CELLULAR AND MOLECULAR EFFECTS OF SURFACE MODIFIED MAGNETIC NANOPARTICLES IN RAT MODEL

Sabareeswaran, A

Ph.D. THESIS

2015

SREE CHITRA TIRUNAL INSTITUTE FOR MEDICAL SCIENCES AND TECHNOLOGY

THIRUVANANTHAPURAM, INDIA

DECLARATION

I, Sabareeswaran. A, hereby certify that I had personally carried out the work depicted in the thesis entitled, **"CELLULAR AND MOLECULAR EFFECTS OF SURFACE MODIFIED MAGNETIC NANOPARTICLES IN RAT MODEL",** except where due acknowledgment has been made in the text. No part of the thesis has been submitted for the award of any other degree or diploma prior to this date.

Thiruvananthapuram — Sabareeswaran, A

-04-2015 — Reg No: PhD/2010/02

SREE CHITRA TIRUNAL INSTITUTE FOR MEDICAL SCIENCES & TECHNOLOGY

Thiruvananthapuram – 695011, INDIA
(An Institute of National Importance under Govt. of India)
Phone: (91)0471-2520271 Fax: (91)0471-2341814
Email: tvkumari@sctimst.ac.in Web site – www.sctimst.ac.in

CERTIFICATE

This is to certify that **Dr. Sabareeswaran. A**, in the Histopathology laboratory of this institute has fulfilled the requirements prescribed for the Ph. D. degree of the Sree Chitra Tirunal Institute for Medical Sciences and Technology, Thiruvananthapuram. The thesis entitled, **"CELLULAR AND MOLECULAR EFFECTS OF SURFACE MODIFIED MAGNETIC NANOPARTICLES IN RAT MODEL"** was carried out under my direct supervision. No part of the thesis was submitted for the award of any degree or diploma prior to this date.

* Clearance was obtained from the Institutional Animal Ethics Committee for carrying out the study.

Thiruvananthapuram
-04-2015

Dr. T.V Kumary. PhD
(Research Supervisor)

Scientist G & SIC
Tissue culture Laboratory,
BMT wing, SCTIMST,
Thiruvananthapuram

The thesis entitled

CELLULAR AND MOLECULAR EFFECTS OF SURFACE MODIFIED MAGNETIC NANOPARTICLES IN RAT MODEL

Submitted by

Sabareeswaran, A

for the degree of

Doctor of Philosophy

Of

SREE CHITRA TIRUNAL INSTITUTE
FOR MEDICAL SCIENCES AND TECHNOLOGY,
THIRUVANANTHAPURAM - 695011

is evaluated and approved by

…… ……..

Dr. T.V.Kumary. PhD., Examiner

(Research Supervisor)

Dedicated To My family &

My teachers

ACKNOWLEDGEMENT

I would like to express my heartfelt gratitude and respect to my supervisors Dr. T.V Kumary, Scientist G, Tissue culture laboratory and Dr Mira Mohanty, Scientist G(Sr Grade), Histopathology laboratory-BMT Wing, SCTIMST. Their guidance, timely advice, lively discussions, critical evaluations and encouragement helped in nurturing my passion for science throughout the course of study. This work would not have been possible without both of their support and encouragement. Their guidance not only added my knowledge but also increased my confidence and dedication in work. I thank them for the entire support offered during my Ph.D programme.

I am grateful to the former and present Director of SCTIMST and the present Head and the previous Heads, BMT Wing for all support provided during the course of my work.

I thank members of the doctoral advisory committee, Dr. Annie John, (Scientist-F, Transmission electron microscopy lab, BMT Wing, SCTIMST) and Dr K Sreenivasan, (Scientist G, Polymer Analysis Lab for their timely suggestions, support and critical comments.

I am thankful to Dr. Sundar Jayasingh, Deputy Registrar, Dr. Prabha D. Nair, Associate Dean for PhD affairs, Dean, and all members of academic division and Director's office for their administrative support.

I thank Dr P R AnilKumar , Mrs Deepa K Raj, Mr Balu V Gopal, Mr Vinod, Mrs Lakshmi, Mrs Shabeena and former staffs and students of Tissue culture laboratory, SCTIMST for the help extended during tissue culture experiments.

I thank Dr.Shivaram Selvam, Dr Sunitha and Dr G.T.Finosh, Polymer Division, Mrs Sreedevi of NIIST, Trivandrum for providing technical help during synthesis.

I thank Dr. Sachin J Shenoy, DIMT, Dr. Harikrishnan V S and all the staffs of DLAS, Dr.Anugya Bhatt of TRU lab, Dr P.V Mohanan, scientist F and Ms Lakshmi of Division of Toxicology for their support during animal experiments.

I thank Dr. Francis Fernandez, Mrs. Sunitha, Mr. Mir Mahmoud and Mrs. Susan, TEM, Dr. Rekha, BioSurface Technology lab, Mr.Willi Paul, Mr. Durgadas, FADDS, Mr.Jaseer mohamad of Experimental pathology, Dr.Ranjith P Nair and Ranjith Kartha of TRU lab, Dr. Suresh Babu, Mr.Ansar, Bioceramic laboratory, Dr. C.L.Gopu, Dr.Radhakumary,LPA, Mrs. Swapna and Mr Bejoy, MOM, Mr. Merlin, DTERT, Mr Sudhin thampi, Mr Vinodkumar, Mr Arun Anirudhan for their assistance during the evaluations.

I thank all my friends of our department, Mrs Sulaikha Baby, Mr Joseph Sebastian, Dr Anupama, Mrs. Sandhya Rani, Mrs. Anju, Mr Thulaseedhran, Dr Josna joseph and Dr Bernadette Madathil for their timely help and encouragement.

I extend my thanks to all friends in BMT Wing and Hospital Wing, SCTIMST.

Thanks to the staff of various administrative departments and library of the Institute and fellow students in the campus for their lively companionship.

I am thankful to DBT and DST-nanomission, GOI for funding through research grants.

I further thank many who directly or indirectly helped me to prepare this thesis.

Last but not the least: I thank my family members who provided the most precious support. I am indepted to my wife Ms Shanthi and my kid's Sharvesh and Kavin kumar for their love and support.

Sabareeswaran, A

TABLE OF CONTENTS

LIST OF FIGURES

LIST OF TABLES

ABBREVIATIONS

DLS	Dynamic Light Scattering
DEX-SPIONS	Dextran coated SuperParamagnetic IronOxide Nanoparticles
FTIR	Fourier Transform Infra Red Spectroscopy
H&E	Haematoxylin and Eosin
IONPs	Iron Oxide Nanoparticles
MEM	Minimum Essential Medium
MNPs	Magnetic Nanoparticles
MRI	Magnetic Resonance Imaging
MTT	3-(4, 5- dimethylthiazol-2-yl)-2.5-diphenyl tetrazolium bromide
NNI	National Nanotechnology Initiative
NPs	Nanoparticles
PB	Pearls' Prussian blue
PEG	poly(ethyleneglycol)
PEG-SPIONS	poly(ethyleneglycol) coated SuperParamagnetic IronOxide Nanoparticles
PEI	polyethyleneimine
RBC	Red Blood Cells
RES	Reticulo Endothelial Cells
ROS	Reactive Oxygen Species
SGOT	Serum Glutamic Oxaloacetic Transaminase
SGPT	Serum Glutamic Pyruvic Transaminase
SPIONS	SuperParamagnetic IronOxide Nanoparticles
TEM	Transmission Electron Microscopy
TGA	Thermo Gravimetric Analysis
VSM	Vibration Sample Magnetometry
WBC	White Blood Cells
XRD	X-ray Diffraction

SYNOPSIS

Use of nanoscale materials for biomedical application has yielded many promising technologies for the diagnosis and treatment of diseases. The development of nanotechnology as diagnostic and or therapeutic agents, coined as theranostics, has accelerated because nanoparticles can be functionalized in many different ways to simultaneously enable drug delivery and imaging, propelling the personalized medicine trend forward. The growing use of nanoscale materials in commercially available products and therapeutics has created an urgent need to determine the toxicity of these materials so that they can be designed and employed safely. As nanoparticles have unique physical and chemical properties, the challenges in determining their physiological impact have been numerous. It is, therefore, important to fundamentally understand how the nanoparticles interact with cells in relevant models. Our study investigates the system when exposed to well-characterized surface modified super paramagnetic iron oxide nanoparticles (SPIONS) with respect to - (1) the mechanism or cause of changes in cell function, including assessment of nanoparticle uptake. (2) Biocompatibility and biosafety, particularly related to their accumulation in tissues and their elimination and (3) the mast cell response.

Chapter 1 introduces the topic of the thesis. Nanomaterials for biomedical applications are mainly used in the imaging and drug delivery. A family of such nanomaterials which has found widespread use in imaging in particular is iron oxide nanoparticles. The compliance of SPIONS with the tissue, excellent physio-chemical properties and notable magnetic properties make SPIONS the material of choice for

biomedical imaging applications. Magnetic nanoparticles offer exciting new opportunities toward developing effective drug delivery systems, as it is feasible to produce, characterize, and specifically tailor their functional properties.

However biocompatibility and biodegradation in the biological system is a matter of concern in the use of SPIONS as contrast agent. The degradation in the biological milieu leads to oxidative stress and redox homeostasis is affected causing the cellular pathology.

Chapter 2 gives a comprehensive account of literature related to the study. The established methods of synthesis of SPIONS specifically the chemical co-precipitation and Massorts procedure are reviewed. The standard techniques used to characterise SPIONS such as Transmission Electron Microscopy (TEM), Dynamic Light Scattering (DLS), Fourier Transform-Infra Red (FT-IR) spectroscopy, X-Ray Diffraction (XRD), Thermo Gravimetric Analysis (TGA) and Vibrational Sample Magnetometry (VSM) are discussed. The commonly used SPION contrast agents require nonspecific uptake by mononuclear phagocytes to improve the local contrast, and at the hydrodynamic size of over 50 nm, these particles have very limited extravasation ability and are subject to easy uptake by the reticuloendothelial system (RES), which undermines severely their targeting specificity.

Physiological mechanisms for cellular internalization of particles include fluid phase or receptor-mediated endocytosis, phagocytosis and non-endocytic pathways. Enhancement of SPIONS internalization by magnetic forces and subsequent short-term viability are poorly understood. Little is also known of intracellular trafficking following magnetically enhanced endocytosis and potential iron cytotoxicity from

particle degradation. Additionally, the effects of cytosolic SPIONS degradation processes are not understood so far or untested. By contrast, intravascular SPIONS targeting of specific cell receptors must contend with opsonisation by proteins and phagocytosis by the RES. Hence, coatings such as polyethylene glycol (PEG) have been used to reduce macrophage recognition and uptake. Encapsulation of SPIONS with negative or positive surface charge (zeta potential) is useful for corrosion protection, colloidal dispersion and as substrate for particle functionalisation. Iron oxide particles are usually coated with different organic shells including dextran, albumin or polyethylene glycol. Coated nanoparticles can be manufactured with a variety of functional groups (such as amino, aldehyde, hydroxyl, sulphate and carboxyl groups) on their surfaces. Potential iron leaching and toxicity, an aspect of short-term SPIONS viability, has limited data. Normal intracellular iron homeostasis involves internalization of the complex iron bound transferrin via the transferrin receptor but excessive intracellular iron ions are potentially toxic through the formation of oxygen radicals and peroxidative damage. Intracellular iron balance could be upset if SPIONS were to leach iron. Nevertheless, studies on magnetic resonance imaging showed ferrite nanoparticles as compatible with hepatic reticuloendothelial cells and cause no hepatocellular injury.

Few studies have been published on the immunotoxicological risks of engineered nanomaterials. However, in vivo interaction of surface modified iron oxide nanoparticles with mast cells are occasional and limited to clinical reports. Mast cells are derived from hematopoeitic precursor cells in the bone marrow and mature and reside in tissues especially in the connective tissues. They produce, store, and secrete a large spectrum of biologically active mediators and have roles in many

physiological processes such as tissue remodeling, wound healing, angiogenesis, and innate immunity.

The present study attempts to gain a better understanding of the cellular and molecular changes due to surface modification of SPIONS. In particular oxidative stress, haematology, biochemistry, histopathological, biodistribution, ultrastructural changes and gene expression were investigated. The hypothesis for the study is that accumulation of surface modified iron oxide nanoparticles in the body following intravenous administration can produce a pro-oxidant environment in tissues and cells leading to adverse biological consequences.

Chapter 3 describes the experimental approach of the entire study including materials and methods used. The study was divided in to three phases.

In phase I, SPIONS was synthesised using a published protocol and its surface was modified with dextran and polyethylene glycol. Synthesised nanoparticles were characterised using standard techniques like size by transmission electron microscopy, hydrodynamic diameter by DLS and colloidal stability by the zeta potential of solutes. The magnetite phase of SPIONS was confirmed by XRD and Surface modifications were analysed by FT-IR and quantity of dextran and polyethylene glycol coating was measured by TGA. The magnetic properties of the synthesised nanoparticles were evaluated by VSM.

In Phase II, the in-vitro interaction of DEX-SPIONS, PEG-SPIONS, SPIONS were analysed using murine macrophage cell line RAW264.7 and L929 fibroblast. The cytocompatibility was assessed by MTT assay and cell viability was assessed by Live and dead assay. Haemocompatibility was assessed by cell count, total and

plasma haemoglobin content and % hemolysis. Oxidative stress induction was assessed in HepG2 cells by analysing the antioxidants namely GSH, SOD, NO level and lipid peroxidation in the cells 12 h post treatment with DEX-SPIONS, PEG-SPIONS and SPIONS.

In addition to above, particle uptake was studied using confocal Raman spectroscopy in macrophage cell line RAW264.7 and L929 fibroblast.

In phase III, details of animal experiments using female Wistar rats are given. The rats were grouped into four groups with 6 animals in each group namely DEX-SPIONS, PEG-SPIONS, SPIONS and saline Control. Under Ketamine (80 mg/Kg) and xylazine (8 mg/kg) anaesthesia, each healthy rat received 5 mg Fe/kg body weight of DEX-SPIONS, PEG-SPIONS and SPIONS suspended in normal saline and normal saline only in control group as a single dose via lateral tail vein. The maximum injected volume was 500 µl per animal. The animals were observed closely for 24 h and clinical signs and mortality were recorded.

Haematology, biochemistry, histology of organs, oxidative stress, mast cell distribution in major organs viz., heart, lung, liver, spleen and kidney, transmission electron microscopy of liver, Quantitative expression of following genes were studied namely, Heat Shock Protein-70 (HSP-70), Haemeoxygenase-1(HO-1), Transferrin and Ceruloplasmin in liver. Fe, Cu, Ca, Co, Cr, Mg, Mn, Mo, Ni, Se, Sr, V, Zn elemental distribution in liver, spleen and kidney were also evaluated.

Chapter 4 includes the results and discussion obtained from above three phases. The SPION was synthesised by chemical co-precipitation method and average particle diameter using TEM was around 10 nm. The surfaces were modified

with Dextran (MW40,000 da) and PEG (MW8,000 da). The hydrodynamic diameter of SPIONS, DEX-SPIONS and PEG-SPIONS were 45 and 89.30, 67.13 nm respectively and zeta potentials were -11.00, + 7.67, + 6.07 mV respectively. XRD results have shown that the synthesised particles were magneteite and FT-IR spectra indicated the presence of characteristic peaks for dextran and PEG specific molecules over the surface of SPIONS. VSM results have shown the superparamagnetic property of synthesised particles.

The cytotoxicity results have shown that the synthesised SPIONS, DEX-SPIONS, PEG-SPIONS were non cytotoxic to L929 and RAW 264.7 cells after 24h exposure. In vitro cytocompatibility, results of fibroblasts and RAW 264.7 cells showed more favorable cell proliferation and metabolic activity in coated particles than uncoated ones. SPIONS affected the metabolic activity in concentration dependent manner when they were added in the concentration range of 50-12.25 µg to the cells. It was observed that the cell proliferation/viability decreased when the concentration of SPIONS increased. Live and dead assay also indicated that more than 95 % cell viability in treated groups and substantial increase in viability was observed in coated groups compared to SPIONS group. Haemocompatibility results have shown that the hemolysis percentage of SPIONS, DEX-SPIONS and PEG-SPIONS were well within the acceptable limit.

The Confocal Raman microscopic studies demonstrated the uptake of nanoparticles by L929 fibroblast cells and RAW 264.7 macrophages. The nanoparticles were mostly distributed in the cytoplasm.

Oxidative stress results in HepG2 cells showed significant ($p<0.05$) increase in lipid peroxides level in cell lysates of SPIONS treated cells when compared with control. The level of reduced glutathione (GSH), superoxide dismutase and nitrite level in cell lysates of SPIONS, DEX-SPIONS and PEG-SPIONS treated cells were increased significantly ($p<0.05$) when compared to control.

Animal experiment results shown that there were no adverse signs and symptoms observed in animals treated with SPIONS, DEX-SPIONS and PEG-SPIONS. The results of haematological and biochemical parameters show that in haematology, the mixed cell populations of treated groups were significantly increased when compared to control values which, could be expected from an acute immune response to foreign materials, here SPIONS. In biochemical parameters, the SGOT level was significantly increased in DEX-SPIONS group when compared to control group. Bilirubin content was detected in the serum of treated groups and found to be within the normal range for this species but in the control group it is below the detectable limit.

Oxidative stress results showed that significant ($p<0.05$) increase in lipid peroxides level in liver, lung and heart tissue homogenates of SPIONS treated animals was measured when compared control groups. The level of reduced glutathione in liver, lung, spleen and kidney tissue homogenates of SPIONS, DEX-SPIONS and PEG-SPIONS treated animals were decreased significantly($p<0.05$) except lung of DEX-SPIONS when compared to control group. The level of SOD in liver, lung, spleen, kidney and heart tissue homogenates of SPIONS, DEX-SPIONS and PEG-SPIONS treated animals were decreased but not statistically significant

when compared to control group. The level of nitrite in liver, lung, spleen, kidney and heart tissue homogenates of SPIONS, DEX-SPIONS and PEG-SPIONS treated animals were decreased significantly($p<0.05$) except kidney of PEG-SPIONS when compared to control group.

Liver architecture was normal in all groups. In SPIONS group, hepatocytes with discreet nucleus, moderate granular cytoplasmic degeneration and multi focal intra hepatocyte cholestasis were found compared to control group. In DEX-SPIONS group, few polymorphonuclear cells and moderate proliferation of Kuppfer cells with brown-yellow cytoplasmic pigments were seen in the sinusoidal space. Hepatocytes with discrete nucleus and eosinophilic dark granular cytoplasm were observed. In PEG-SPIONS group, very few Kuppfer cells with occasional brown-yellow cytoplasmic pigments were seen in the sinusoidal space and hepatocytes with discrete nucleus and granular cytoplasm was observed. Blue iron deposits in the cytoplasm of Kupffer cells were observed in the SPIONS, DEX-SPIONS group and iron deposits were also seen in sinusoids and cytoplasm of hepatocytes in PEG-SPIONS group. Mast cells were observed more in DEX-SPIONS but not statistically significant and also in SPIONS and PEG-SPIONS group compared to control group. Mast Cells were mostly distributed in the periportal region in all groups.

The histological micrographs of kidneys show normal architecture. In SPIONS group, glomeruli appeared normal in the cortex region. Protein casts were observed in the collecting tubular lumen. Tubular epithelial cells with enlarged nuclei, formation of prominent nucleoli and marked granular cytoplasm were observed. In DEX-SPIONS group, focal tubular degeneration was seen with the tubular

epithelium showing moderate granular cytoplasmic degeneration. In PEG-SPIONS group, glomeruli architecture was normal; Protein casts were noted in the convoluted tubular lumen. Blue pigment deposits in the cytoplasm of convoluted tubule cells were observed in the SPIONS group, DEX-SPIONS group and PEG SPIONS group. These deposits were also seen in the glomerular region in PEG-SPIONS group. Mast cells were absent in the cortex region in all three groups and control group. They were mostly distributed in the hilus and medulla region in all groups.

Pulmonary architecture was preserved in all groups. In SPIONS group, infiltration of macrophages in the alveolar septa was seen. In DEX-SPIONS group, infiltration of macrophages in the alveolar septa and peribronchial region was seen. In PEG-SPIONS group, mild peribronchial infiltration of macrophages was noted. Blue iron pigment deposits in the cytoplasm of macrophage cells were observed in the SPIONS group in the alveolar region, macrophages of peribronchial region in DEX-SPIONS group and perivascular region in PEG SPIONS group. Mast cells were observed significantly ($p<0.05$) more in DEX-SPIONS group and in SPIONS, PEG-SPIONS group it was more but not statistically significant compared to control group. Mast Cells were mostly distributed in the peribronchial and alveolar region in DEX-SPIONS group and in the ventral border of alveolar region in PEG-SPIONS and SPIONS group.

Spleenic architecture was normal in all groups. In SPIONS and DEX-SPIONS group, the spleenic red pulp with macrophages laden with brown siderotic pigments was seen. In PEG-SPIONS group, there was relatively increased number of macrophages were observed in the spleenic red pulp area. Blue pigment deposits in

the cytoplasm of macrophage cells in the red pulp region were observed in the SPIONS group, DEX-SPIONS group and PEG SPIONS group with more intensity in the later group. Mast cells were absent in DEX-SPIONS and SPIONS group and were scant in PEG-SPIONS group as compared to control group.

Histological sections of heart show normal architecture. There were no changes in striations and no nuclear changes. Blue iron pigment deposits in the perivascular region were observed in the SPIONS group, DEX-SPIONS group and PEG SPIONS group. Mast Cells were mostly distributed in the peri vascular region in all groups and in addition in the sub endocardial region of SPIONS group. Mast cells were observed significantly ($p<0.05$) more in PEG-SPIONS and followed by DEX-SPIONS group and SPIONS group compared to control group.

The ultrastructural images of liver injected with DEX-SPIONS, PEG-SPIONS and SPIONS are shown. In SPIONS, DEX-SPIONS group, Kuppfer cells with aggregates of iron particles were seen in the cytoplasm but in PEG-SPIONS group the particles could not be identified in the cytoplasm of Kupffer cells in the ultra thin sections examined. There were also few Kuppfer cells observed in H&E section.

Gene expression studies revealed that transferrin and ceruloplasmin genes were up regulated in coated groups when compared to control group which could be due to iron over load. Similarly heat shock protein-70 (HSP-70) and Haemeoxygenase-1 (HO-1) genes were also up regulated when compared to control group which could be due to oxidative stress induced by the excessive load of transitional metal ions.

Elemental analysis showed that iron content was increased significantly in spleen of treated groups when compared to control. Copper content was significantly

inceresed in SPIONS group alone when compared to control. Calcium level was significantly increased in kidney of PEG-SPIONS group and spleen of DEX-SPIONS group when compared to control group. Magnesium and Zinc level was significantly increased in spleen of DEX-SPIONS group. Manganese was significantly increased in liver and spleen of SPIONS, PEG-SPIONS and DEX-SPIONS group and significantly decreased in kidney of SPIONS, DEX-SPIONS group when compared to control group.

Chapter 5 summarises the whole study and provides the conclusion drawn out. The results of this study indicate the successful in house synthesis of SPIONS and surface modification. Cytocompatibility and haemocompatibility studies qualified the material for animal experimentation.

The surface modification of iron oxide nanoparticles has shown improvement in vivo biocompatibility and their interaction with the biological system. The coating material has influenced the rate of metabolism to a greater extent than either the cellular distribution or the clearance. These results indicate that the degradation of iron oxide coating is a critical factor affecting their cytotoxicity and suggest that exposure of cell mileu to iron oxide makes the cell more sensitive to oxidative stress. The study for the first time assessed the mast cell induction by surface modified SPIONS. These results also indicate that the surface modification of the iron oxide core is an important factor and influences the mast cell induction differently in different organs. Gene expression studies indicated that cellular homeostasis has disrupted and molecular cell defence mechanisms were activated. The divalent metal

cations were altered acutely due to SPIONS infusion which is very relevant when viewed from clinical perspective.

In future, investigations can be carried out to elucidate the long term effect of SPIONS on divalent metal cation homeostasis. Need to study the gene expression associated to the iron transport and other divalent metal cation transport using specific knock out models.

Introduction

1 INTRODUCTION

1.1 *Nanotechnology*

Nanotechnology is defined by the American National Nanotechnology Initiative (NNI) as ‘‘the understanding and control of matter at dimensions between approximately 1 and 100 nm, where unique phenomena enable novel applications’’ (Hubbs et al., 2013).

Use of nanoscale materials for biomedical applications has yielded many promising technologies for the diagnosis and treatment of diseases. The development of nanotechnology as diagnostic and or therapeutic agents, coined as theranostics, has accelerated because nanoparticles can be functionalized in many different ways to simultaneously enable drug delivery and imaging, propelling the personalized medicine trend forward. The growing use of nanoscale materials in commercially available products and therapeutics has created an urgent need to determine the toxicity of these materials so that they can be designed and employed safely. As nanoparticles have unique physical and chemical properties, the challenges in determining their physiological impact have been numerous. It is, therefore, important to fundamentally understand how the nanoparticles interact with cells in relevant models.

1.2 *Nanotoxicology*

Nanotoxicology is emerging as an important subdiscipline of nanotechnology (Jia and Zhuang, 2010). It refers to the study of the interactions of nanostructures

with biological systems with an emphasis on elucidating the relationship between the physical and chemical properties (e.g. size, shape, surface chemistry, composition, and aggregation) of nanostructures with induction of toxic biological responses (Kunzmann et al., 2011).

1.3 *Nanoparticles*

According to the EUROPEAN COMMISSION 'Nanomaterial' means a natural, incidental or manufactured material containing particles, in an unbound state or as an aggregate or as an agglomerate and where, for 50 % or more of the particles in the number size distribution, one or more external dimensions is in the size range 1 nm - 100 nm (Vogel et al., 2013). The major benefit of using nanoparticles is that, due to their size, they can be accurately manoeuvred. Their unique electronic, optical and magnetic properties coupled with their specific dimensions have favoured their attractiveness in this field. Also, they may be best suited for biological applications due to their size being in the range of many biological entities. Furthermore, nanoparticles can be customised for a specific biological purpose such as cell isolation, drug delivery, diagnostics (magnetic resonance imaging, MRI), cellular imaging and hyperthermia (Neuberger et al., 2005). As such, it is necessary to identify and characterize the effects of nanoparticles (NPs) on various biological systems and cell types and evaluate the possibility of exploiting NP for use in novel biomedical applications. Engineered nanoparticles are composed of a much wider variety of materials and occur in monodisperse sizes and shapes. Iron oxide nanoparticles, in particular, have wide-spread biomedical applications and are frequently found in many different products.

1.3.1 Magnetic nanoparticles

Magnetic nanoparticles for use in biomedical applications are desired to exhibit superparamagnetic properties. The magnetic property of the iron oxide nanoparticles depends upon shape and size of the particle. Spherical iron oxide nanoparticles with small size have emerged as one of the primary nanomaterials for biomedical applications due to their superparamagnetic property characterised by high coercivity, low Curie temperature and high magnetic susceptibility (Neuberger et al., 2005).

Superparamagnetic iron oxide nanoparticles (SPIONS) are typically small particles composed of either a magnetite (Fe_3O_4) or maghemite (γ-Fe_2O_3) core coated with a biocompatible organic/inorganic polymer. Both maghemite and magnetite are traditionally ferromagnetic in nature. However, as they decrease in size to $\leq$ 30 nm, they lose their permanent magnetism and become superparamagnetic. SPIONS have been used clinically as negative contrast agents in magnetic resonance imaging (MRI) for detecting liver and lymph node lesions. Due to the intrinsic and unique magnetic properties of SPIONS, they have been used for broad range of bio-applications such as diagnostic imaging, targeted drug delivery, cell tracking and magnetic fluid hyperthermia to generate heating for cancer therapy. However, small size iron oxide nanoparticles tend to cause adverse tissue response due to the high surface to volume ratio. Furthermore, iron oxide nanoparticles can be easily oxidized in air, resulting in the loss of magnetism. Therefore, surface coating is essential to stabilize the magnetic iron oxide nanoparticles. These strategies comprise grafting or coating with organic molecules, including small organic molecules, polymers and biomolecules or coating with an inorganic layer (silica, metal and carbon). In many

cases, the protecting shells not only stabilize the magnetic iron oxide nanoparticles but can also be used to improve their biocompatibility, for further functionalization to use in biological applications.

Surface coatings contribute significantly to the hydrodynamic diameter and the net surface charge, both critical design parameters that determine the in vivo fate of nanoparticles. Studies have indicated that cancer targeting and therapy may require several hours of circulation time to reach the affected sites and possibly remain at the site for days, if repeated therapeutic exposure and imaging is desired. The mononuclear phagocytic system of the liver and spleen, has to be studied in detail to understand mechanism of nanoparticle handling at cellular level (Jokerst et al., 2011).

Limitation

Although great strides have been made in the worldwide production and use of metal-based nanoparticles, there is a serious lack of information about the impact of nanoparticles on human health and environment, especially the potential for nanoparticle induced toxicity (Canesi et al., 2008). Preliminary reports of the inherent toxicity of some nanoparticles are available and indicate that they can affect biological behavior at the organ, tissue, cellular, subcellular, and protein levels (Shaw et al., 2008). From a safety perspective, more information on the in vivo toxicity and metabolism of SPIONS is required.

1. The physical properties such as the particle size, shape and surface coating can also evoke a toxic response by aggregating and coagulating according to size and shape (Singh et al., 2010). When addressing the possible *in vivo* application of

magnetic nanoparticle, it is equally important to consider the fate of the magnetic nanoparticles after they have been released by the cells. Further issues arise when considering the degradation of the magnetic nanoparticles and the outcome of accumulated magnetic nanoparticles or magnetic nanoparticle by-products in various tissues and organs. Degradation products are thought to possibly react with various components of the body or cells. Therefore, the effects of the breakdown products on the surrounding tissue should be fully investigated. Assumptions on this matter cannot be made, and appropriate investigations should always be performed.

2. Even though SPIONS-based MRI contrast agents have been used and approved, the use of these for cell-based therapies still requires FDA approval as their intended use is different from their use as contrast agents. An essential requirement of contrast agents is that the particles need to be excreted relatively quickly and not remain in the body in the long term. However, for some applications, especially within the remit of regenerative medicine, for long-term treatment by magnetic nanoparticles, long term residence in the body may be necessary.

3. In cases where the magnetic nanoparticles are incorporated into the therapy and transplanted within the body, the risk of magnetic nanoparticles migrating through the organism, entering and accumulating within organs is a constant concern. This could trigger an immunological or an inflammatory response by the body. More studies are needed in order to know the potential deleterious or beneficial effects of nanostructures in the immune system. The role of mast cells in this inflammatory response to nanomaterials has still not been studied enough. Mast cells are well known for their involvement in allergic and anaphylactic reactions,

during which immunoglobulin E (IgE) receptor aggregation leads to exocytosis of the content of secretory granules, commonly known as degranulation and secretion of multiple mediators (Sismanopoulos et al., 2012).

4. Though the dose of SPIONS administered intravenously accounts for 1.255% of the total body iron stores, SPIONS are required to be magnetically targeted to a particular tissue/organ in order to maximally benefit a therapeutic or diagnostic application, leading to high concentrations in a localised area. Consequently, this iron overload can have toxic implications as excessive accumulation of the SPIONS, and in particular, high levels of free Fe ions in the exposed tissue can lead to an imbalance in its homeostasis and can cause aberrant cellular responses including cytotoxicity, DNA damage, oxidative stress, epigenetic events and inflammatory processes (Bulte et al., 2001) (Häfeli et al., 2009) (Ankamwar et al., 2010).

Iron is essential for many physiological processes; however, iron overload has been known as a risk factor in progression of atherosclerosis (Pourmoghaddas et al., 2014). So from a clinical perspective, the risk associated with infusion of iron based contrast agents, drug carriers has to be assessed.

More importantly, in the absence of cytotoxicity, this exposure can still lead to subtle but deleterious cellular disruption in the form of DNA damage that may initiate carcinogenesis or have a significant impact on future generations if the fidelity of the genome in germ cells is not maintained (Singh et al., 2009). Furthermore, there are possibilities for their direct contact with DNA during the process of mitosis when the nuclear membrane breaks down.

This thesis is a detailed investigation into the mechanism or cause of changes in cell function, with respect to a) biocompatibility, b) their accumulation in tissues and their elimination and c) the mast cell response and assessment of nanoparticle uptake, following exposure to surface modified super paramagnetic iron oxide nanoparticles.

The development of iron oxide based nanoparticles for biomedical applications including medical imaging and drug delivery is currently undergoing a dramatic expansion. However, as the range of SPIONS types and applications increase, it is also clear that the potential toxicities of these novel materials and the properties driving such toxic responses must also be understood. Indeed, a detailed assessment of the factors that influence the biocompatibility and/or toxicity of SPIONS are crucial for the safe and sustainable development of these emerging SPIONS.

Aim

The aim of this study was to find out the hitherto less studied adverse effects associated with SPIONS following acute intravenous exposure, including general and specific toxicological actions (on the major organs, immune system and on certain macromolecules). Both, in vivo and in vitro examinations have notable advantages and disadvantages. By combining these in a complex experimental model, early detection of possible toxicological effects can be achieved and new relationships between the primary outcomes can be revealed. In summary, this thesis comprises both in vitro and in vivo tests for toxicological examination of superparamagnetic iron oxide nanoparticles.

As iron oxide based nanomaterials expand as therapeutics and as diagnostic tools, parenteral administration of SPIO nanomaterials should also be recognized as a critical aspect for toxicity consideration. Due to the complex nature of nanomaterial coatings, opposing studies have led to different views of their safety. In this investigation, the cellular effects of surface modified iron oxide nanomaterials after systemic exposure was studied.

Approach with hypothesis

Iron oxide is one of the mostly used nanoparticles in biomedical applications, more specifically in imaging. Surface modification with dextran a natural and immunogenic polymer and polyethylene glycol, a synthetic polymer and nonimmunogenic were selected for this study. Intravenous was employed as this route is the most commonly used route for administering nanoparticle formulations, including in-vivo imaging and presents several physiological barriers.

Hypothesis

Accumulation of surface modified iron oxide nanoparticles in the body following intravenous administration, produces a pro-oxidant environment in tissues and cells leading to adverse biological consequences.

Approach

In phase I, superparamagnetic iron oxide nanoparticle (SPION) was synthesised and surface was coated using dextran (DEX-SPION) and polyethylene glycol (PEG-SPION). Synthesised nanoparticles were characterised using techniques like TEM, XRD, FT-IR spectra, VSM and TGA.

In phase II, SPION induced bio-effects were studied in- vitro using cell lines namely L929 mouse fibroblast, RAW 264.7 macrophage and HepG2 cell lines. To study the blood compatibility, haematology and hemolysis tests were carried out. To study particle uptake in *in vitro* cell culture system, confocal Raman spectroscopy has been used.

In phase III, the acute in-vivo cellular responses to intravenously administered surface modified SPIONS were evaluated in a rat model. Acute changes in haematological and biochemical parameters were investigated. Oxidative stress was assessed by evaluating the anti-oxidant enzymes namely super oxide dismutase, glutathione sulfhydryl, tissue nitrite level and lipid peroxidation level of major organs. Gross and histopathological evaluation of all organs and tissues were carried out. The tissue response to SPIONS has been evaluated using the techniques of light microscopy and transmission electron microscopy. In this study special staining techniques have been adopted, toluidine blue to demonstrate mast cells, Prussian blue to identify iron and cresyl violet stain to evaluate the neural tissue. A genomic approach also was adopted to elucidate the expression levels of specific genes that are expressed to surface modified SPIONS, using Real time polymerase chain reaction. The elemental iron distribution and other essential divalent metal cations distribution also were studied.

Review of Literature

2 REVIEW OF LITERATURE

2.1 *Nanotechnology*

Even long before the start of “nanoera”, people have come across various nano sized materials and the related nano level processes and used them in practice. The first mention of purposely created and applied technological processes and means, which were subsequently termed nanotechnology, is usually connected with the well-known lecture of Mr. R. Feynman, the professor of Californian institute of technology, delivered in 1959 at the session of the American Physical Society. In this lecture entitled “There is a lot of space down there” the possibility to create nanosized products with the use of atoms as building particles was considered for the first time. Presently, this lecture is referred to as the origin of the nanotechnological paradigm.

Publications and products in the field of nanotechnology are rapidly increasing. A PubMed search of papers published in the year 2011 (Hubbs et al., 2013) and 2015 using the search term **nanotechnology** yielded 6,369 and 51,327 publications respectively; a search using the term **nanomedicine** yielded 953 and 9,618 publications respectively, a search using the term **nanotoxicology** recovered 214 and 953 references respectively, a search of **nanotoxicology and pathology** recovered only 17 publications in 2011 but 108 publication in 2015. These searches demonstrate the tremendous increase in the scientific investigation of

nanotechnology and nanomedicine as well as the scarcity of information regarding the safety of nanotechnology products, particularly the potential toxicity to tissues.

2.2 *Nanotoxicology*

Majority of nanotoxicity research was focused on cell culture systems; however, the data from these studies could be misleading and will require verification from animal experiments. *In vivo* systems are extremely complicated and the interactions of the nanostructures with biological components, such as proteins and cells, could lead to unique biodistribution, clearance, immune response, and metabolism. An understanding of the relationship between the physical and chemical properties of the nanostructure and their *in vivo* behavior would provide a basis for assessing toxic response and more importantly could lead to predictive models for assessing toxicity (Fischer and Chan, 2007). Among the growing debate related to the human health and safety risks of nanotechnology warranted simultaneous discussion for stringent regulation of nanotechnology (Samuel Reich, 2011). Very little attention has been directed towards the potential immunogenicity of nanostructures. Nanostructures can activate the immune system, inducing inflammation, immune responses, allergy, or even affect to the immune cells in a deleterious or beneficial way (immunosuppression in autoimmune diseases, improving immune responses in vaccines). In comparison to conventional pharmaceutical agents, nanostructures have very large sizes and immune cells, especially phagocytic cells, recognize and try to destroy them (Nel et al., 2006).

2.3 *Superparamagnetic iron oxide nanoparticles (SPIONS)*

Magnetite (Fe_3O_4) or maghemite (γ-Fe_2O_3) cores stabilised with a hydrophilic surface and nanoparticles with diameters below 30 nm are of particular interest because they exhibit superparamagnetic behaviour. This means that once the magnetic field is removed, they do not retain any magnetization (no hysteresis). Superparamagnetism is obtained by nanoparticles that contain only a single magnetic domain (Laurent et al., 2008). Magnetic nanoparticles based on iron oxides or iron oxide shells are recognized as the most prominent magnetic materials, as they are reported to possess unique physicochemical properties.

2.4 *Use of SPIONS in medicine*

SPIONS with different surface chemistry have been used for a great number of biomedical applications including MRI contrast agent, drug delivery (Laurent et al., 2014), hyperthermia (Laurent et al., 2011), cell labelling, in-vivo imaging and gene delivery (Alvarim et al., 2014).

2.5 *Synthesis of SPIONS*

SPIONS can be synthesised chemically using different methodology (Laurent et al., 2008). The most common method for the production of magnetite nanoparticles is the chemical co-precipitation technique of iron salts. For obtaining water-soluble and biocompatible iron oxide nanoarticles, co-precipitation often has been employed. However, this method presents low control of the particle shape, broad distributions of sizes and aggregation of particles (Kang et al., 1996) (Massart, 1981).

2.5.1 Chemical synthesis by co-precipitation technique

The co-precipitation technique is probably the simplest and most efficient chemical pathway to obtain magnetic particles. Iron oxides (either Fe_3O_4 or γFe_2O_3) are usually prepared by an aging stoichiometric mixture of ferrous and ferric salts in aqueous medium followed by precipitation of magnetite by addition of a base (Gupta and Gupta, 2005). Fe_3O_4 nanoparticles may then be superficially oxidized to the more stable maghemite (γ-Fe_2O_3) by addition of ferric nitrate to the colloidal suspension. Shape and composition of iron oxide nanoparticles are reported to depend on various operating conditions such as pH, nature of the base, Fe^{2+} and Fe^{3+} ratio (Massart et al., 1995).

Although, co-precipitation is probably the most widely used method to obtain commercial magnetic nanoparticles for biomedical applications, particles prepared by co-precipitation tend to be rather polydisperse and their shapes are difficult to control (Gupta and Gupta, 2005). A wide variety of factors can be adjusted in the synthesis of the iron oxide nanoparticles in order to control size, magnetic characteristics, stability in solution, surface properties and coatings (Gupta and Gupta, 2005). In addition, the ionic strength and pH of the coprecipitation solution can be adjusted to control nanoparticle size over an order of magnitude (2–15 nm) (Cabuil et al., 1995). Babes et al, (1999) have studied the influence of different parameters, the most important factor to be the Fe^{2+}/ Fe^{3+} molar ratio. The mean size increased with the Fe^{2+}/ Fe^{3+} ratio, whereas the preparation yield decreased. The second most important factor influencing the synthesis is the iron concentration. The evolution of this factor is similar to that of the Fe^{2+}/ Fe^{3+} ratio, with an optimum between 39 and 78 mM. The particle mean size of magnetite is strongly dependent

upon the acidity and the ionic strength of the precipitation medium. Higher the pH and ionic strength, smaller will be the particle size and size distribution width, because these parameters determine the chemical composition of the crystal surface and consequently the electrostatic surface charge of the particles. Increase of the mixing rate tends to decrease particle size. In the same way, a decrease of the size as well as the polydispersity is observed when the base is added to the reactives as compared to the opposite process (Massart et al., 1995). Studies have shown that the formation of magnetite particles decreases with an increase in the temperature and also supported the theory of nucleation and growth of the particles. Bubbling nitrogen gas through the solution not only protects against critical oxidation of the magnetite but also reduces the particle size when compared to methods without oxygen removal (Gupta and Wells, 2004a) (Kim et al., 2003). The existence of a superparamagnetic state in Fe_2O_4 metal oxide system has been determined by magnetic measurements in combination with neutron diffraction. In addition, the relaxation time had been correlated with the particle size and temperature which was consistent with Néel theory (Chen et al., 1999).

2.6 *Surface modification of SPIONS*

Magnetite nanoparticles, need to be stabilized with organic and inorganic molecules which are of great importance for the stability of the nanoparticles. Various organic molecules including monomeric and polymeric molecules and inorganic molecules such as silica, manganese, gold and quantum dots have been used for surface modification of iron oxide (Laurent et al., 2008). Various methods of coating have been developed to prepare small (60-100 nm) and ultra small (20-35

nm) particles without size-separation processes. Polymers are often employed to coat the surface of small magnetic iron oxide nanoparticles during or after the synthesis to avoid agglomeration (Moghimi et al., 2001). Coatings provide a means of engineering the surface of the magnetic iron oxide nanoparticles, to tailor its characteristics such as surface charge and chemical functionality. In general, polymers can be chemically attached or physically adsorbed on to magnetic iron oxide nanoparticles to form a single or double layer structure resulting in a repulsive (mainly steric repulsion) force to prevent a magnetic attraction between the iron oxide nanoparticles (Mohapatra and Anand, 2010). A variety of natural and synthetic polymers have been used for coating of nanoparticles. The most common coatings cited in literature are dextran, carboxymethylated dextran, carboxy- dextran, starch, arabinogalactan, glycosaminoglycan, sulfonated styrene-divinylbenzene, polyethylene glycol (PEG), polyvinyl alcohol (PVA), poloxamers, polyoxamines, poly (pyrrole), poly (aniline), poly (alkylcyanoacrylates), poly (methylidene malonate) and polyesters, such as poly (lactic acid) and poly (glycolic acid), (Barratt, 2000).

Several approaches have been developed to coat iron oxide nanoparticles, like in situ coating in which the nanoparticles are coated during the synthesis and post-synthesis coating method in which the polymer is grafted on to the magnetic particles once synthesised (Mohapatra and Anand, 2010).

2.6.1 Dextran

Dextran is a polysaccharide polymer composed exclusively of R-D-glucopyranosyl units with varying degrees of chain length and branching. It has been used often as a polymer coating mostly because of its biocompatibility.

Dextran has been functionalized after iron oxide stabilization by oxidation with periodate to create more hydroxyl groups to allow for the binding of the amino groups of proteins (Pardoe et al., 2001), with good magnetic and structural properties of iron oxide formed in the presence of dextran (40,000 g/mol). Results of analysis suggest that the presence of the polymer limits the particle size compared to particles prepared without the polymer. An important factor in the choice of dextran appears to be the favorable size of dextran chains, which enables optimum polar interactions (mainly chelation and hydrogen bonding) with iron oxide surfaces. Although single hydrogen bonds are relatively weak, the total bonding energy of hydrogen bonds over the length of a polysaccharide molecule can be very high because of the large number of hydroxyl groups per molecule (Pardoe et al., 2001).

Carmen Bautista et al, (2005) described dextran surface modification of pure superparamagnetic iron oxide nanoparticles prepared by laser pyrolysis and the coprecipitation method. Physical characterization techniques were used to delineate the nature and the mechanism of dextran particulate adsorption. The favored mechanism of adsorption of dextran on the surface of maghemite nanoparticles prepared by laser pyrolysis seems to be the collective hydrogen bonding between dextran hydroxyl groups and the iron oxide particle surface (Laurent et al., 2011) (Berry et al., 2003).

2.6.2 Polyethylene Glycol (PEG)

PEG is a hydrophilic, water-soluble, biocompatible polymer. Several investigators have reported the use of PEG to increase the biocompatibility of iron oxide dispersions and duration in blood (Gupta and Curtis, 2004) (Kim et al., 2003) (Zhang et al., 2002). Many of the good ligands (like surfactants, dendrimers, phosphine moieties etc.) which stabilize iron oxide nanoparticles will not meet the biocompatibility criteria for in vivo applications. A biofriendly approach is the PEGylation of nanoparticles to impart biocompatibility, where a PEG-SH ligand of appropriate molecular weight acts as the stabilizing shell of the core iron oxide nanoparticles. Researchers have reported that the PEGylation of nanoparticles could provide better stability in the biological fluids and in cell culture media and also prevent macrophage binding and protein adsorption (Fang et al., 2006). Feruglose (Clariscan) can be regarded as true "stealth nanoparticles", because the PEGylation of the coating starch, makes the particles unrecognizable by the macrophage-monocytic system (Gupta and Wells, 2004b).

2.7 *Physico-chemical characterization of SPIONS*

Different methods can be used to determine sizes of the nanoparticles. However, "size" is an ambiguous concept. First, it could define different parts of the nanoparticle: the crystalline part of the core, the whole iron core (crystalline and amorphous), the core, the shell, and the hydrated layer, or even a size with no geometrical meaning on the particle but just a physical meaning. Second, in almost all cases, nanoparticles are polydisperse. This heterogeneity of sizes gives rise to different values (even if characterizing the same size) depending upon whether the

technique gives access to a number, volume, or even intensity (volume to the power of two) weighted mean size. In the case of volume and, even more, of intensity weighted, the mean size is boosted toward high values even in the case of very small quantities of the biggest nanoparticles (Kang et al., 1996).

2.7.1 Transmission electron microscopy (TEM)

Transmission electron microscopy is a technique that is used to characterize the morphology and size of nanomaterials. The size of the particle core can be determined by TEM images (Kim et al., 2003). Furthermore, it provides details on the size distribution and the shape. However, this technique needs an analysis by image treatment, and it has to be performed on a statistically significant number of particles. Moreover, the sample preparation can induce aggregation of the colloids, and the TEM measurements may consequently not reflect the size and the distribution in solution (Alcalá and Real, 2006).

2.7.2 X-Ray Diffraction (XRD)

X-ray diffraction is a method used to characterize the crystal structure and analyse the parrticular phase of the material. XRD is basically used to identify unknown substances, by comparing diffraction data with a database maintained by the International Centre for Diffraction Data (ICDD). These techniques are based on collecting the scattered intensity of an X-ray beam hitting a sample as a function of incident and scattered angle, polarization and wavelength or energy. The peak intensity in XRD result can be used to quantify the proportion of iron oxide formed in a mixture by comparing experimental peak and a reference peak intensity. The crystal size also can be calculated from line broadening from the XRD pattern using

the Scherrer's equation. XRD can be performed to obtain the crystalline structure of the particles. In a diffraction pattern, the intensity can be used to quantify the proportion of iron oxide formed in a mixture by comparing experimental peak and reference peak intensities (Calvin et al., 2003).

2.7.3 Dynamic Light Scattering Study (DLS)

Dynamic light scattering is a common method to characterize dilute and transparent dispersions of magnetic nanoparticles. DLS is also known as photon correlation spectroscopy. This technique is based on the analysis of fluctuations of the scattered intensity pattern caused by the Brownian motion of particles and is used to determine the suspended particle size from nanometer up to a few microns. Hydrodynamic radius of objects can then be evaluated through the Stokes-Einstein law. Surface coatings contribute significantly to the hydrodynamic diameter (HD) and the net surface charge both critical design parameters that determine the in vivo fate of nanoparticles (Murdock et al., 2008).

2.7.4 Fourier Transform Infrared Spectroscopy (FT-IR)

Fourier Transform infrared spectroscopy is a technique which is used to determine the chemical functional groups in the sample. In infrared spectroscopy, IR radiation is passed through a sample. Some of the infrared radiation is absorbed by the sample and some of it is passed through (transmitted). The resulting spectrum represents the molecular absorption and transmission, creating a molecular fingerprint of the sample. Like a fingerprint no two unique molecular structures produce the same infrared spectrum. This makes infrared spectroscopy useful for several types of analyses. The possibility of deducing the magnetite in the solid

phase of ferro fluids from FT-IR spectra using the characteristic vibrational bands at 572 cm^{-1} and 628 cm^{-1} has been suggested (Beeran et al., 2015).

2.8 *Effect of size, surface charge and surface coating on toxicity of SPIONS*

Size and surface of nanoparticles are important with respect to pharmacokinetics in vivo, where the major limitations are quick blood clearance and non-specific uptake by macrophages. To maximize circulation times and targeting ability, it is suggested that the optimal size should be less than 100 nm in diameter and the surface should be hydrophilic. It is also reported that amphiphilic coatings are preferred to prolong plasma half-life by extending the circulation time of the particulates from minutes to hours, thereby increasing the targeting capabilities of the contrast agent (Mornet et al., 2004). The physicochemical properties of SPIONS are of importance in terms of the corresponding biological responses (e.g., clearance, biodistribution, cell response/uptake, and cytotoxicity). The bare particles are cleared from the blood due to their opsonization and corresponding clearance by the reticuloendothelial system (RES). This clearance would be overcome by modifying the particles' surface using organic and inorganic materials (Gupta et al., 2007).

Nanoparticle size is recognized as being crucially important for biodistribution. Nanoparticles with a hydrodynamic diameter below 10 nm would be typically removed through renal filtration (Almeida et al., 2011). SPIONS with larger hydrodynamic diameter than the average spacing between inter-endothelial slits in the spleen (200-500 nm) will be retained and subsequently cleared by macrophages in the red pulp. Nanoparticles in a size range of 40-200 nm are taken up by the liver

and spleen (Mornet et al., 2004). Ferumoxtran-10 with hydrodynamic diameter of 30 nm has been reported to have a longer blood half-life when compared to few minutes for the substantially larger ferumoxides with hydrodynamic diameter 150 nm (Bourrinet et al., 2006). As the size of a particle decreases, its surface area to volume ratio increases, allowing a greater proportion of its atoms or molecules to be displayed on the surface resulting in increased surface reactivity (Nel et al., 2009) (Oberdörster et al., 2005). It is reported that particles with greater specific surface area per mass were more biologically active and that their biological effects mainly depended on their surface area rather than particle mass. As particle size shrinks, there is a tendency for toxicity to increase, even if the same material is relatively inert in a bulk form (Tarnuzzer et al., 2005). Kyung et al, (2009) demonstrated that smaller SiO_2 nanoparticles, with a higher specific surface area, produced more toxic effects compared to larger- sized nanoparticles.

Nanoparticle surface chemistry and surface charge has been reported to play important roles in toxicity and corresponding safety assessments. Altering the surface chemistry of nanoparticles has been shown to effectively prevent toxicity derived from the core material (Gupta and Gupta, 2005) (Chen et al., 2011) (Wilhelm et al., 2003) (Dumortier et al., 2006). Reducing opsonin binding is critical to designing long-circulation SPIONS, and while numerous factors contribute to protein adsorption on nanoparticle surfaces, surface charge is one of the most significant determinants. Nanoparticles with a neutral surface charge have been reported to have lower opsonization rates than charged particles, thus being retained longer in circulation (Lynch and Dawson, 2008). Metz et al, (2004a) showed that carboxy-dextran (negatively charged) coated SHU 555C with hydrodynamic

diameter ~ 21 nm, showed greater uptake in monocytes than the comparable sized nonionic-dextran coated ferumoxtran-10 with hydrodynamic diameter ~ 20-50 nm. The study also suggested that surface charge induced a greater phagocytic effect than size. The results clearly showed that carboxy-dextran coated Ferucarbotran had shown three times more uptake in monocytes than the significantly larger nonionic-dextran coated Endorem. Positively charged polymers such as poly (ethyleneimine) (PEI) enhance cell penetration due to electrostatic attraction to the negative charge of phospholipids lining the cell membranes (Albanese et al., 2012).

The physicochemical property of surface coatings influences the final hydrodynamic size, surface charge and hydrophobicity of SPION formulations. Hydrophobic surfaces, due to their insolubility in aqueous environments, often undergo rapid non-specific protein adsorption and are unsuitable for designing long-circulating SPIONS (Laurent et al., 2011). Conversely, hydrophilic polymer coatings, such as the polysaccharides (e.g. dextran) and the polyethers (e.g. PEG), which allow sufficient hydration are widely used in stabilizing SPIONS. PEG coatings are particularly attractive due to their exceptional resistance to protein adsorption characteristics (Gupta and Gupta, 2005). It is reported that hydrophilic polymers are often used to encapsulate and stabilize nanoparticle cores that are either intrinsically hydrophobic or coated with hydrophobic surfactants such as oleic acid, and large exposed regions, due to insufficient polymer coverage, can lead to protein adsorption and subsequent removal by the mononuclear phagocytic system (Hume et al., 2002).The density or surface coverage of coatings is a critical parameter in designing long-circulating SPIONS. In the mushroom state, PEG chains are more flexible, and on average lay closer to the surface. Critically, the low coverage

exposes significant portions of the underlying core to opsonins. At the other extreme, high surface coverage extends PEG chains further into the solvent, but also reduces chain flexibility and mobility – critical features responsible for steric stabilization and non-fouling characteristics (Jokerst et al., 2011). Thus, optimal PEG conformation facilitates both, sufficient cloaking of the underlying core from opsonins, and chain mobility to enhance nanoparticle solubility – a balance between the 'mushroom' and 'brush' configurations (Greish, 2010). For example, polysaccharide coatings have been used to promote biocompatibility as well as better dispersion in solution (Schrand et al., 2008) (Lemarchand et al., 2005). With regard to surface charge, positively charged Au nanoparticles caused greater toxicity than those with negative surface charges (Goodman et al., 2004).

2.9 *In-vitro cell culture evaluation*

In vitro assessments are the study of cells, either isolated from animals or an immortalized cell line, in a culture dish. In general, the use of primary cells (isolated directly from animals) will give a more realistic toxicity result because immortal cell lines transform over time. However, the use of immortal cell lines is often preferred simply because they do not require animal sacrifice (Mahmoudi et al., 2012). Generally, both in vivo and in vitro studies have limitations (Sharifi et al., 2012) (Brunner et al., 2006). Despite extensive research on the biological effects of nanotherapeutic materials, there is relatively little information about the toxicity of these materials or the tools needed to assess this toxicity. Maurer-Jones et al, (2009) have extensively reviewed various toxicological assessment techniques currently in use as well as considerations in nanoparticle dosing. For most IONPs, levels below

20 μg Fe/ml are generally not advisable; because the overall internalization of the IONPs would be too low for most applications. Conversely, higher concentrations of more than 200 μg Fe/ml are generally not necessary for efficient internalization and, therefore, most studies employ concentrations of 50, 100 or 200 μg Fe/ml. Multiple time points would allow full assessment of both the short- and long-term effects, as toxicity effects can often be quite variable in time (Soenen et al., 2007). When investigating IONP toxicity, incubation times of 2, 4, 8 and 24 h would allow the assessment of any acute cytotoxic effect, by means of an MTT or an LDH assay. If desirable, the IONPs can also be incubated for longer time points, although 24 - 48 h is generally more than sufficient to reach adequate intracellular levels of IONPs (Soenen et al., 2007) (Wilhelm and Gazeau, 2008). Understanding the cell – material interactions, arising from these tests, form the basis for a model-based evaluation of nanoparticles behavior in 3D tissues (Mahmoudi et al., 2012).

One important aspect that has not received adequate attention till date is the important link between toxic effects and the intracellular concentration of the NPs. Several studies have shown that high intracellular amounts of NPs can lead to drastic effects on cellular proliferation (Soenen et al., 2010b) (Hu et al., 2006). However, till date, most studies link any cytotoxicity data to the concentration of particles present in the incubation medium (Huang et al., 2008) (Mahmoudi et al., 2009b) (Choi et al., 2010). Any such findings therefore cannot be well interpreted, as the reduced toxicity of a novel type of iron oxide formulation might simply be due to reduced internalization efficiency. It is therefore of crucial importance to simultaneously study uptake efficiency and cytotoxicity of SPIONS at the same time and to correlate any data obtained.

2.9.1 Cytotoxicity

Cell metabolic activity of Polyethyleneglycol, Polyethyleneglycol co fumerate, Polyvinyl alcohol, dextran, poly (ethyleneimine) and chitosan coated iron oxide nanoparticles have been evaluated by MTT assay and no toxicity has been observed even in the high applied dosage (about 1 mg/ml). A trace of toxicity was detected for bare iron oxide at the same concentrations (Gupta and Wells, 2004a) (Kim et al., 2006) (Dumortier et al., 2006) (Mahmoudi et al., 2009a) (Mahmoudi et al., 2009b). Studies using C10 lung epithelial cells show that the dose rate effects of stable agglomerates of iron oxide nanoparticles in conventional culture medium can be substantial and vary by over an order of magnitude difference in cellular dose in some cases (Sharma et al., 2013). Results are contradictory and a detailed and in depth evaluation is warranted to determine the effects on cells.

2.9.2 Study of intracellular uptake

A nanoparticle can be internalized simply because of its physical proximity to the membrane or because of interactions with specific receptors, originating via a number of different internalization paths. Interpretation of toxicity results depends upon an understanding of how nanoparticles and the living systems interact. Fluorescence microscopy has been employed to study nanoparticle uptake. Cellular uptake of nanoparticles was observed and subsequently quantified using fluorescently labeled nanoparticles (Panyam et al., 2003). Chnari et al, (2006) and co-workers employed confocal fluorescence microscopy to evaluate the location of fluorescently-labeled micelles within individual cells.

Transmission electron microscopy (TEM) has lot of advantage and allows determination of internalized nanoparticle localization, concurrent characterization of nanoparticle and cell/tissue morphology, and complementary elemental analysis using spectroscopic methods. But the technique has some limitations like, time-intensive preparation that may induce artifacts while providing only a static picture of a small sample population.

Inductively Coupled Plasma-Mass Spectroscopy (ICP-MS) has been used to probe the Au content of HeLa and A594 cells, cancer cell lines (Dykman and Khlebtsov, 2014). It allows easy sample preparation and quick results. But, it gives limited information about the cellular location of the nanoparticles. It cannot distinguish between internalized or externally adherent nanoparticles. It is applicable to only a subset of nanomaterial elements, and does not discriminate between nanoparticles and preexisting ions of the same element (Giljohann et al., 2007).

Raman microscopy has been used to spectroscopically image biological cells previously exposed to fluorescently labelled nanoparticles and in combination with K-means clustering. The nanoparticles could be localised and subcellular environment was identified based on the molecular spectroscopic signatures (Dorney et al., 2012). Raman imaging of plant cell walls represented a nondestructive technique that has provided insights into chemical composition in context with structure at the micrometer level (<0.5 μm) (Gierlinger et al., 2012). High spatial resolution Raman maps have been obtained of fixed cells in an aqueous environment (Diem et al., 2012). These maps were obtained by collecting individual Raman spectra via a Raman microspectrometer in a raster pattern on a 0.5-microm grid and

assembling pseudocolor maps from the spectral hypercubes by multivariate methods. This was the first report of label-free detection of mitochondria inside a somatic mammalian cell using Raman microspectroscopy (Matthäus et al., 2007). Confocal Raman Microscopy, a non-invasive, non-destructive and label-free technique, has been employed to study the uptake and localization of nanoparticles in the Hepatocarcinoma human cell line (HepG2) at the level of single cells (Estrela-Lopis et al., 2011a).

Fluorescence spectroscopy offers highly sensitive measurements with time resolution, but requires confocal fluorescence techniques to determine nanoparticle localization. For nanoparticles that are not natively fluorescent, a tag or label is crucial that may alter nanoparticle characteristics and toxicity. As stated previously, understanding nanomaterial interaction (both amount and localization/association of nanoparticles) is essential for determining mechanisms of interaction and the limitations of these common techniques necessitates the further development of new methods to assess nanoparticle uptake.

Though confocal Raman microscopy has been explored in many label free methods for detection and imaging, a confocal imaging of the cell and uptake of iron oxide nanoparticles has not been studied so far. Confocal Raman microspectroscopy has been used in this study to evaluate cellular uptake of the nanoparticles.

2.10 *Haemocompatibility*

Infusion of nanoparticles into the vascular system, being an important aspect in use of these materials, in vivo assays to assess their biosafety assume importance. Incompatibility with bio fluids such as blood, could lead to haemolysis, coagulation,

and blood clots due to adsorption and/or activation of biomolecules, for example, plasma protein and complement factors. As such it is critical to assess these properties before clinical use. One such test is the haemolysis assay which uses erythrocytes to assess the MNP toxicity.

Ostomel et al, (2007) have investigated the hemostatic response due to surface charges of a variety of metal oxide particles which did not include SPIONS. Li et al, (2008) have investigated the influence of nano- TiO_2 on erythrocyte. Singh et al, (2010) have investigated the disturbance in iron homeostasis caused by SPIONS. The hematologic effects of the above-described SPIONS and their separated components on the coagulation process have been studied by measuring both Prothrombin time (PT) and activated Partial Thromboplastin time (*a*PTT). In addition, by measuring erythrocyte, leucocytes, haemoglobin, hematocrit and platelets blood count, their hemolytic effects have also been tested (Ali et al., 2013).

The *in vitro* biocompatibility studies should also include evidence of hemolysis and quantification of leukocytes, erythrocytes and platelets to rule out immediate cytotoxicity of nanoparticles or contact spontaneous platelet aggregation (Mayer et al., 2009) (Gulati et al., 2010). Therefore, it is essential to investigate the effects of both, nanoparticles and coatings on blood.

2.11 *Comet assay /genotoxicity*

Understanding the genotoxic potential of iron oxide nanoparticles is important as these particles are commonly targeted to cells. Different nanoparticles and nanotubes have been compared with respect to their cytotoxicity and ability to cause DNA damage and oxidative stress (Singh et al., 2009). Focus was on different metal

oxide particles (CuO, TiO_2, ZnO, $CuZnFe_2O_4$, Fe_3O_4, Fe_2O_3), and the toxicity was compared to that of carbon nanoparticles and multiwalled carbon nanotubes (MWCNT). The human lung epithelial cell line A549 was exposed to the particles, and cytotoxicity was analyzed using trypan blue staining. DNA damage and oxidative lesions were determined using the comet assay, and intracellular production of reactive oxygen species (ROS) was measured using the oxidation-sensitive fluoroprobe 2′,7′-dichlorofluorescin diacetate (DCFH-DA) (Karlsson et al., 2008). The results showed a high variation among different nanoparticles concerning their ability to cause toxic effects.

In another study, the surface of the magnetic nanoparticles (MNPs) was coated with two thiol-containing hydrophilic ligands: mercaptosuccinic acid (MSA) or dimercaptosuccinic acid (DMSA), leading to thiolated MNPs. Free thiols groups on the surface of MSA- or DMSA-MNPs were nitrosated leading to NO-releasing MNPs. The genotoxicity of thiolated-coated MNPs on human lymphocyte cells was studied by the comet assay (Lima et al., 2013). No genotoxicity was observed due to exposure of human lymphocytes to MSA- or DMSA-MNPs.

Ahamed et al, (2013) have recently reported that IONPs induced cytotoxicity in mammalian cells. The authours investigated the cytotoxicity, oxidative stress and genotoxicity of IONPs on two human cell lines; skin epithelial A431 and lung epithelial A549 cells. Prepared IONPs were polygonal in shape with a smooth surface and had an average diameter of 25 nm. IONPs (25-100 μg/ml) induced dose-dependent cytotoxicity in both types of cells, which was demonstrated by cell viability (3- (4,5-dimethylthiazol-2-yl)-2,5-diphenyltetrazoliumbromide) and lactate

dehydrogenase leakage assays. IONPs were also found to induce oxidative stress in a dose-dependent manner, evident by depletion of glutathione and induction of reactive oxygen species (ROS) and lipid peroxidation. Comet assay revealed that level of DNA damage was higher with concentration of IONPs in both types of cells. Quantitative real-time PCR analysis showed that following exposure of cells to IONPs, the expression levels of mRNA of caspase-3 and caspase-9 genes were higher. They also observed the higher activity of caspase-3 and caspase-9 enzymes in IONPs treated cells. Moreover, western blot analysis showed that protein expression level of cleaved caspase-3 was up-regulated by IONPs in both types of cells. Taken together, their data demonstrated that IONPs had potential to induce genotoxicity in A431 and A549 cells, which was likely to be mediated through ROS generation and oxidative stress. The authors suggested that genotoxic effects of IONPs should be further investigated at in vivo level (Ahamed et al., 2013).

2.12 *In-vivo studies*

In vivo studies are whole organism studies where nano therapeutics is delivered via one of four pathways: inhalation, dermal, ingestion, or injection. Using a variety of techniques, typical in vivo assessments include the determination of physiological localization and the concentration of material in specific tissues, rate of excretion, and macroscopic tissue and organismal toxicity.

The most widely investigated exposure pathway for nanotherapeutics has been injection. Nanoparticle injectables have been explored because they could potentially eliminate the negative side effects of traditional injectable drugs, particularly chemotherapy, where solubility and stability of drug molecules limit their use. In

fact, most of the approved nanoproducts are aimed at diagnosis or therapy as are many injectable nanomaterials in development (Weissleder et al., 1989).

The various interactions of NPs with fluids, cells and tissues need to be considered from the route of entry through the wide range of possible pathways ending at potential target organs. Nanoparticles may be able to enter the body via routes such as the gastrointestinal tract, injection into the blood stream, and passage through the skin (Oberdörster et al., 2005).

Following systemic administration, NPs may be able to penetrate into very small capillaries throughout the body and efficiently distribute to certain tissues. NPs passing through epithelia and biological membranes can potentially affect the physiology of any cell in the body (Kim et al., 2006).

It is reported that in nanotherapeutics to treat cancer much of the in vivo toxicity assessments focus on the nanoparticle uptake into tumors followed by various characterizations of the progression of cancer along with the systemic biodistribution of administered nanoparticles to assess clearance and potential sites of unintentional toxicity (Al-Jamal et al., 2008) (Devalapally et al., 2008) (Gannon et al., 2007).

The vasculature network is the most commonly employed route for administering nanoparticle formulations, and presents several physiological barriers. Continuous vessels with pore sizes of ~6-15 nm in the kidneys (Sarin, 2010) prevent extravasation of larger SPIONS, which are ultimately cleared in highly fenestrated filtration organs like the liver and spleen. In a healthy biological system, the liver, spleen and kidneys are primarily responsible for nanoparticle clearance. Liver and

spleen have a significant portion of immune cells comprised of the mononuclear phagocytic system. Macrophages remove large foreign particles through endo-phagocytic pathways, for example, SPIONS that are hydrophobic, aggregating, cationic or tagged with specific proteins called opsonins are quickly recognized and taken up by mononuclear phagocytic system cells. The resident macrophages called Kupffer cells in the liver, line the interior of fenestrated sinusoidal capillary walls. Macrophages in the spleen are located in the red pulp, the primary site of splenic filtration, and also the marginal zone between the red and white pulps (Hume et al., 2002). The red pulp is part of the "open" circulation route in the spleen, which lacks direct connections between the arterial and venous capillaries. Blood from the arterial capillary openings flows into the red pulp and re-enters blood circulation by seeping through the 200-500 nm inter-endothelial slits in the venous bed. The deformability of healthy erythrocytes allows passage through the inter-endothelial slits, while dead or rigid erythrocytes accumulate in the red pulp and are eventually cleared by the resident macrophages.

The pharmacokinetics (distribution, metabolism, bioavailability, excretion) and toxicity (acute and subacute toxicity, mutagenicity) of a superparamagnetic iron oxide preparation (AMI-25), presently used in clinical trials, has been evaluated by 59Fe radiotracer studies, measurements of relaxation times, the ability to reverse iron deficiency anemia, histologic examination, and laboratory parameters (Arbab et al., 2005). One hour after administration of AMI-25 to rats (18 μM Fe/kg; 1 mg Fe/kg), 82.6 +/- 0.3% of the administered dose was sequestered in the liver and 6.2 +/- 7.6% in the spleen. Peak concentrations of 59Fe were found in liver after 2 h and in the spleen after 4 h. 59Fe slowly cleared from liver (half-life, 3 days) and spleen (half-

life, 4 days) and was incorporated into hemoglobin of erythrocytes in a time-dependent fashion (Weissleder et al., 1989). Ferumoxides, dextran-coated superparamagnetic iron oxide nanoparticles, form ferumoxide-transfection agent (FE-TA) complexes that are internalized into endosomes/lysosomes and have been used to label cells for in vivo MRI tracking and localization studies (Arbab et al., 2005).

Kermanizadeh et al, (2013) believed that nanoparticles accumulate, often preferentially, in the liver, investigated the effect of silver nanoparticles (20 nm) on the liver and in particular, the role of Kupffer cells in the overall inflammatory response in the organ. The study revealed that the liver function was unaffected by the silver nanoparticles.

In a study, mice were injected intravenously with a single dose of TiO_2 NPs at varying dose levels (0, 140, 300, 645, or 1387 mg/kg). Animal mortality, blood biochemistry, hematology, genotoxicity and histopathology were investigated 14 days after treatment (Xu et al., 2013).

The biological fate of SPION microbubbles was determined in Sprague-Dawley rats after intravenous administration. The rats were sacrificed and perfusion-fixated at different time points. The magnetic resonance imaging results obtained were compared with histopathologic findings in different organs (Barrefelt et al., 2013). Results showed macrophages with increasing signs of cytoplasmic iron accumulation, initially in the lungs followed by other major organs.

The acute toxicity of nickel (Ni) nanoparticles (50 nm) has been evaluated by injecting the particles intravenously into the dorsal penile vein of Sprague Dawley

rats. Fourteen days after injection, it was found that nanoparticles induced liver and spleen injury, lung inflammation, and caused cardiac toxicity (Magaye et al., 2014).

2.13 *Oxidative stress*

Reactive oxygen species (ROS) are molecules and ions containing unpaired valence shell electrons and constitute a type of free radical, specifically involving oxygen. The unpaired valence shell electrons make ROS highly reactive, and although ROS play an important role in cell signaling, excess ROS (called oxidative stress) can result in significant cellular damage which can ultimately lead to cellular demise by both necrotic and apoptotic processes. Types of ROS formed as a result of the sequential reduction of molecular oxygen include superoxide radical ($\cdot O_2^-$) superoxide anion (O_2^-), hydrogen peroxide (H_2O_2) and the hydroxyl radical (OH-). Major endogenous sources of ROS are mitochondria, which produce H_2O_2 from $\cdot O_2^-$ as a natural by-product of ATP production as oxygen is reduced along the electron transport chain (Bergamini et al., 2004). This can damage cells both directly and indirectly as H_2O_2 interacts with Fe^{2+} or other catalytic metals (a process known as the Fenton reaction) and is converted into the highly destructive OH- radical (Bačić et al., 2008).

Cellular processes, in the form of intracellular enzymes, have evolved to neutralize the potentially harmful effects of ROS produced in physiologically moderate amounts. These enzymes include superoxide dismutase, catalase, and the glutathione enzymes (e.g. glutathione-peroxidase, glutathione-reductase and S-glutathione transferase) (Apel and Hirt, 2004).

Hussain et al, (2005) evaluated the acute toxic effects of metal/metal oxide nanoparticles proposed for future use in industrial production methods using the in vitro rat liver derived cell line BRL 3A. Different sizes of nanoparticles such as silver (Ag; 15, 100 nm), molybdenum (MoO_3; 30, 150 nm), aluminum (Al; 30, 103 nm), iron oxide (Fe_3O_4; 30, 47 nm), and titanium dioxide (TiO_2; 40 nm) were evaluated for their potential toxicity. Cellular morphology, mitochondrial function (MTT assay), membrane leakage of lactate dehydrogenase (LDH assay), reduced glutathione (GSH) levels, reactive oxygen species (ROS), and mitochondrial membrane potential (MMP) were assessed under control and exposed conditions (24 h of exposure). Results showed that mitochondrial function decreased significantly in cells exposed to Ag nanoparticles at 5–50 μg/ml. However, Fe_3O_4, Al, MoO_3 and TiO_2 had no measurable effect at lower doses (10–50 μg/ml), while there was a significant effect at higher levels (100–250 μg/ml).

2.13.1 Superoxide dismutase (SOD)

Superoxide dismutase was reported to be involved in the dismutation of superoxide radical to hydrogen peroxide. Superoxide dismutase is found in both the mitochondrial matrix and cytoplasm and catalyzes the formation of H_2O_2, O_2 and water from the potent highly damaging superoxide radicals (O_2^-) produced in the electron transport chain (McCord and Fridovich, 1969) (Rapoport et al., 1994). Under conditions in which superoxide dismutase becomes overwhelmed (e.g. during oxidative stress), excessive amounts of H_2O_2 are produced resulting in the formation of OH- via the Fenton reaction (Benzie, 1996).

2.13.2 Reduced glutathione (GSH)

Glutathione is a cofactor of several detoxifying enzymes against oxidative stress, e.g. glutathione peroxidase (GPx) and glutathione-S-transferase. GSH scavenges hydroxyl radical and singlet oxygen directly, detoxifying hydrogen peroxide and lipid peroxides by the catalytic action of glutathione peroxidase. Glutathione is an important antioxidant tri-peptide synthesised from the amino acids L- cysteine, L-glutamic acid and glycine, and in its reduced state participates in conjugation reactions to remove various toxic metabolites and donates electrons to unstable ROS molecules (Devasagayam et al., 2004). During oxidative stress glutathione precursors become depleted and glutathione production is insufficient in neutralizing the ROS generated (Townsend et al., 2003).

2.13.3 Lipid peroxidation (LPO)

ROS attack cellular components like polyunsaturated fatty acid residues of phospholipids, which are extremely sensitive to oxidation. Once formed, peroxyl radicals (ROO•) can be rearranged *via* a cyclisation reaction to endoperoxides (precursors of malondialdehyde) with the final product of the peroxidation process being malondialdehyde (MDA). The process of lipid peroxidation and the atherogenicity of peroxidied lipids are reviewed Laboratory methods of assessing antioxidant defences, lipid peroxidation and the effects of lipid peroxidation are also reviewed and discussed with particular reference to their ability to assess in vivo oxidative stress and lipid peroxidation status (Benzie, 1996).

2.13.4 Tissue nitrite level

Nitric oxide (NO) is a potent mediator with diverse roles in regulating cellular functions, including nitrosylation of proteins involved in signaling pathways. NO is

produced by the oxidation of the amino acid L-arginine by the enzyme nitric oxide synthase (NOS). This family of enzymes are generally classified as constitutive, calcium dependent (neuronal NOS, nNOS, NOS1 and endothelial NOS, eNOS, NOS3) or inducible, calcium independent (inducible NOS, iNOS, NOS2). The constitutive isoforms release relatively low levels of NO, while iNOS is induced by inflammatory conditions and releases larger amounts of NO (Alderton et al., 2001) (Stamler et al., 2001). Furthermore, Ag, Cu, and Al NPs may induce oxidative stress and generate free radicals that could disrupt the endothelial cell membrane (Sharma and Sharma, 2007).

2.14 *Mast cells*

Mast cell is a less studied cell with respect to the nanomaterials. Mast cells are involved in both the adaptive and innate immune system and play an important role in our body's effective response towards foreign bodies. They develop from progenitor cells that in turn arise from uncommitted hematopoietic stem cells in the bone marrow and are found in highest numbers in areas of the body that interface with the environment, such as the skin, lung and gastrointestinal tract (Abraham and John, 2010). They occur in virtually all vascularized tissues where they ordinarily reside in close proximity to blood vessels, nerves, smooth muscle cells, epithelial cells, mucus-producing glands and hair follicles. Mast cells tend to be located perivascularily and in sentinel locations to respond to noxious stimuli as well as to allergens (Galli et al., 2008). Presently, mast cells have assumed importance in multiple biological processes including phagocytosis, processing of antigen,

production of cytokines and other vasoactive substances like histamines and protein slicing enzymes such as chymase and tryptase (Abraham and John, 2010).

2.14.1 Mast cell activation and effects

Mast cells are typically activated by cross-linking of their FcεR1 by IgE/antigen complexes. Cross-linkage of IgE by the interaction of allergen with specific determinants on the Fab portion of the molecule brings the receptors into juxtaposition and initiates mast cell activation and mediator generation and release. Although the process can be triggered by a variety of immunological and non immunological stimuli, the most important signaling pathway in vivo is by aggregation of surface bound immunoglobulin E (IgE) by specific antigen. Activation of mast cells then result in three types of biological effects, 1) Mast cells undergo regulated secretion in which preformed contents stored in their granules are rapidly released by exocytosis 2) They enzymatically synthesize lipid mediators derived from precursors stored in cell membranes and in lipid bodies and 3) Mast cells initiate transcription, translation and secretion of a diverse array of cytokines (Abraham and John, 2010). Mast cells may also be activated by non immunological stimuli induced by substances such as neuropeptides, basic compounds, complement components, and certain drugs such as opiates. Morphologically degranulation produced by immunologic and non immunologic stimulation appears similar. However, biochemical processes that lead to mediator release may differ. Human mast cells express a multitude of G protein coupled receptors and other recognition sites on their surface which are involved in mast cell activation under physiological and patho physiological conditions (Sismanopoulos et al., 2012).

Mast cells may be able to orchestrate different biological processes through their ability to release pro-inflammatory mediators selectively without the degranulation typical of allergic reactions. Even though the importance of mast cells as mediators in allergic inflammatory responses and various other diseases have been well studied, their role in the biological responses to nanomaterials have yet to be investigated. The information about the possible relation between the nanoparticles in biological system and mast cells may help in developing strategies to prevent or alleviate complications which are often associated with nanoparticle administration.

2.14.2 Role of oxidants in mast cell activation

Reactive oxygen species (ROS), such as superoxide, hydrogen peroxide (H_2O_2), and hydroxyl radical, have for a long time been considered as accidental by-products of respiratory energy production in mitochondria and as being useless and rather deleterious to biological systems. Contrary to such a classical view, accumulating evidence (Zhao et al., 2014) indicates that upon stimulation of divergent receptor systems, ROS are intentionally produced and even required for appropriate signal transduction and biological responses. Work by our group (unpublished) and that of others have shown that stimulation of mast cells through the high-affinity IgE receptor (FcεR1) induces the production of ROS such as superoxide and H_2O_2 possibly by the phagocyte NADPH oxidase homologue and that these endogenously produced oxidants have important functions in regulation of various mast cell responses, including degranulation, leukotriene secretion, and cytokine production. Subsequent studies (Frossi et al., 2003) have enumerated particular biochemical pathways that can be targeted by ROS and/or cellular redox balance. More recent research reveals that ROS may also play an important role in

mast cell activation by divergent allergy-relevant environmental substances, like heavy metals and polycyclic aromatic hydrocarbons (Suzuki et al., 2005).

2.15 *Iron homeostasis*

It is reported that dextran-coated SPIONS have the potential to cause perturbation in the regulation of iron homeostasis. Indeed preliminary studies (Mackenzie et al., 2008) have found that although ferritin (iron storage protein complex) and ferroportin (iron export molecule) were not altered following exposure to dextran-coated SPION, transferrin-receptor 1 (TfR1) and hepcidin were significantly down-regulated in HepG2 hepatocellular carcinoma cells. The TfR1 is a cell-surface receptor that controls iron uptake and its down-regulation following exposure to dextran-coated SPION therefore suggested that the cells were reacting as though they were in a state of iron overload.

In another study, the acute toxicity of polyethylene glycol tethered gold nanoparticles has been verified in vivo by measurement of inflammation and apoptosis related gene expression levels in liver tissues (Cho et al., 2009).

Biodistribution of gold nanoparticles (AuNPs) in more than 25 organs were examined on 1 day, 1 week, 1 month and 2 months after a single intravenous (i.v.) injection in rats (Balasubramanian et al., 2010). Microarray results of liver and spleen point to significant effects on genes related to detoxification, lipid metabolism, cell cycle, defense response, and circadian rhythm. These results demonstrate that significant biodistribution of Au occurs in the body over 2 months after a single i.v. injection of AuNPs, accompanied by gene expression changes in target organs (Balasubramanian et al., 2010).

It is reported that long-term exposure to TiO_2 NPs resulted in obvious titanium accumulation in the liver and TiO_2 NP aggregation in hepatocyte nuclei, an inflammatory response, hepatocyte apoptosis and liver dysfunction (Cui et al., 2012). The microarray data has shown striking changes in the expression of 785 genes related to the immune/inflammatory response, apoptosis, oxidative stress, the metabolic process, response to stress, cell cycle, ion transport, signal transduction, cell proliferation, cytoskeleton, and cell differentiation in TiO_2 NP–exposed livers (Cui et al., 2012).

Gene expression following administration of nanoparticles in vivo has been investigated in various studies. In on such study (Ma et al., 2012) Kumming mice were exposed to Fe_3O_4-nanoparticles via intraperitoneal injection daily for 1 week at doses of 0, 5, 10, 20, and 40 mg/kg. Hepatic and renal tissues were sliced for physiological observation. Injuries were found in the high-dose groups (20 and 40 mg/kg) compared with the control group. Biomarkers of reactive oxygen species, glutathione, malondialdehyde, DNA-protein crosslinks, and 8-hydroxy-2′-deoxyguanosine in the hepatic and renal tissues were detected. Injury to tissues and oxidative damage to cells at the molecular level was observed (Ma et al., 2012).

Important biomarkers for evaluation of iron homeostasis have been assessed by gene expression of Transferrin, Ceruloplasmin, Haemoxygenase-1 and Heat shock protein-70 for evidence of oxidative stress.

2.15.1 Transferrin

Transferrins are iron-binding blood plasma glycoproteins that control the level of free iron in biological fluids. Transferrin has a molecular weight of around 80

KDa and contains two specific high-affinity Fe^{3+} binding sites. The affinity of transferrin for Fe^{3+} is extremely high (10^{23} M^{-1} at pH-7.4) but decreases progressively with decreasing pH below neutrality (Mackenzie et al., 2008). Liver is the main site of transferrin synthesis. Transferrin plays a key role where erythropoiesis and active cell division occur. The receptor helps maintain iron homeostasis in the cells by controlling iron concentrations (Macedo and de Sousa, 2008).

Earlier studies have shown that expression of transferrin and its receptor genes was considerably increased during supplementation of animals by selenium nanopaerticles for 10 or 20 days (Kojouri et al., 2012).

2.15.2 Ceruloplasmin

Ceruloplasmin is a ferroxidase enzyme, synthesised in the liver containing 6 atoms of copper in its structure. Ceruloplasmin is the major copper carrying protein in the blood, and in addition plays a role in iron metabolism. Ceruloplasmin exhibits a copper-dependent oxidase activity, which is associated with possible oxidation of Fe^{2+} (ferrous iron) into Fe^{3+} (ferric iron), therefore assisting in its transport in the plasma in association with transferrin, which can carry iron only in the ferric state (Harris et al., 1999) (Hellman and Gitlin, 2002).

2.15.3 Haemoxygenase-1

Haemoxygenase (HO) is an enzyme that catalyzes the degradation of heme. This produces biliverdin, iron, and carbon monoxide. Biliverdin is subsequently converted to a potent physiological anti-oxidant called bilirubin, by biliverdin reductase (Maines, 1997). Three isoforms of heme oxygenase are known namely

HO-1, HO-2 and HO-3. Among them, HO-1, unlike the other two (HO-2 and -3), shows limited expression under normal situations and is induced by oxidative stress, hypoxia, heavy metals, cytokines, etc. Haemeoxygenase expression is induced by oxidative stress, and in animal models increasing this expression seems to be protective. Carbon monoxide released from hemeoxygenase reactions can influence vascular tone independently or influence the function of nitric oxide synthase (Ryter et al., 2006).

2.15.4 Heat shock protein-70

The 70 kilodalton heat shock proteins (HSP-70) are a family of conserved ubiquitously expressed heat shock proteins. HSP70s are involved in signal transduction, cell cycle regulation, cell differentiation and programmed cell death. The HSP70 protein family and their co-chaperones constitute a complex network of folding machines which help to protect the cells from stress. Members of the HSP70 family are strongly upregulated by heat stress and toxic chemicals, particularly heavy metals. HSP70 proteins can act to protect cells from thermal or oxidative stress (Morano, 2007) (Kregel, 2002).

It is reported that after intratracheal instillation of AgNPs, gene expression was modulated by AgNPs in a tissue and time-dependent manner. At 7 days, selective changes in the expression of genes encoding oxidative stress-related enzymes, namely Gpx1, SOD, FMO2 and GAPDH were observed in hepatic and testicular tissues. Other genes implicated in oxidative stress (Txnrd1, Gss, Gsr), metal toxicity (Mt1), apoptosis/cell cycle (casp3, p53) and protein-folding processes (Hsp70) were not modified (Coccini, 2014).

2.16 *Elemental ion analysis by ICP-OES*

Inductively coupled plasma mass spectrometry (ICP-MS) is a robust and widely used technique for multi elemental and isotopic analysis of environmental materials (Sucharová and Suchara, 2006) (Enamorado-Bais et al., 2013).

Based on survey of literature regarding surface modified superparamagnetic iron oxide nanoparticles, It is hypothesized that accumulation of these nanoparticles in various organs following intravenous administration, can produce a pro-oxidant environment in cells and tissues which could lead to adverse biological consequences. This environment can also initiate induction of mast cells into various organs of the body.

Materials and Methods

3 MATERIALS AND METHODS

3.1 *PHASE I: Synthesis of Superparamagnetic iron oxide nanoparticles*

3.1.1 Materials

$FeCl_3$ anhydrous (Merck)

$FeCl_2.4H_2O$ (Merck)

NaOH (Merck)

35% HCl (Merck)

Dextran (MW40000 da) (Sigma-Aldrich)

Polyethylene glycol (MW8000 da) (Sigma-Aldrich)

All the chemicals and reagents used were of analytical grade.

3.1.2 Synthesis of SPIONS

The SPIONS was prepared by common aqueous co-precipitation method. Briefly, the stoichiometric mixtures of $FeCl_3$ and $FeCl_2.4H_2O$ (Fe^{3+}/Fe^{2+}: 2:1 molar ratio) were dissolved in deionized water and heated at 80°C for 1h under inert atmosphere for deoxygenation. The SPION was precipitated via alkalization of iron precursor by the dropwise addition of 1M NaOH. Thereafter the same reaction condition was kept another two hours for the complete precipitation of SPIO nanocrystals. The precipitate was then washed with deionized water to get neutral pH condition (Gupta and Gupta, 2005).

3.1.3 Surface modification with Dextran and PEG

The surfaces of the colloidal nanocrystals were modified by interaction with polymer dextran and polyethylene glycol. In order to modify the surface of SPIONS

with dextran [DEX-SPIONS], a 3% percentage solution of dextran was prepared in deionized water with continuous magnetic stirring at room temperature followed by drop wise addition of SPIONS colloidal suspension in to the polymer solution and it was kept with magnetic stirring overnight at room temperature. The colloidal suspension was washed with deionized water and centrifuged. Similarly for PEG surface modification of SPIONS [PEG-SPIONS] particles, 5 % PEG solution was prepared in deionized water followed by drop wise addition of SPIONS suspension in to polymer solution and it was magnetically stirred over night at room temperature. The suspension was magnetically separated, washed with deionized water and centrifuged.

3.2 *Physico-chemical characterisation of nanoparticles*

3.2.1 Materials

SPIONS (SPIONS, DEX-SPIONS and PEG-SPIONS)
Copper grid (300 mesh) (Electron microscopy science)
Potassium bromide (Merck)

3.2.2 Transmission electron microscopy

Samples were prepared for TEM imaging by placing a drop of solution containing nanoparticles on to a TEM grid (copper coated) and dried over-night. The sample grid was then lightly tapped to remove any excess particles and the grid was placed in the TEM for imaging.

3.2.3 Dynamic light scattering and Zeta potential

The hydrodynamic size estimation and net ζ potential measurements were carried out using Malvern Instrument-Zeta sizers 2000, UK. These measurements were performed in water medium at 25°C. Sodium phosphate buffer was used to

maintain the pH at 7.4. The ζ potential measurements were measured for 70 s and Smuluchowsky approximation was applied in the calculation of surface charge of the nanoparticles.

3.2.4 X-Ray diffraction

Approximately 10 mg of sample was placed onto a silicon zero-reflectance disc adhered to an aluminum sample plate. XRD data were collected with 2θ ranging from 10 to 80 degree at a rate of 2 degree per minute.

3.2.5 Vibrational sample magnetometry

The magnetic property was measured at room temperature using a Lakeshore model 7410 vibrational sample magnetometer (VSM). The magnetic hysteresis and saturation magnetization of SPIONS, DEX-SPIONS and PEG-SPIONS were evaluated.

3.2.6 Fourier Transform-Infra Red spectroscopy

The Fourier Transform Infrared (FT-IR) spectrum was recorded in the transmission mode on a Thermo Nicolet 5700 FTIR spectrometer (USA). The dried samples of bare SPIONS, DEX-SPIONS and PEG-SPIONS were ground with KBr and tablets of 10 mm diameter pellets were prepared by pressing the powder mixture at a load of 5 tons for 2 min. The spectrum was taken from 4000 to 400 cm^{-1} with resolution 4 and 128 times scanning.

3.2.7 Thermogravimetric analysis (TGA)

TGA was used to evaluate the thermal properties of the prepared nanoparticles and to estimate the amount of dextran and polyethylene glycol bound to the SPIONS to calculate the dose for in-vivo experiment. TGA of lyophilized SPIONS, DEX-

SPIONS and PEG-SPIONS were performed using SDT 2960 V2.2B (Simultaneous TGA-DTA, TA Instruments, Delaware, USA). TGA was run within a temperature range of 25 - 800^{o}C applying a constant heating rate of 10^{o}C/min.

3.3 *PHASE II: Cell culture studies*

3.3.1 Materials

Nanoparticles (SPIONS, DEX-SPIONS, PEG-SPIONS), Minimum Essential Medium (MEM) (Sigma), Dulbecco's modified Eagle's medium (DMEM) (Gibco/BRL, Bethesda, MD), Fetal bovine serum (FBS-Invitrogen), Isopropanol (Merck, India), Glutamine, Trypsin solution 2.5% (10×) (Gibco/Invitrogen, 100 mL), EDTA 2% (sodium salt) solution (ICN Biomedicals), Penicillin-streptomycin (Sigma), trypsin EDTA (Sigma), DMSO >99.9% (ACS reagent, Sigma), Teflon cell scrapers (Fisher, UK), Phosphate-buffered saline (PBS), Dulbecco's, without Ca, Mg, 1× (Gibco/Invitrogen, 500 mL), Hemocytometer (cell-number counter bright-line/dark-line counting chambers 0.1 mL volume, Hausser Scientific, UK), MTT - 3-(4,5-dimethylthiazol-2-yl)-2,5-diphenyltetrazolium bromide (Sigma), Fluorescein diacetate (FDA) (Invitrogen) and Propidium iodide (PI) (Invitrogen), 24 well plate and coverslips

Cell lines

L929 mouse fibroblast cell line (ATCC, USA),
RAW264.7 macrophage cell line (NCCS, Pune),
HepG2 cell lines (NCCS, Pune)

Macrophages were used between passage numbers 5 and 15 and mouse fibroblasts L929 between passage numbers 10 and 20.

Nanoparticles: SPIONS, DEX-SPIONS and PEG-SPIONS were diluted in serum free medium just before any experiment.

3.3.2 MTT assay

To evaluate the cytotoxicity of the synthesised SPIONS, DEX-SPIONS and PEG-SPIONS, the MTT assay was used (Mosmann, 1983). SPIONS, DEX-SPIONS and PEG-SPIONS were mixed with equal volume of MEM-2X to get initial concentration of 50 µg/ml in medium. Test materials SPIONS, DEX-SPIONS and PEG-SPIONS were evaluated with L929 cells. A serial dilution from 50 – 12.25 µg/ml was prepared using culture medium containing serum. 96 well plates were seeded with 1×10^4 cells per well and maintained until subconfluency. The culture medium was replaced with various dilutions of test samples and cell control (normal medium). After 24 h incubation, the medium was removed and cells were washed with serum free MEM. To each well, 50 µl of MTT reagent (1 mg/ml in serum free medium) was added and incubated for minimum two hours. MTT reagent was replaced with 100 µl isopropanol and absorbance was read at 570 nm in a multiwell plate reader (Tykon, USA). The data was exported to Microsoft Excel and analyzed statistically. Cell activity was determined by the formula Cell activity (%) = (OD test cells/OD cell control) × 100. The cellular activities of cells exposed to test samples were also compared with the cell control.

Similarly, MTT assay was carried out using RAW 264.7 macrophage cells for SPIONS, DEX-SPIONS and PEG-SPIONS.

3.3.3 Live/dead assay

Viability of L929 fibroblasts in the presence of SPIONS, DEX-SPIONS and PEG-SPIONS was evaluated. 12 well plates with coverslips were seeded with 1×10^4 cells per well and maintained until subconfluency. SPIONS, DEX-SPIONS and PEG-SPIONS were mixed with equal volume of MEM-2X to get initial concentration of 50 µg/ml in medium. Test nanoparticles were added to the wells. After 24 h incubation, the medium was removed and cells were washed with serum free MEM. To each well, 50 µl of freshly prepared FDA/PI staining working solution (Appendix) was added and incubated at room temperature for 4 to 5 minutes in the dark. Staining solution was removed and PBS was added. The sample was viewed under inverted fluorescence microscope with filter sets for Texas Red and FITC (Leica DM6000, GmbH). Images were captured and analysed using ImageJ software.

3.4 *Haemocompatibility studies*

3.4.1 Materials

Nanoparticles (SPIONS, DEX-SPIONS, PEG-SPIONS), 0.1% Sodium carbonate and EDTA -2K coated vaccutainer.

3.4.2 Haematology

Test was done as per ISO 10993 Part-4. In brief samples at different concentration were exposed to 2.0 ml human blood. 0.5 ml blood was collected as initial sample. Cell count was measured using an automatic hematology analyzer (Sysmex-K4500) in initial samples as well as in samples after 30 mins exposure. Percentage change in cell count was analyzed by applying following formula.

$$\text{Percentagechange} = \frac{\text{InitialCount} - \text{FinalCount}}{\text{InitialCount}} \text{X} 100$$

3.4.3 Hemolysis assay

The total hemoglobin in the initial blood sample was measured using an automatic hematology analyzer (Sysmex-K4500). The free hemoglobin liberated in the plasma after exposure to the materials was estimated in sample by measuring the absorbance of diluted plasma with a diode array spectrophotometer (HP 8453, Hewlett-Packard GmbH, Germany).

$$\text{Percentage hemolysis} = \frac{\text{Free Hb}}{\text{Total Hb}} \text{X } 100$$

3.5 *Oxidative stress studies in HepG2 cell lines*

3.5.1 Materials

Nanoparticles (SPIONS, DEX-SPIONS, PEG-SPIONS), Reduced glutathione (GSH), Dithio-bis-2-nitrobenzoic acid [DTNB], Riboflavin (Sigma, USA), Thiobarbituric acid (TBA), Disodium hydrogen phosphate (Na_2HPO_4), Sodium dihydrogen phosphate (NaH_2PO_4), Ethylene triamine tetra acetic acid (EDTA) (Merck, Germany) and Physiological saline (Parenteral Drugs Ltd., India).

3.5.2 HepG2 cell culture

HepG2 cell line was maintained in Dulbecco's modified eagles media (Appendix) supplemented with 10% FBS and grown to confluency at 37°C in 5 % CO_2 in a humidified atmosphere in a CO_2 incubator (NBS, EPPENDORF, GERMANY).

- The cells were trypsinized (500 µl of 0.025% Trypsin in PBS/ 0.5 mM EDTA solution) for 2 minutes and passaged to T flasks in complete aseptic conditions.

- Nanoparticles were added to grown cells at a final concentration of 50 µg/ml and incubated for 24 h.

- The isolation was done by spinning at 6000 rpm for 10 minutes.

- Supernatant was discarded and 200 µl of cell lysis buffer (1M Tris HCl, 0.25M EDTA, 2M NaCl, 0.5% Triton) was added.

- The incubation was done for 30 minutes at 4°C and SOD, GSH, LPO and tissue nitrite level assays were done in pellet suspended in a small amount of supernatant.

3.5.2.1 Estimation of SOD activity (Misra and Fridovich, 1972)

The enzyme superoxide dismutase catalyzes the dismutation of superoxide in to oxygen and hydrogen peroxides. As such, it is an important antioxidant defense in nearly all cells exposed to oxygen. 50 µl of cell lysate were added to the reaction mixture containing 50 mM phosphate buffer (pH-7.8), 45 µM methionine, 5.3 mM riboflavin, and 84 µM potassium ferricyanide. The tubes were then incubated at 25^0C for 10 minutes and the absorbance was read on spectrophotometer at 600 nm.

% inhibition = 100 - (Test/Blank) X100

Enzyme units = % inhibition/50

3.5.2.2 Estimation of reduced Glutathione level (Moron et al., 1979)

1.0 ml of cell lysate was taken in a test tube and 0.5 ml of phosphate buffer (0.2M, pH-8), 1.3 ml of distilled water and 0.2 ml of DTNB (0.6 mM) was added.

The contents were mixed well and read on spectrophotometer at 420 nm. The GSH levels were compared with a standard reduced glutathione graph.

3.5.2.3 Estimation of Nitrite levels (Lepoivre et al., 1990)

To 0.5 ml of cell lysate, 0.1 ml of sulphosalicylic acid was added and vortexed well for 30 minutes. The samples were then centrifuged at 5,000 rpm for 15 minutes. The protein-free supernatant was used for the estimation of nitrite levels. To 200 µl of the supernatant, 30 µl of 10% NaOH was added, followed by 300 µl of Tris-HCl buffer and mixed well. To this, 530 µl of Griess reagent was added and incubated in dark for 10–15 minutes, and the absorbance was read at 540 nm against a Griess reagent as blank. Sodium nitrite solution was used as the standard. The amount of nitrite present in the samples was estimated from the standard curves obtained.

3.5.2.4 Estimation of Lipid peroxidation (Ohkawa et al., 1979)

To 50 µl of cell lysate, 500 µl of 70% alcohol and 1ml of 1% TBA were added. Then all the tubes were kept in boiling water bath for 20 minutes. After cooling to room temperature, 50 µl of acetone was added to all the test tubes and the absorbance was read at 535 nm in spectrophotometer and the concentration of MDA was calculated by using the extinction coefficient of MDA (1.56×10^5).

3.6 *Raman chemical mapping of L929 and RAW cells treated with SPIONS, DEX-SPIONS and PEG-SPIONS*

3.6.1 Materials

Nanoparticles (SPIONS, DEX-SPIONS, PEG-SPIONS), CaF_2 Slides (Crystran, UK) and Cover slips (Blue star, India).

3.6.2 Method

Particle uptake study was performed with the confocal Raman microscope (Witec Inc. alpha300R). For the measurements a frequency-doubled NdYAG laser: l = 532 nm was used. The excitation light was polarized horizontally (in the x-direction) with respect to the Raman image. All measurements were performed using a SP2300i spectrometer and back illuminated Peltier cooled CCD camera DU401A.

The live L929 cells were cultured on a Raman grade CaF_2 substrates (Crystran, UK) and cover slips in 12-well culture plates treated with SPIONS, DEX-SPIONS and PEG-SPIONS taken in physiological medium (PBS). Cells were viewed using a 60 x Nikon (NA=1.0) water objective and were illuminated using LED light from bottom to record a phase contrast image. Samples were excited with the 532 nm excitation wavelength laser and Stokes shifted Raman spectra were collected in the range of 400 to 4000 cm^{-1} with 1 cm^{-1} resolution. Prior to every measurement, a calibration with a silicon standard (Raman peak centered at 520 cm^{-1}) was performed. The distribution of chemical species on the L929 cell was obtained in Raman spectral imaging mode. In this imaging mode a complete Raman spectrum was recorded (integration time of 0.5s) at every imaging point (100 x 100 points for 40 x 40 μm^2), leading to a 2D array of Raman spectra. Background subtraction, cosmic ray removal, averaging a certain region manually, and spectral de-mixing were performed on this 2D array of Raman spectra. Three distinct spectra for nanoparticles, cell and the buffer were extracted using Cluster Analysis (CA) utilizing Witec Project plus software. In the cluster analysis method Raman images are sorted according to their similarities. As a result, one gets a certain number of areas or masks, which indicate where the spectra belonging to the various clusters

were acquired as well as the average spectra of each cluster. Spectral mapping was based on K-means, Manhattan distance cluster analysis. The distribution of these three Raman spectra over the examined cell is colour coded which can distinctly show the cell and the nanoparticles.

Similarly, SPIONS uptake study was carried out using RAW 264.7 macrophage cells.

3.7 *In vitro evaluation of Genocompatibility by comet assay*

3.7.1 Materials

Nanoparticles (SPIONS, DEX-SPIONS, PEG-SPIONS), Normal melting point agarose (NMA), low melting point agarose (Hi-Media), NaCl (Merck), Ethidium bromide, Na_2EDTA, Tris, and Sodium dodecyl sulphate (Sigma)

3.7.2 Method

Nanoparticles were added to a sub-confluent layer of L929 fibroblasts and incubated at 37 ^oC for 48 h. These cells were then subjected to comet assay as per the following procedure. The microscope slides were pre-coated with 1 ml of 0.75% normal melting point agarose (NMA) and stored at 4^0C. This layer was removed before use and 120 µl of 0.75% NMA was pipetted on to the slides, which were then covered with cover slips. Cells were trypsinized, mixed with 50 µl of low melting point agarose and pipetted over the first layer of agarose. NMA (80 µl) was used as a final protective layer. Slides were placed in cold lysing solution (2.5 M NaCl, 100 mM Na_2EDTA, 10 mM Tris, pH-10 & 1% SDS to which 10% DMSO and 1% Triton X 100 were added immediately before use) for overnight at 4^oC. After lysis slides were placed in electrophoresis buffer (300 mm NaOH and 1 mM Na_2EDTA pH-13)

for 20 min to allow unwinding of DNA. Then electrophoresis was conducted in the same buffer by applying an electric current of 0.8 V/cm (300 mA) for 15 min. Finally, slides were washed in neutralization buffer (0.4 µl Tris, pH-7.5) three times for 5 min and stained with 50 µl ethidium bromide (20 µg/ml). The excess stain was washed with PBS and viewed under fluorescent microscope using green filter. The extent of DNA damage was quantified by the comet reading software TriTek cometScore Freeware 1.6.1.13 with respect to a control and H_2O_2 treated cells (200 mM H_2O_2 was added to the culture and incubated for 24 h) (Thankam and Muthu, 2014).

3.8 *PHASE III: Animal experiment*

3.8.1 Materials

Pellet rat feed (M/s. Tetragon Chemie Private Limited, India), Xylazine, Ketamine, normal saline, 26G needle, insulin syringe, EDTA coated vials, 2 ml syringe, 22G needle, Bard-Parker (BP) handle (No. 3&4), Bard-Parker (BP) blade (No.11, 22&23), Scissors 4,6,8 inches with blunt ends, forceps, dissection board, absorbent cotton, blotting paper, 250 ml glass tissue collection container, sterile petridishes, Tissue collection vials (Eppendorf), 10% neutral buffer formalin (Appendix).

The diagnostic kits for glucose, total protein, cholesterol, triacylglycerides, uric acid, creatinine, Alkaline phosphatase, Gamma Glutamyl Transferase, Serum Glutamate Pyruvate Transaminase, Serum Glutamate Oxaloacetate Transaminase were purchased from M/s Agappe diagnostics, India.

For flowcytometry, cuvettes (BD FACS Aria, USA), Optilyse (Sigma), Nanoparticles (SPIONS, DEX-SPIONS, PEG-SPIONS)

3.8.2 Experimental animals

Female Wistar rats of 6-8 weeks age, weighing about 200 - 230 gram were obtained from Division of Laboratory Animal science, SCTIMST, India. All animals were housed in cages with 12/12 hours light/dark cycle. The animals were fed *ad libitum* feed and water throughout the experimental period. The animals were acclimatized for one week prior to the start of the experiment. The animal experiments were carried out after prior approval of Institutional Animal Ethical Committee (IAEC), SCTIMST.

3.8.3 Experimental design

Twenty four female Wistar rats were randomly divided into four groups (Table.1), each consisting of six animals. The study was designed for twenty four hours, after nanoparticle administration. A dose of 5 mg Fe/kg body wt. was fixed for this study since it was the highest dose tested in the clinical Phase II studies for MRI imaging (Wang et al., 2001).

Table 1: Experimental design

GROUPS	**Treatments**	**Number of Animals**
Group – I (Control)	Saline only control	6
Group – II (DEX-SPIONS)	Dextran coated Fe_3O_4 i/v @ 5 mgFe/kg b.wt	6
Group – III (PEG-SPIONS)	PEG coated Fe_3O_4 i/v @ 5 mgFe/kg b.wt	6
Group – IV (SPIONS)	Bare Fe_3O_4 i/v @ 5 mgFe/kg b.wt	6
	Total	24

3.8.4 Administration of nanoparticles

Under anesthesia given through intramuscular injections of ketamine (80 mg/kg) and xylazine (8 mg/kg), each animal received a single intravenous lateral tail vein injection of 5 mg Fe/kg body weight of DEX-SPIONS, PEG-SPIONS or bare SPIONS suspended in 500 µl normal saline.

Clinical observation was for 24 h. At the experimental end point of 24 h, all animals were humanely sacrificed.

3.8.5 Collection of blood and tissue samples

Blood samples for haematology and biochemical analysis were collected at the end of experiment by cardiac puncture under anaesthesia. The blood for hematology was collected into tubes treated with dipotassium ethylenediaminetetraacetate (EDTA-2K). The blood for biochemistry was collected in a 3 ml plastic tube without coagulant activators and the serum was separated by centrifugation at 3000 rpm for 10 minutes.

Tissue samples for assay of tissue antioxidant status in lung, heart, liver, kidney and spleen were taken from control and experimental rats in ice cold PBS.

Organs collected for histopathology studies included lung, heart, liver, kidneys, spleen, cerebrum, cerebellum, stomach, duodenum, jejunum, ileum, colon, caecum, rectum, eyes, ovary, uterus, cervix and vagina from control and experimental rats.

Liver tissue was collected for RNA isolation from normal and experimental rats and stored at -80°C.

Organs collected for elemental analysis included liver, kidney and spleen taken from control and experimental rats. Wet weight of collected tissues was measured before digestion.

3.8.6 Haematology

The hematological examination was carried out using an automatic analyzer (Sysmex KX-21NV; Sysmex Corporation), to determine the

Red blood cell count (RBC),
Hemoglobin concentration (Hb),
Hematocrit level (HCT),
Mean corpuscular volume (MCV),
Mean corpuscular hemoglobin (MCH),
Mean corpuscular hemoglobin concentration (MCHC),
White blood cell count (WBC) and
Platelet count (PLT).

3.8.7 Biochemical Assays

Assays were carried out as per the manufacturers protocol described in the standard kits (Agappe diagnostics) with an automatic analyzer (ERBA XL 300 Biochemical Fully automated analyzer) to estimate

Alkaline phosphatase,
Gamma Glutamyl Transferase (GGT),
Serum Glutamate Pyruvate Transaminase (SGPT),
Serum Glutamate Oxaloacetate Transaminase (SGOT)
Glucose,
Cholesterol,
Triglycerides,
Uric acid,
Creatinine,

Chloride,
Calcium,
Phosphorous,
Albumin and
Total protein

3.8.8 Flow Cytometry

The whole blood was analysed for forward and side scattering using a flowcytometer (BD FACS Aria, USA). 100 µl of RBC lysis buffer was added to 500 µl of anticoagulant added blood and mixed well in a cuvette. About 10,000 cells were acquired and the FSC vs SSC dot plot was developed using BD FACS Diva software. The difference in cell size and granularity were compared.

3.8.9 Oxidative stress studies in tissues

3.8.9.1 Preparation of tissue homogenate

Approximately 100 mg of lung, heart, liver, spleen and kidney tissues were taken in a porcelain mortar and 5 ml of liquid nitrogen was added and tissues were triturated to powder using the pestle.

3.8.9.2 Estimation of SOD activity (Misra and Fridovich, 1972)

The enzyme superoxide dismutase catalyzes the dismutation of superoxide in to oxygen and hydrogen peroxides. As such, it is an important antioxidant defense in nearly all cells exposed to oxygen. 50 µl of tissue homogenate was added to the reaction mixture containing 50 mM phosphate buffer (pH-7.8), 45 µM methionine, 5.3 mM riboflavin, and 84 µM potassium ferricyanide. The tubes were then incubated at 25^0C for 10 minutes and the absorbance was read on spectrophotometer at 600 nm.

$$\% \text{ inhibition} = 100 - \frac{Test}{Blank} \text{ X } 100$$

$$Enzyme\ unit = \% \text{ inhibition} / 50$$

3.8.9.3 Estimation of reduced Glutathione (Moron et al., 1979)

1.0 ml of tissue homogenate was taken in a test tube. 0.5 ml of phosphate buffer (0.2M, pH-8), 1.3 ml of distilled water and 0.2 ml of DTNB (0.6 mM) was added. The contents were mixed well and read on spectrophotometer at 420 nm. A series of standards treated in a similar manner were also run to determine the glutathione content. The GSH levels were compared with a standard reduced glutathione graph.

The amount of glutathione in tissues is expressed as nanomoles / mg of protein

3.8.9.4 Estimation of Lipid peroxidation (Ohkawa et al., 1979)

To 50 µl of tissue homogenate, 500 µl of 70% alcohol and 1ml of 1% TBA were added. Then all the tubes were kept in boiling water bath for 20 minutes. After cooling to room temperature, 50 µl of acetone was added to all the test tubes and the absorbance was read at 535 nm in spectrophotometer and the concentration of MDA was calculated using the extinction coefficient of MDA (1.56×10^5).

The level of lipid peroxides is expressed as nanomoles of MDA released per mg of protein.

3.8.9.5 Estimation of tissue Nitrite levels (Lepoivre et al., 1990)

To 0.5 ml of tissue homogenate, 0.1 ml of sulphosalicylic acid was added and vortexed well for 30 minutes. The samples were then centrifuged at 5,000 rpm for 15 minutes. The protein-free supernatant was used for the estimation of nitrite levels. To

200 µl of the supernatant, 30 µl of 10% NaOH was added, followed by 300 µl of Tris-HCl buffer and mixed well. To this, 530 µl of Griess reagent was added and incubated in the dark for 10–15 minutes, and the absorbance was read at 540 nm against a Griess reagent as blank. Sodium nitrite solution was used as the standard. The amount of nitrite present in the samples was estimated from the standard curves obtained.

3.8.10 Histopathology

3.8.10.1 Tissue fixation & Grossing

3.8.10.1.1 Materials

10% Neutral buffer formalin, plastic containers, BP handle (No. 4), BP blade (No. 23), tissue cassettes.

3.8.10.1.2 Method

Tissue and organs were collected in the plastic container containing 10% neutral buffer formalin.

Organs were examined for any gross pathological changes. 2-3 mm thick tissue pieces were cut from organs and kept in plastic cassette (Leica) in buffered formalin prior to processing.

3.8.10.2 Tissue Processing

3.8.10.2.1 Materials

Tissue cassettes (Leica), isopropyl alcohol, xylene and paraffin (Merck).

3.8.10.2.2 Method

Tissues were processed using the Automatic Tissue processor (LEICA ASP300). The following protocol was followed:

10% Neutral buffered formalin	10 minutes
80% isopropyl alcohol	1 hour
95% isopropyl alcohol I	1 hour
95% isopropyl alcohol II	1 hour
100% isopropyl alcohol I	1 hour
100% isopropyl alcohol II	1 hour
100% xylene I	1 hour
100% xylene II	1 hour
Paraffin wax I	2 hours
Paraffin wax II	2 hours

3.8.10.3 Embedding

3.8.10.3.1 Materials

Stainless steel molds, Tissue cassette lids, molten paraffin and marker pen.

3.8.10.3.2 Method

Processed tissues were embedded into molten paraffin blocks using the Paraffin embedder (LEICA EG 1160).

3.8.10.4 Sectioning

3.8.10.4.1 Materials

Charged slides (Starfrost), Lead pencil, disposable steel knife, forceps, brushes, ice blocks in ice trays and slide racks.

3.8.10.4.2 Method

5 µm thick paraffin sections were taken using the Automatic Microtome (LEICA RM 2155) collected onto charged glass slides (Starfrost, GmbH). The sections were air dried and kept stored in an incubator at 37^{o}C, overnight or at 50^{o}C for 1-2 hours.

3.8.10.5 Hematoxylin and Eosin staining

Hematoxylin and eosin staining is usually done to study the architecture of tissue sections at light microscopic level based on the histological affinity of various tissue components. The nucleus stains blue and cytoplasm stains pink or red.

3.8.10.5.1 Materials

Incubator, Autostainer (Leica Autostainer XL) , Microscope (Nikon., Japan), slide racks, staining troughs, forceps, Isopropyl alcohol of different grades (Merck), Harris hematoxylin solution (Appendix), Eosin (in alcohol or water) (Appendix), Scott's tap water (Appendix), acid alcohol (Appendix), Xylene (Merck), Cytoseal ™ 60 (Richard Allan scientific), cover slip, identity label.

3.8.10.5.2 Method

Sections were stained with hematoxylin and eosin using the following schedule in an autostainer (Leica Autostainer XL).

Xylene I	-	10 minutes
Xylene II	–	5 minutes
90% alcohol	–	5 minutes
70% alcohol	–	5 minutes
Wash I (with tap water)	–	3 minutes
Hematoxylin solution	–	30 minutes
Wash II (tap water)	–	3 minutes.
Acid alcohol	–	10 minutes.
Wash III (tap water)	–	5 minutes
Scott's tap water	–	7 minutes
Wash IV (tap water)	–	5 minutes
1% eosin	–	5 minutes
Wash V (tap water)	–	15 seconds
70% alcohol	–	2 minutes
100% alcohol	–	5 minutes

100% alcohol	–	5 minutes
Xylene I	–	10 minutes
Xylene II	–	10 minutes

After these schedule slides were removed from xylene and cleaned with tissue paper without allowing the sections to dry. The slides were then mounted with Cytoseal ™ 60, cover slipped and dried overnight before observing under light microscope.

3.8.10.6 Toluidine blue staining

Sections of lung, heart, liver, spleen and kidneys were stained with toluidine blue for identification of mast cells.

Principle

Toluidine blue is a basic dye commonly used for the identification of mast cells. Under the highly acidic conditions only the sulfated proteoglycans remains positively charged and are therefore capable of binding these basic dyes. Binding of toluidine blue to repetitively charged side chains of heparin brings the coloured ionic portion of the dye into close alignment causing a shift in wavelength of the light absorbed. This colour shift is metachromasia and mast cell is seen in bluish purple colour.

3.8.10.6.1 Materials

Incubator, Toluidine blue stain (Appendix), Isopropanol (Merck), Xylene (Rankem), Cytoseal ™ 60, coplin jar, distilled water.

3.8.10.6.2 Method

The tissue sections were taken on to charged slides and kept in an oven at 50^{o}C for 2 hours, deparaffinised by placing in two solutions of Xylene for ten minutes and

dehydrated by passing through descending grades of alcohol (90%, 70%) for 5 minutes each and then kept in distilled water for 3 minutes. They were then stained with toluidine blue for 10 minutes at 37^{o}C. The sections were blotted carefully and dipped in absolute alcohol for 10 seconds and then put in xylene for clearing. The slides were mounted with cytoseal and cover slipped and air dried overnight before observing under the microscope. Control used was normal rat muscle tissue sections.

3.8.10.7 Perl's Prussian blue

Sections of lung, heart, liver, spleen and kidneys were stained with Perl's Prussian blue for identification of iron.

Principle

Perl's Prussian blue is used to demonstrate ferric iron in tissue sections. The reaction occurs with the treatment of sections in acid solutions of ferrocyanides. Any ferric ion (+3) in the tissue combines with the ferrocyanide which results in the formation of a bright blue pigment called Prussian blue or ferric ferrocyanide.

3.8.10.7.1 Materials

Incubator, microscope, Potassium ferrocyanide (Merck), Con. HCl, Nuclear fast red (Sigma), Glacial acetic acid (Merck), Isopropanol (Merck), Xylene (Rankem), Cytoseal ^{TM} 60, cover slips, micro slides, distilled water, tap water.

3.8.10.7.2 Method

The tissue sections were taken on to charged slides and kept in an oven at 50^{o}C for 2 hours, deparaffinised by placing in two solutions of Xylene for ten minutes and dehydrated by passing through descending grades of alcohol (90%, 70%) for 5 minutes each and then kept in distilled water for 3 minutes. Sections were covered

with potassium ferrocyanide for 5 minutes the potassium ferrocyanide-HCl mixture (Appendix) for 20 minutes. Sections were rinsed well in distilled water. Then sections were stained with nuclear fast red (Appendix) for 5 minutes at 37^{o}C. Sections were rinsed well in tap water. The sections were blotted carefully and dipped in absolute alcohol for 10 seconds and then put in xylene for clearing. The slides were mounted with cytoseal and cover slipped and air dried overnight before observing under the microscope. Control used was normal rat spleen tissue sections.

3.8.10.8 Cresyl violet staining

Sections of cerebrum and cerebellum were stained with cresyl violet for identification of neural cells.

Principle

Cresyl violet is a basic dye. Neurons contain Nissl substance, which is primarily composed of rough endoplasmic reticulum, with the amount, form and distribution varying in different types of neurons. Because of the RNA content, Nissl substance is very basophilic and will be very sharply stained with basic aniline dyes. By varying the pH and the degree of differentiation, both Nissl substance and nuclei or only Nissl substance may be demonstrated.

3.8.10.8.1 Materials

Incubator, microscope, Cresyl fast violet (Appendix), acetic alcohol (Appendix), Isopropanol (Merck), Xylene (Rankem), Cytoseal ^{TM} 60, cover slips, micro slides, distilled water, tap water.

3.8.10.8.2 Method

The tissue sections were taken on to charged slides and kept in an oven at 50^{o}C for 2 hours, deparaffinised by placing in two solutions of Xylene for ten minutes and dehydrated by passing through descending grades of alcohol (90%, 70%) for 5 minutes each and then kept in distilled water for 3 minutes. Sections were covered with filtered cresyl fast violet, stain for 20 minutes and rinsed in distilled water. Differentiation was carried out in 0.25 % acetic alcohol until most of the stain had been removed. The sections were blotted carefully and dipped in absolute alcohol for 10 seconds and then put in xylene for clearing. The slides were mounted with cytoseal and cover slipped and air dried overnight before observing under the microscope.

3.8.11 Light microscopy

All stained sections were observed by transmitted light microscopy (Nikon Eclipse E 600, Japan). H&E stained sections were observed for histopathological changes. Iron distribution was examined in Prussian blue stained tissue sections.

Images from different zones (selected after qualitative microscopy) at a magnification of 40X of the stained sections were captured with a digital camera (Nikon Digital Camera DSi, Japan).

3.8.11.1 Mast cells and image analysis

Mast cells were identified in toluidine blue stained section as round oval cells with deep blue granules. Total numbers of mast cells in each section were quantified. The surface areas of each section were calculated using image proplus (Media

cybernetics, Inc: version 5.1, USA). Data was exported to an excel sheet and total number of mast cells per mm^2 section were calculated for comparison.

3.8.12 Transmission Electron Microscopic Analysis

3.8.12.1 Materials

Tissues pieces of liver, Gluteraldehyde (Electron microscopy sciences, USA), acetone, propylene oxide, epoxy resin, embedding kit (Polysciences Inc, USA).

3.8.12.2 Tissue fixation & Grossing

Tissue blocks from liver were collected in 3% buffered gluteraldehyde (Appendix) and fixed for 48 h at 4^oC. Gluteraldehyde fixed tissues were cut to 1-2 mm thin pieces. The samples were washed with cold phosphate buffer (pH 7.4), 4 changes, for 10 minutes each, with sample vials standing in an ice bath. Tissues were then placed in 1% OsO_4 for 2 hours and thereafter washed with phosphate buffer, 4 changes for 15 minutes each, in an ice bath. Tissues were then rinsed in distilled water for five minutes.

3.8.12.3 Dehydration

The tissues were dehydrated in ascending grades of acetone using the following protocol:

50% acetone	-10 minutes (2 changes) in cold.
70% acetone	-10 minutes in cold (stored overnight in refrigerator).
70% acetone	-10 minutes at RT.
90% acetone	-10 minutes (2 changes) at RT.
100% acetone	-15 minutes (4 changes) at RT.
100% dry acetone	-15 minutes at RT.

3.8.12.4 Infiltration

Tissues were placed in two changes of propylene oxide for five minutes each and then transferred into propylene oxide-resin mixtures of ratio 3:1 for two hours, 1:1 for two hours and finally kept overnight in vacuum in propylene: epoxy resin mixture of ratio of 1:3. Final infiltration was carried out in pure resin prior to embedding.

3.8.12.5 Embedding

The tissues were embedded in molds containing the epoxy resin - Polybed 812 mixed with dodecenyl succinic anhydride (DDSA – Hardener), Nadic methyl anhydride (NMA – Hardener), Dimethylaminomethyl phenol (DMP – Accelerator) in appropriate ratios as per the kit instructions (Polysciences Inc, USA) and polymerized at 60°C in an oven for three days.

3.8.12.6 Sectioning

For light microscopy semithin sections (~ 1µm) were cut using a glass knife in an ultramicrotome (Leica Ultracut UCT). Once the area of interest was identified, the remaining area of the block was trimmed off.

For TEM, ultrathin sections (50-70 nm) were cut using a diamond knife (Diatome®) and collected onto the shiny side of copper grids of 300 mesh sizes.

3.8.12.7 Staining

- The semithin sections were stained with Toludine blue.
- Sections were taken onto a few drops of water on a slide and a drop of toludine blue was added.
- Sections were heated on a hot plate for a few seconds.

- The sections were washed well in distilled water and air dried.
- The sections were mounted using DPX and the photographs were taken using the trinocular microscope (Nikon Eclipse Model E600, Japan) and images captured using a digital camera (Nikon model DSi, Japan).
- Area of interests was located in the semi thin sections to take ultrathin sections.
- Ultrathin sections were viewed under TEM without staining.

3.8.12.8 TEM observation and ultramicrographs

The grids were then dried and viewed under the Transmission Electron Microscope (Hitachi-H 7650, Japan) at an accelerating voltage of 80kV and multiple digital images were taken.

3.8.13 Gene expression studies

3.8.13.1 Materials

Tissues pieces of liver from all groups, Qiagen RNA easy fibrous tissue kit (Cat.No.74704), liquid nitrogen, pestle and mortar, Refrigerated centrifuge, Minispin (Eppendorf), Tissue homogeniser (Polytron, Germany), Full velocity master mix, (Stratagene, USA), forward and reverse primers (Table.2) (ITD, India), SYBR green master mix and kit (Roche).

Table 2: Primers used for *in vivo* gene expression studies

Name of gene	Primer Sequence	Tm
HSP-70	Forward : 5'-CTG ACA AGA AGA AGG TGC TGG-3' Reverse : 5'-AGC AGC CAT CAA GAG TCT GTC-3'	55.7°C 57°C
HO-1	Forward : 5'-ACT TTC AGA AGG GTC AGG TGT CC-3' Reverse : 5'-TTG AGC AGG AAG GCG GTC TTA-3'	59°C 55°C
Transferrin	Forward : 5'-GGC ATC AGA CTC CAG CAT CA-3' Reverse : 5'-GCA GGC CCA TAG GGA TGT T-3'	57.2°C 57.5°C
Ceruloplasmin	Forward : 5'-ATG TGA TGG CTA TGG GCA ATG-3' Reverse : 5'-TTC CCC TGT GCT TGT ATT GGA-3'	56.4°C 55.6°C
Beta actin	Forward : 5'-AGA GGA AAA TCG TGC GTG AC-3' Reverse : 5'-AGG AGC CAG DGC AGT AAT C-3'	57.5°C 56.8°C

3.8.13.2 RNA isolation

Total RNA was isolated from retrieved rat liver tissue samples according to the manufacturer's description. On the day of isolation, around 30 mg tissue was weighed out from fresh/frozen samples from control, DEX-SPIONS and PEG-SPIONS group without thawing and homogenized with a rotor stator homogenizer in 350 µl of RPE buffer (lysis buffer). Proteinase digestion was done by incubating the sample at 55^0C after the addition of 10 µl proteinase K, followed by ethanol precipitation after which the homogenate was applied to RNeasy mini-spin columns sitting in 2 ml collection tubes. The columns and tubes were then centrifuged for 1 min at 13,000 rpm (Eppendorf minispin), the flow-through was discarded and the columns were washed with 350 µl buffer and spun at 9,500 rpm for 15 seconds. The purified sample was DNAse treated with 10 µl DNase I and 70 µl buffer and

incubated at RT for 15 minutes. Thereafter, the columns were washed with 350 µl buffer and spun at 9500 rpm for 15 seconds. The columns were subsequently washed with 500 µl buffer twice with the flow through being discarded after each centrifugation. The columns were transferred to new collection tubes and 50 µl RNase freewater was applied to each column twice. The accumulated flow through was collected after the centrifugations. Yield and purity of isolated RNA was checked in spectrophotometer (Colibri, GmbH) at an absorbance of 260/280 nm. The isolated RNA samples were stored in -80^{o}C till downstream analysis was carried out.

3.8.13.3 Reverse transcription

cDNA synthesis of RNA samples was carried out. Total RNA at a concentration of 1 µg was taken for each reverse transcription using Thermal cycler (Appollo Cycler, USA) at annealing temperatures of 53-58^{0}C. In 25 µl total volume, 1 µl dNTP, 2.5 µl stratascript buffer, 0.5 µl RNase inhibitor, 1 µl each forward and reverse primer and 0.5 µl (50U/ µl) reverse transcriptase (Stratagene, USA) and the RNA template were added. The primer sequences were derived from cited literature and are listed in Table 2. All cDNA samples were stored at -20^{o}C until use.

3.8.13.4 Real time PCR with SYBR green dye

Real time PCR was performed to determine the mRNA expression of HSP-70, HO-1, Transferrin and ceruloplasmin using light cycler system (Roche, USA). All reactions were carried out in a total volume of 20 µl containing 10 µl SYBR green master mix, 1 µM forward and reverse primers each and 8 µl template cDNA. For each gene, quality and specificity was assessed by examining Melting curves following Real-time PCR. The cDNA copy numbers of the target gene were

analyzed after normalizing with the copy number of beta actin, the house keeping gene. The relative gene expression was calculated using delta-delta Ct method. The gene expression in control liver tissue acted as the baseline for comparison. The Roche light cycler run was used with the following parameters: 35 cycles, denaturation at 94^0C for six minute, annealing temperature at 53-58.5^{0}C (depending on T_m of primers) for 30 seconds and elongation temperature at 72^0C for one minute.

3.8.14 Elemental analysis by inductively coupled plasma Optical emission spectroscopy (ICP-OES)

3.8.14.1 Materials

Tissues pieces of liver, spleen, kidney from all groups, Con. HNO_3, Con. $HClO_4$ (Merck) and digestion tubes.

3.8.14.2 Method

Weighed quantity of wet tissues were taken in a boiling tube and digested by heating in 5 ml of 50% HNO_3, 5 ml of Conc: HNO3 and finally in a mixture of 2 ml each of Conc: HNO_3 and Conc: $HClO_4$. Heating was done on a sand bath. The clear soution thus obtained were diluted to 50 ml in deionized water and then analysed. The analysis was carried out (ICP-OES system Perkin Elmer OES-ICP, Model : 5300DV) as per the work procedure for ICP-OES Analysis(Anderson KA, 1999)(AOAC International, 2006). The concentration of the analyte element was determined from the calibration plot obtained by analyzing standard solutions. The results were recorded and processed using Win Lab 32 software to find the total amount of the analyte element contained in the tissue

$$\text{Total amount}\,(g/g) = \frac{\text{Concentration}\ x10^{-6}\ x\ 50}{\text{Weight of sample}}$$

$$\text{Total amount } (\mu g/g) = \frac{\text{Concentration x 50}}{\text{Weight of sample}}$$

3.9 *Statistical Analysis*

All values were expressed as mean ± S.D with $n \geq 4$ per group. All data were tested for significance with one-way analysis of variance (ANOVA) using Tukey post-hoc test using Graph Pad Prism 6 (San Diego, USA) with p value ≤ 0.05 considered statistically significant.

Results

4 RESULTS

4.1 *PHASE I: Synthesis and surface modification of SPIONS*

Superparamagnetic iron oxide nanoparticles synthesised appeared as a dark black colour suspension. The DEX-SPIONS and PEG-SPIONS suspensions were black brown in colour.

4.2 *Physico-chemical characterisation of nanoparticles*

4.2.1 Transmission electron microscopy

High resolution is essential to visualize nanoparticles. Transmission electron microscopy (TEM) is a technique that is used to characterize the morphology and size of nanomaterials. The TEM images of SPIONS indicated uniform size distribution of SPIONS, DEX-SPIONS and PEG-SPIONS (Figure 1). The histogram of nanoparticle was evaluated using ImageJ software. The corresponding average particle size was calculated with the help of a Gaussian fit and the average diameter was found to be 10.3 ± 1.4 nm.

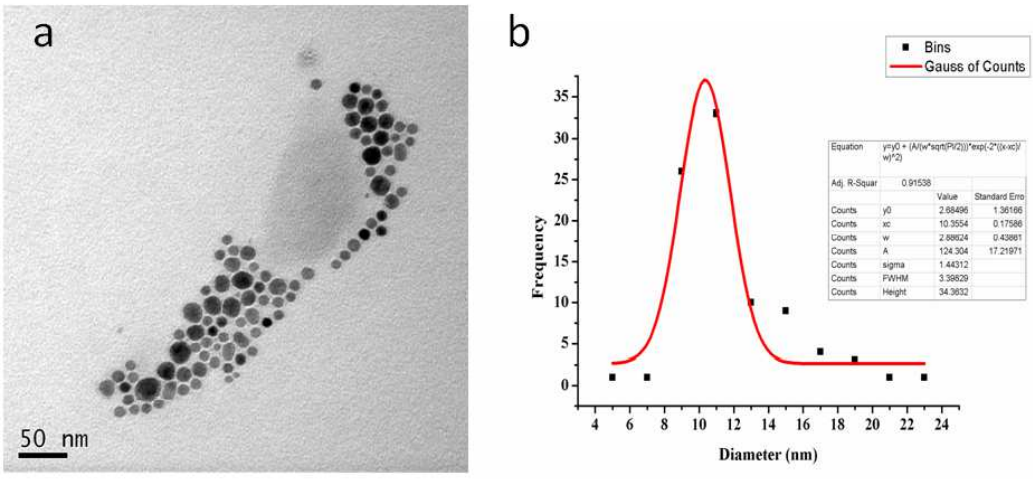

Figure 1. Transmission electron micrograph of SPIONS.

4.2.2 Dynamic light scattering and Zeta potential

The hydrodynamic diameter and Zeta potential values of synthesised and surface modified nanoparticles are shown in Table.3. The hydrodynamic diameter of synthesised SPIONS, DEX-SPIONS and PEG-SPIONS nanoparticle were 45 nm, 89.3 nm and 67 nm respectively with zeta value of -11, +7.67 and +6.07 mV respectively.

Table 3: Hydrodynamic diameter and Zeta potential value of synthesised nanoparticles

Particle	Hydrodynamic size (nm)	Zeta potential value (mV)
SPIONS	45.00	-11.00
DEX-SPIONS	89.30	+ 7.67
PEG-SPIONS	67.13	+ 6.07

4.2.3 X-Ray Diffraction analysis

Powder XRD analysis of SPIONS nanoparticles (Fig. 2) showed an inverse spinel structure of magnetite with the indices (2 2 0), (3 1 1), (4 0 0), (4 2 2), (5 1 1), and (4 4 0). The peak positions exactly matched with PDF number 01-071-6336, which further confirmed the formation of magnetite phase of iron oxide particles. Furthermore, the DEX-SPIONS and PEG-SPIONS (Fig. 2) XRD pattern also showed SPIONS peak positions which matched with PDF number.

4.2.4 Vibrational sample magnetometry

In VSM analysis, the magnetization curve at room temperature showed zero coercivity and remanence for all materials which is a characteristic property of superparamagnetic materials. SPIONS (Fig.3a) showed high saturation magnetization of 71 emu/g followed by PEG-SPIONS (Fig.3b) and DEX-SPIONS (Fig.3c), 59 emu/g and 38 emu/g respectively.

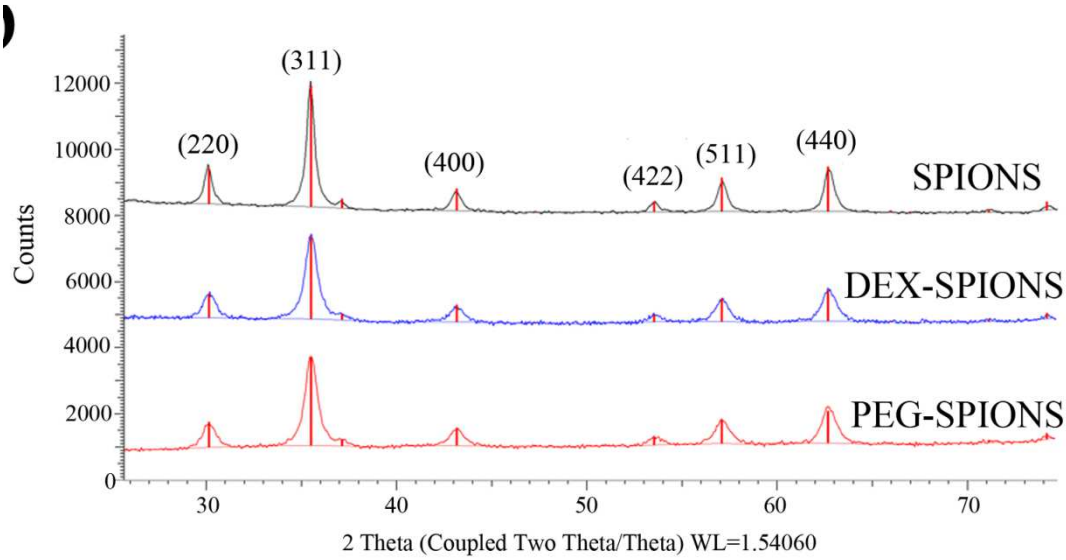

Figure 2. X-Ray Diffraction patterns of SPIONS, DEX-SPIONS and PEG-SPIONS.

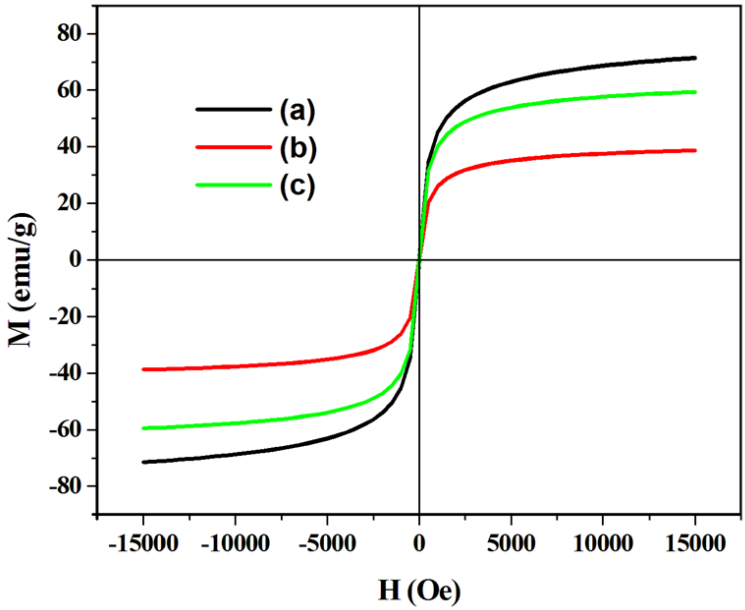

Figure 3. Vibrational sample magnetometry of a) SPIONS, b) DEX-SPIONS and c) PEG-SPIONS.

4.2.5 Fourier Transform –Infra Red spectra

The FT-IR spectra of SPIONS, DEX-SPIONS (Fig 4A) and PEG-SPIONS (Fig 4B) show the vibrational modes associated with C-O and Fe-O groups individually. The FT-IR spectrum of SPIONS has shown the prominent peaks at 573, 1621 and 3382 cm^{-1}. Distinct peaks around 570, 912, 1074, 1102, 1333, 1608, 2920 and 3317 cm^{-1}were noted in the FT-IR spectra of DEX-SPIONS. Spectrum of PEG-SPIONS showed peaks at 566, 842, 969, 1108, 1342, 1467, 1618, 2888 and 3385 cm^{-1}.

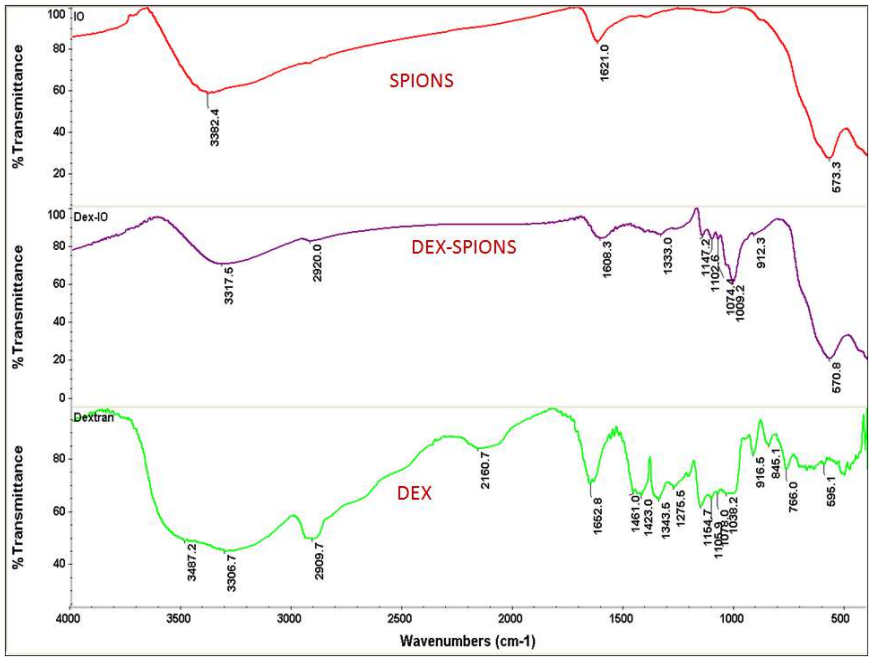

Figure 4A. FT-IR spectra of SPIONS and DEX-SPIONS.

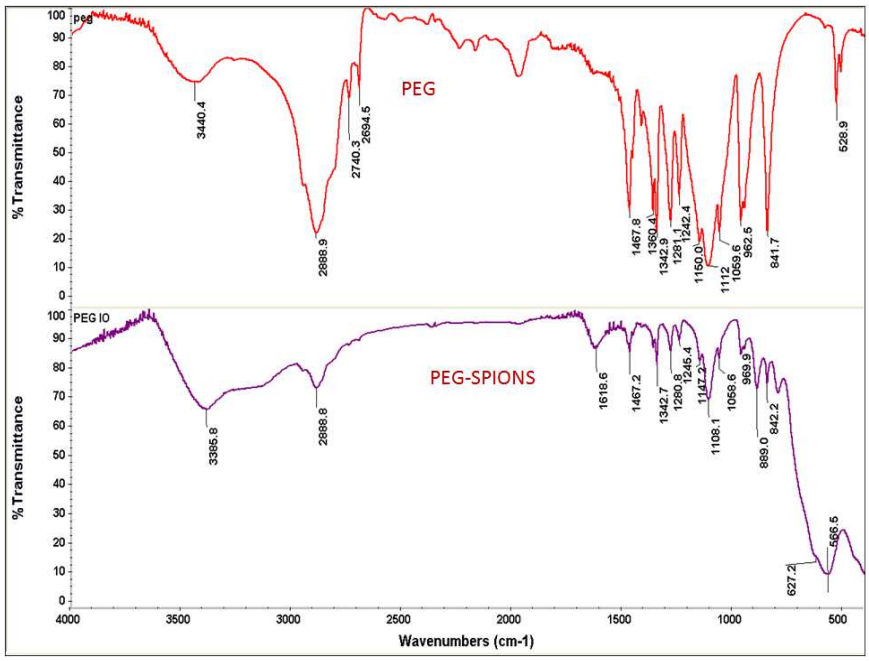

Figure 4B. FT-IR spectra of PEG-SPIONS.

4.2.6 Thermo Gravimetric Analysis

The TGA plot of SPIONS, DEX-SPIONS and PEG-SPIONS (Fig 5) showed the distinct stages of thermal decompositions at different temperatures. TGA plot of SPIONS shows four similar stages of decomposition around 58.14^{o}C, 216.77^{o}C, 333.65^{o}C, 583.96^{o}C and 794.60^{o}C corresponding to the total weight loss of 0.72%, 2.76%, 4.09%, 6.54% and 7.86%. TGA plot of DEX-SPIONS shows four distinct stages of thermal decompositions around 126.56^{o}C, 200.74^{o}C, 413.07^{o}C and 794.74^{o}C corresponding to the total weight loss of 1.08%, 12.59%, 24.75%, and 28.25%. TGA plot of PEG-SPIONS also shows four similar stages of decomposition around 119.81^{o}C, 218.24^{o}C, 270.91^{o}C, 519.27^{o}C and 794.51^{o}C corresponding to the total weight loss of 0.69%, 7.61%, 18.31%, 23.08% and 24.72%.

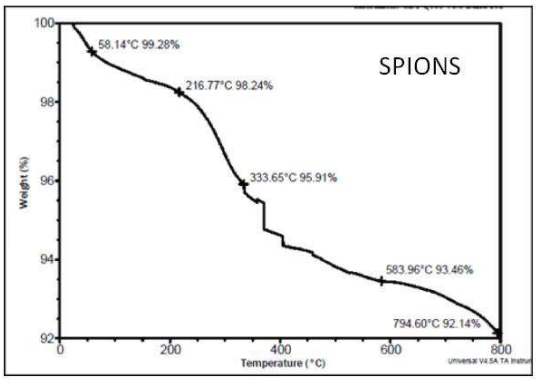

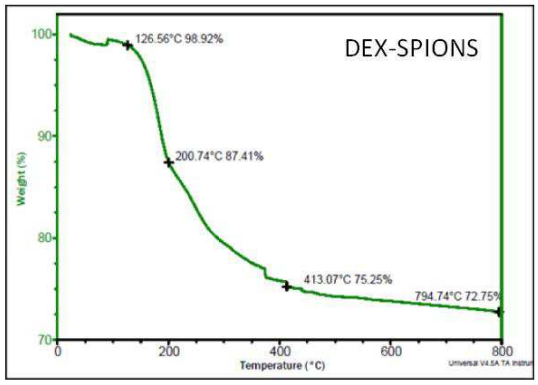

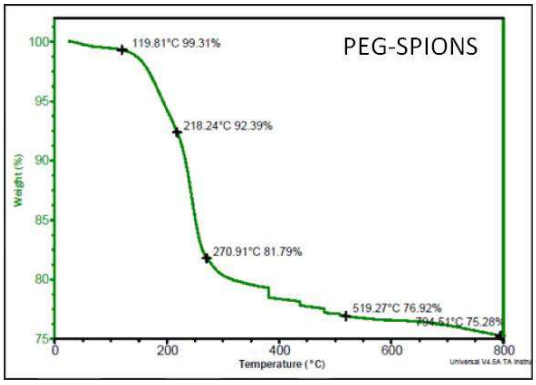

Sample	Total Weight loss
SPIONS	7.86 %
DEX-SPIONS	28.25 %
PEG-SPIONS	24.72%

Figure 5. Thermogravimetric analysis of SPIONS, DEX-SPIONS and PEG-SPIONS

4.3 *PHASE-II: Phase contrast microscopic studies*

Phase contrast microscopic evaluation of the L929 and RAW 264.7 cultures after 24 h showed the control cultures to have obtained confluency. The cells of L929 had attained the characteristic elongated spindle shaped morphology and RAW264.7 macrophages had attained the stellate shape with processes adhering to the surface of culture plate and round cells floating in the medium. When cultured in presence of 12.5, 25 and 50 µg/ml of SPIONS, DEX-SPIONS and PEG-SPIONS, the morphology of the cells was similar to that of control in L929 fibroblast (Fig 6). RAW264.7 macrophage cell line also showed similar results. The cells had also attained confluency. It was observed that the SPIONS nanoparticles tend to cluster and adhere to the fibroblasts and macrophages. Changes in cellular morphology were apparent with the cells appearing round with vacuolation in the cytoplasm at higher concentration of 50 µg/ml of SPIONS.

4.4 *MTT assay*

The results have shown that the obtained nanoparticles were not cytotoxic to the L929 cells and RAW 264.7 macrophages after 24 h exposure to a suspension of SPIONS, DEX-SPIONS, PEG-SPIONS at dose range of 50-12.25 µg/ml to the cells respectively. The metabolic activity of L929 cells cultured with SPIONS, DEX-SPIONS and PEG-SPIONS at 50 µg/ml were 63%, 105% and 100% respectively (Figure 7a). The metabolic activity of RAW 264.7 macrophage cells cultured with SPIONS, DEX-SPIONS and PEG-SPIONS at 50 µg/ml were 90%, 96% and 78% respectively (Figure 7b).

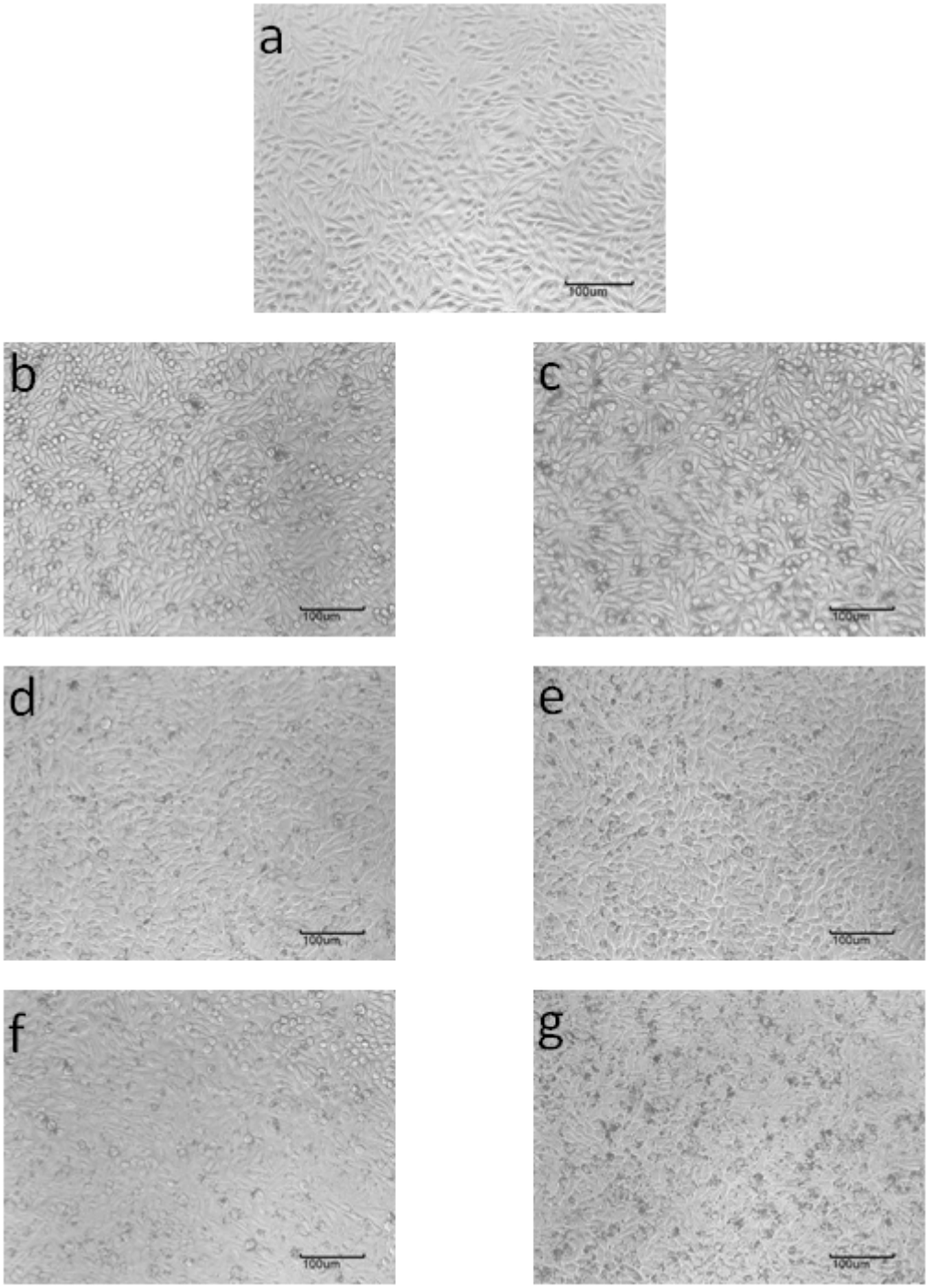

Figure 6. Phase contrast micrographs of L929 cells a) control b&c) 25 and 50 µg/ml SPIONS, d&e) 25 and 50 µg/ ml DEX-SPIONS f&g) 25 and 50 µg/ml PEG-SPIONS.

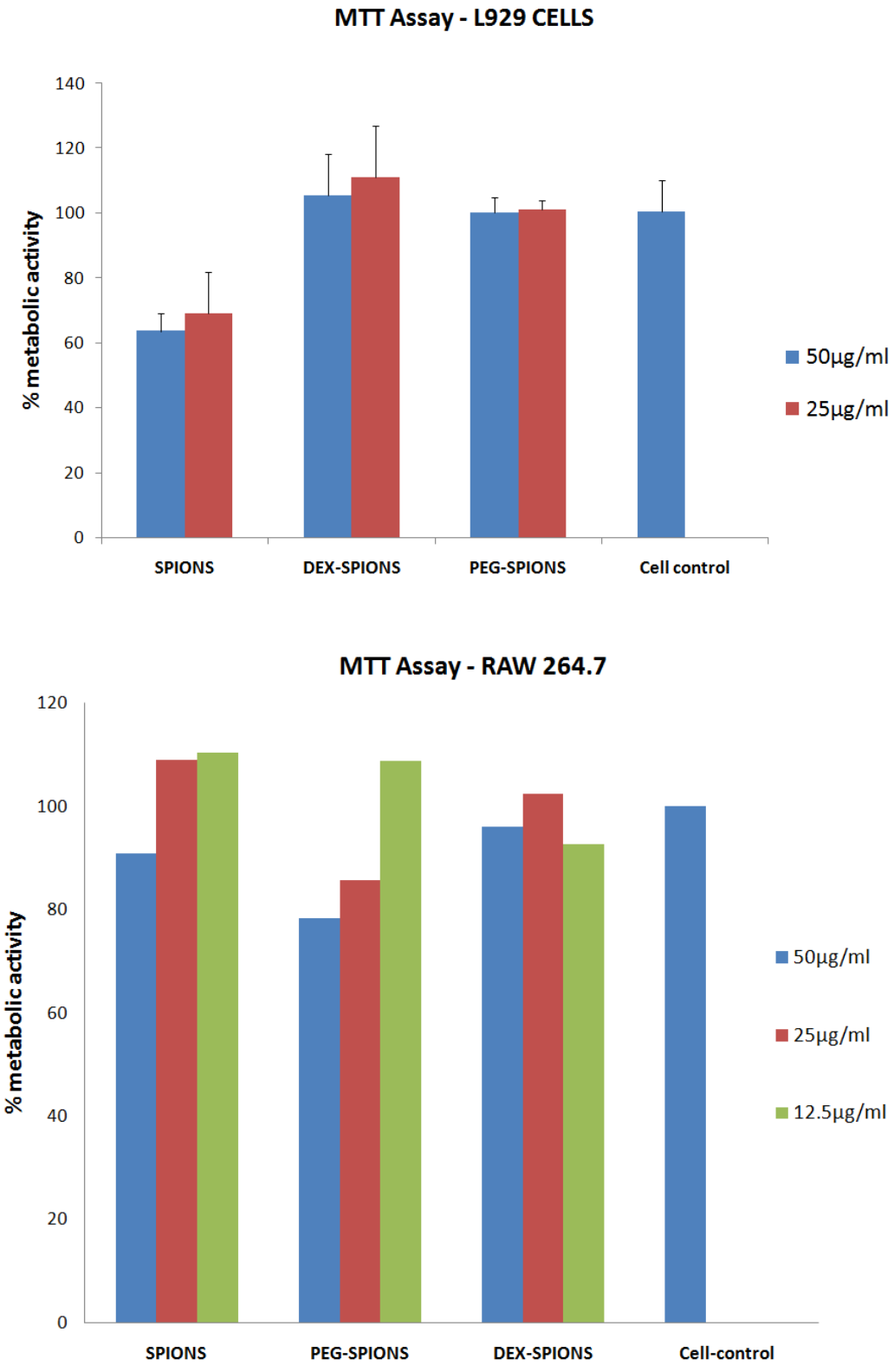

Figure 7. MTT assay in a) L929 cell lines b) RAW 264.7 cell lines

SPIONS affected the metabolic activity in concentration dependent manner when they were added in the concentration range of 50-12.25 µg/ml to the cells. It was observed that the cell proliferation/viability decreased when the concentration of SPIONS increased.

4.5 *Live and dead assay*

Under fluorescent light, live cells appeared green in colour and dead cells appeared orange or red in colour. Examination of the fibroblast cultures 24 h post nanoparticle challenge revealed that at 50 µg/ml concentration, there was a non significant decrease in the viability of the cells in culture with SPIONS (Figure 8b) and was similar to that of the control (Figure 8a). In DEX-SPIONS (Figure 8c) and PEG-SPIONS (Figure 8d) challenged group, more than 95 percentage cells remain viable.

4.6 *In-Vitro Oxidative stress analysis*

4.6.1 SOD activity

The average levels of SOD in HepG2 cells exposed to 50 µg/ml of SPIONS, DEX-SPIONS and PEG-SPIONS were 1.19 ± 0.01, 1.88 ± 0.02 and 1.77 ± 0.01 respectively when compared to control 0.04 ± 0.02. The level of SOD in HepG2 cells increased significantly in SPIONS, DEX-SPIONS and PEG-SPIONS groups (Table.4) when compared to control group. Within nanoparticle treated groups SOD level was significantly low in SPIONS group when compared to PEG-SPIONS group and DEX-SPIONS. Within coated groups it was significantly low in PEG-SPIONS group.

Table 4. *In vitro* oxidative stress studies in HepG2 cells showing the levels (average ± SD) of SOD, GSH, NO and LPO of control, SPIONS, DEX-SPIONS and PEG-SPIONS groups.

Parameter	Control	SPIONS	DEX-SPIONS	PEG-SPIONS
SOD	0.04 ± 0.02	1.19 ± 0.01*	1.88 ± 0.02*$^{\#}$	1.77 ± 0.01*$^{\#@}$
GSH	0.29 ± 0.12	1.00 ± 0.16*	1.09 ± 0.10*	1.27 ± 0.14*
NO	227.70 ± 4.95	297.00 ± 40.52*	245.85 ± 7.56	298.65 ± 29.00*
LPO	3.47 ± 0.02	3.97 ± 0.01* $^{\#}$	3.57 ± 0.02*$^{@}$	3.45 ± 0.02
*,#,@ - Significance level $p < 0.05$ * - Control vs SPIONS, DEX-SPIONS, PEG-SPIONS # - SPIONS vs DEX-SPIONS, PEG-SPIONS @ - DEX-SPIONS vs PEG-SPIONS				

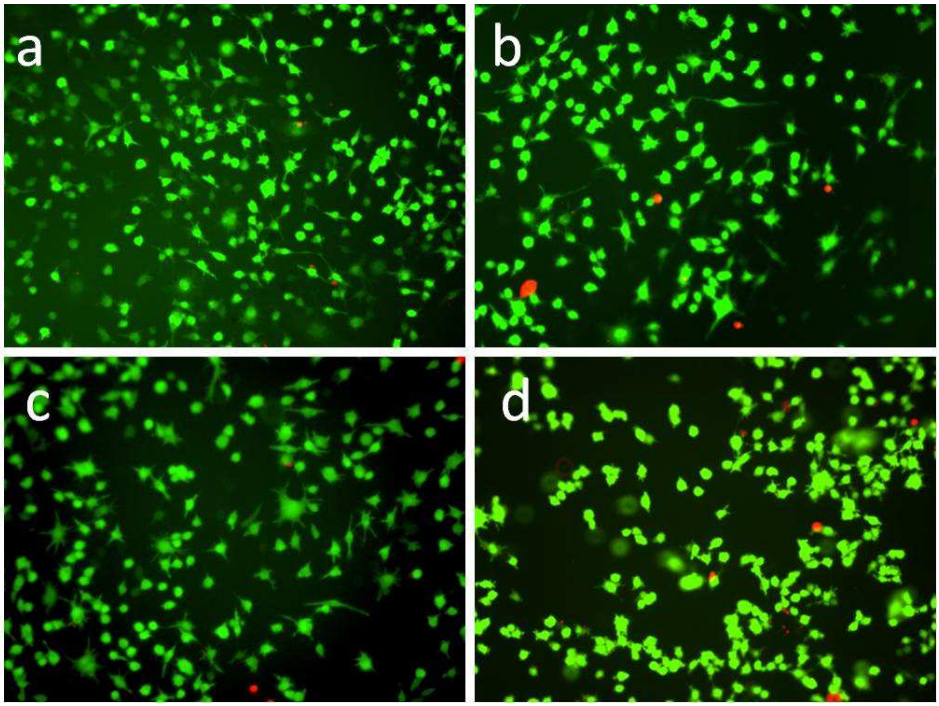

Figure 8. Live and Dead assay a) control, b) SPIONS, c) DEX-SPIONS and d) PEG-SPIONS.

4.6.2 GSH level

The average level of GSH in HepG2 cells exposed to 50 µg/ml of SPIONS, DEX-SPIONS and PEG-SPIONS were 1.00 ± 0.16, 1.09 ± 0.10 and 1.27 ± 0.14 respectively when compared to control 0.29 ± 0.12. The level of reduced glutathione in HepG2 cells was increased (Table.4) significantly in SPIONS, DEX-SPIONS and PEG-SPIONS groups as compared to control group. No statistically significant difference could be observed within treated groups.

4.6.3 Nitrite level

The average level of Nitrite in HepG2 cells exposed to 50 µg/ml of SPIONS, DEX-SPIONS and PEG-SPIONS were 297.00 ± 40.52, 245.85 ± 7.56 and 298.65 ± 29.00 respectively when compared to control 227.70 ± 4.95. The level of nitrite in HepG2 cells was increased significantly in SPIONS and PEG-SPIONS groups but was not significant in DEX-SPIONS group (Table.4) when compared to control group. No statistically significant difference could be observed within treated groups.

4.6.4 Lipid peroxidation

The average level of MDA in HepG2 cells exposed to 50 µg/ml of SPIONS, DEX-SPIONS and PEG-SPIONS were 3.97 ± 0.01, 3.57 ± 0.02 and 3.45 ± 0.02 respectively when compared to control 3.47 ± 0.02. A significant increase in lipid peroxides level was noted in HepG2 cells SPIONS group and DEX-SPIONS group when compared with control groups (Table.4). Within treated groups, lipid peroxide level was significantly high in SPIONS group when compared to PEG-SPIONS group and DEX-SPIONS and within coated groups significantly high in DEX-SPIONS group.

4.7 *Raman chemical mapping of L929 and RAW cells treated with SPIONS, DEX-SPIONS and PEG-SPIONS*

Phase contrast image of representative cells with the corresponding confocal Raman image of SPIONS, DEX-SPIONS and PEG-SPIONS are shown in figures 9 A, B and C and figure 10. Raman bands of water (3350–3550 cm^{-1}, valence band with maximum at about 3400cm^{-1}) and protein (2800–3020 cm^{-1}, C-H stretching region) were identified. The bands at 1664 and 1264 cm^{-1} are related to the amide I and III vibrations. Raman spectra of nucleus region showed, C=N, C=C, and C=O double bond stretching frequencies of the planar bases between 1600 and 1700 cm^{-1}. "Phosphate" of nucleic acid (phosphodiester linkage) band was observed at ca. 1235 and 1085 cm^{-1}. The intense band at 1449 cm^{-1} can be assigned to the CH_2 and CH_3 bending mode of proteins. The cluster analysis was performed on the characteristic Raman spectral scan obtained and the color coded Raman image is also shown in figures along with the corresponding Raman spectra. The blue spectrum and region corresponds to the SPIONS present in the cytoplasm of the L929 cells, green being the cell and black region corresponds to the medium (buffer). Nanoparticles are mostly localized around the cell nucleus in the cytoplasm corresponding to the multiplexed signals at 680 cm^{-1}.

4.8 *Haemocompatibility studies*

4.8.1 Haematology

The percentage change in haematological parameters pre and post treatment with SPIONS, DEX-SPIONS and PEG-SPIONS nanoparticles are given in Table 5.

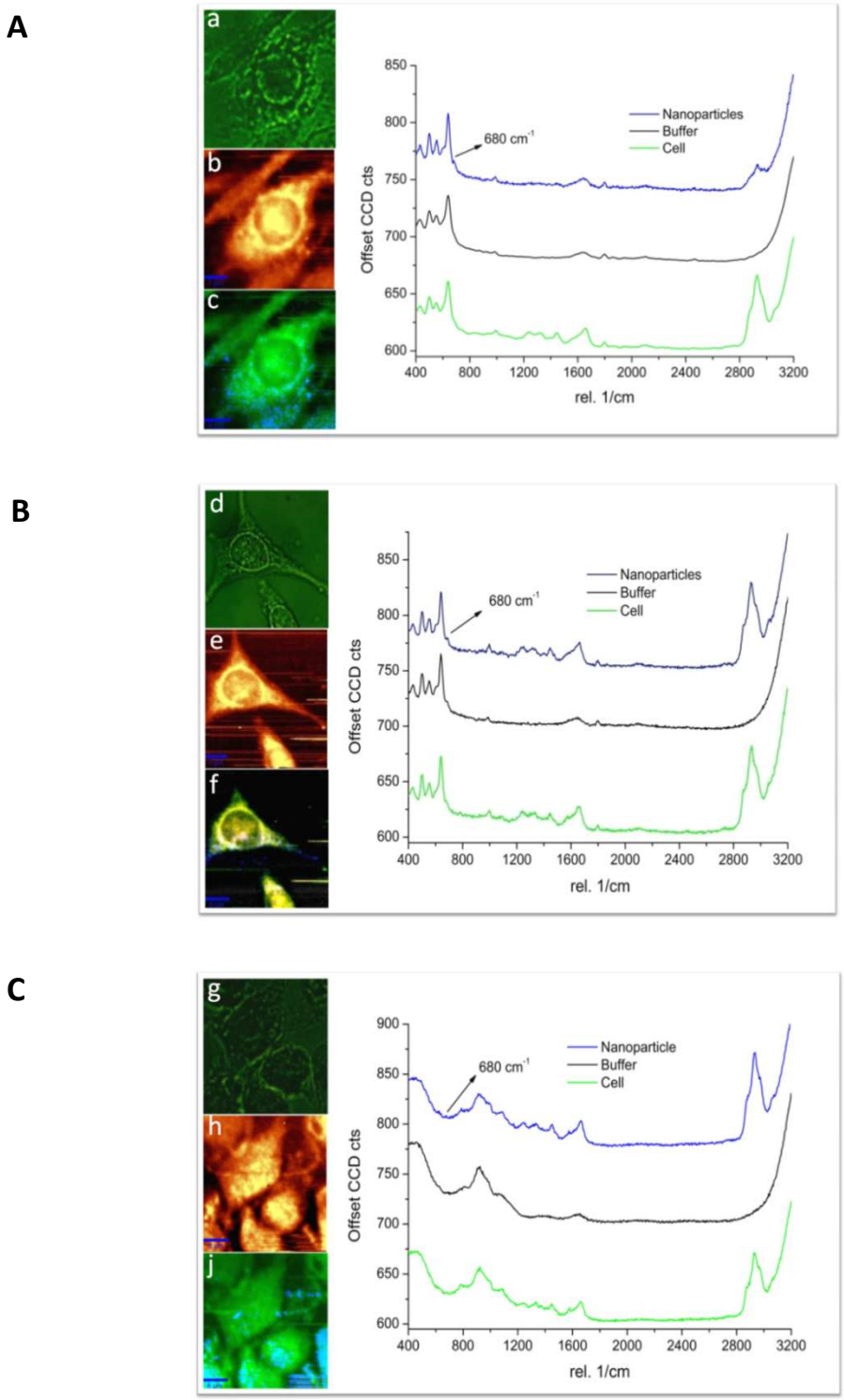

Figure 9. Confocal Raman images of L929 cells with A) SPIONS B) DEX-SPIONS C) PEG-SPIONS. a,d,g) Phase contrast images b,e,h) Confocal Raman images c,f,j) Raman chemical mapping images

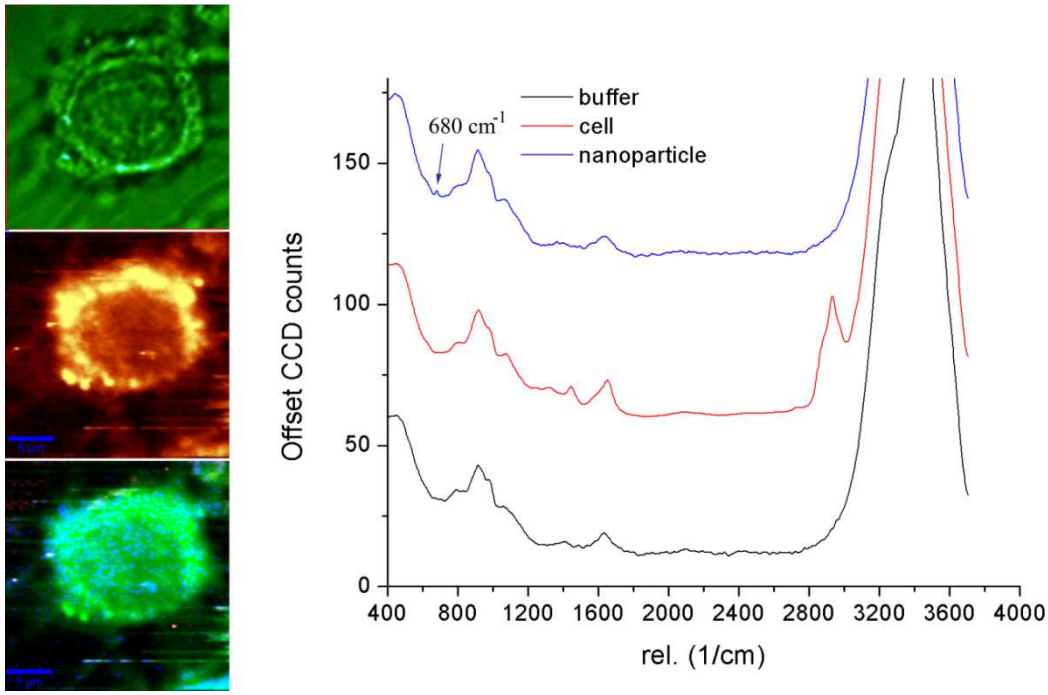

Figure 10. Confocal Raman image of RAW 264.7 with SPIONS.

The difference in percentage change in haematological parameters evaluated was less than 10% and was found to be insignificant for all parameter studied.

Table 5: Percentage change in haematology parameters pre and post treatment

Parameter	SPIONS	DEX-SPIONS	PEG-SPIONS
WBC	4.24±3.78	5.67±3.76	5.28±3.48
RBC	1.80±0.96	6.51±2.44	0.34±0.12
Hb	2.24±1.48	6.80±3.22	1.75±1.12
HCT	1.39±1.77	7.25±2.31	0.90±0.51
MCV	0.79±0.18	0.75±0.30	0.60±0.41
MCH	2.53±2.01	1.45±0.94	1.71±1.05
MCHC	2.12±1.56	1.43±0.18	1.33±1.24
PLT	7.34±4.12	3.06±1.36	1.44±0.66

4.8.2 Hemolysis assay

The hemolysis assay is based on RBC lysis and the release of hemoglobin to the surrounding medium. The hemolytic potential of the SPIONS, DEX-SPIONS and PEG-SPIONS were found to be negligible and fell within the acceptable limit of <5%. Hemolysis percent are given in Table 6. This result is confirmed by the obtained results of haematological parameters where there is no significant decrease in erythrocytes, hemoglobin and hematocrit.

Table 6: Percentage hemolysis post treatment

Group	**% hemolysis**
SPIONS	0.05 ± 0.015
DEX-SPIONS	0.09 ± 0.023
PEG-SPIONS	0.07 ± 0.030

Altogether these data show the safety of SPIONS, DEX-SPIONS and PEG-SPIONS nanoparticles in relation to erythrocytes.

4.9 *Genocompatibility by comet assay*

The determination of DNA damage of cells grown with bare and surface modified nanoparticles give a clear idea about the genotoxic potential of the nanoparticles. The comets resulting from exposure to the SPIONS, DEX-SPIONS and PEG-SPIONS did not differ from that of the control. With control and test nanoparticles the relatively undamaged cells give comets consisting of a compact head without any prominent tail, indicating double-stranded intact DNA (Figure 11). The mean comet lengths for the L929 cells exposed to test nanoparticles as

compared with control are presented in Table 7. For test nanoparticles, DNA in the head region is more than 99% and in the tail region, it is less than 1%.

Table 7: Comet assay attributes

Attributes	CONTROL	SPIONS	DEX-SPIONS	PEG-SPIONS
%DNA in Tail	0.34±0.63	0.02±0.04	0.12±0.17	0.31±0.40
%DNA in Head	99.66±0.63	99.98±0.04	99.88±0.17	99.69±0.40
Olive Moment	0.07±0.13	0.00±0.00	0.00 ±0.01	0.02±0.03

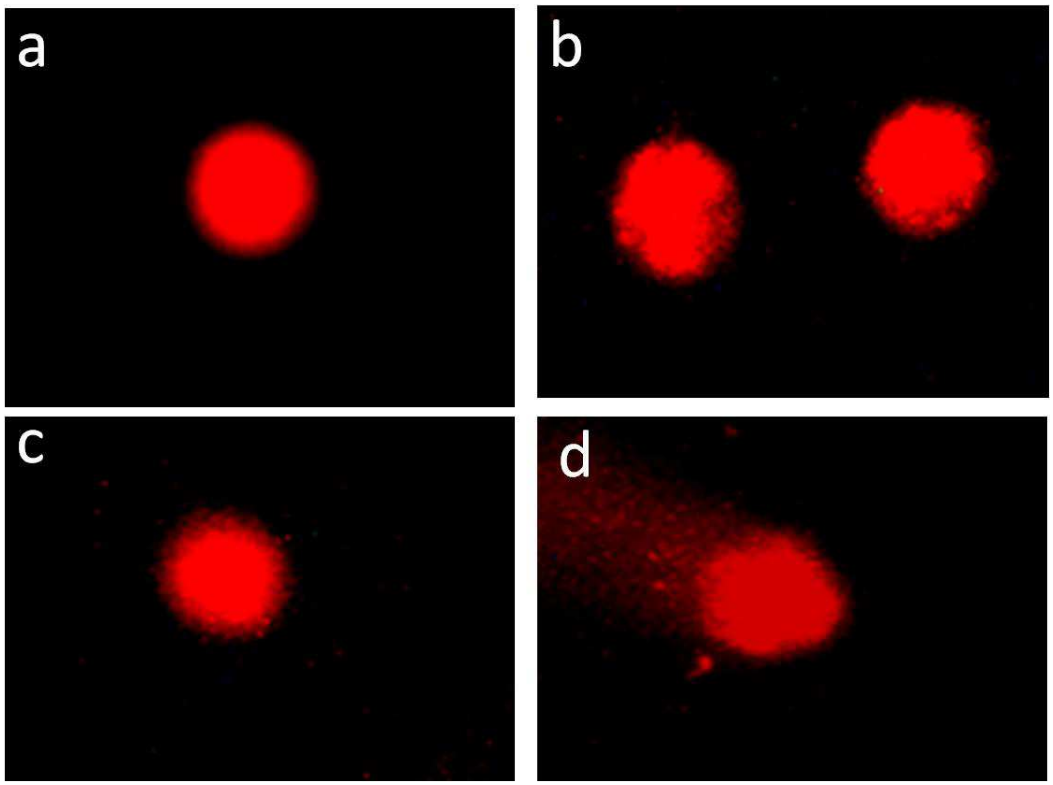

Figure 11. Comet assay a) control, b) SPIONS, c) DEX-SPIONS and d) PEG-SPIONS.

4.10 *Phase-III: Animal experiment-Clinical observation and Gross pathology*

All the animals exposed to nanoparticles were observed closely during the 24 hours. No adverse signs and symptoms were observed in animals treated with SPIONS, DEX-SPIONS and PEG-SPIONS. There was no mortality. At the end of observation period, all animals were sacrificed. Gross examination showed all the organs to be normal.

4.11 *Haematology*

The results of haematological parameters are given in the Fig 12. Haematology results of the SPIONS, DEX-SPIONS and PEG-SPIONS treated groups of rats post 24 h of intravenous injection demonstrated that the white blood cells (WBC), red blood cells (RBC), hematocrit (HCT), mean corpuscular volume (MCV), hemoglobin (HGB), platelets (PLT), mean corpuscular hemoglobin (MCH), and mean corpuscular hemoglobin concentration (MCHC), lymphocytes (LYMP) did not change significantly except mixed cells (MXD). The mixed cell populations of treated groups were significantly increased when compared to control group. Within treated groups, DEX-SPIONS group has shown more number of mixed cells followed by PEG-SPIONS and SPIONS group.

4.12 *Biochemical assays*

The results of biochemical parameters are given in the Fig 13. The blood biochemical parameters like alkaline phosphatase, glucose, cholesterol, triglycerides, uric acid, creatinine, chloride, calcium, phosphorous, albumin and total protein (Fig 13 a,b,c,d) were within normal limits in treated groups. The SGPT level (Fig 13e)

was significantly increased in treated groups and the SGOT level (Fig 13e) was significantly increased in DEX-SPIONS group when compared to control group.

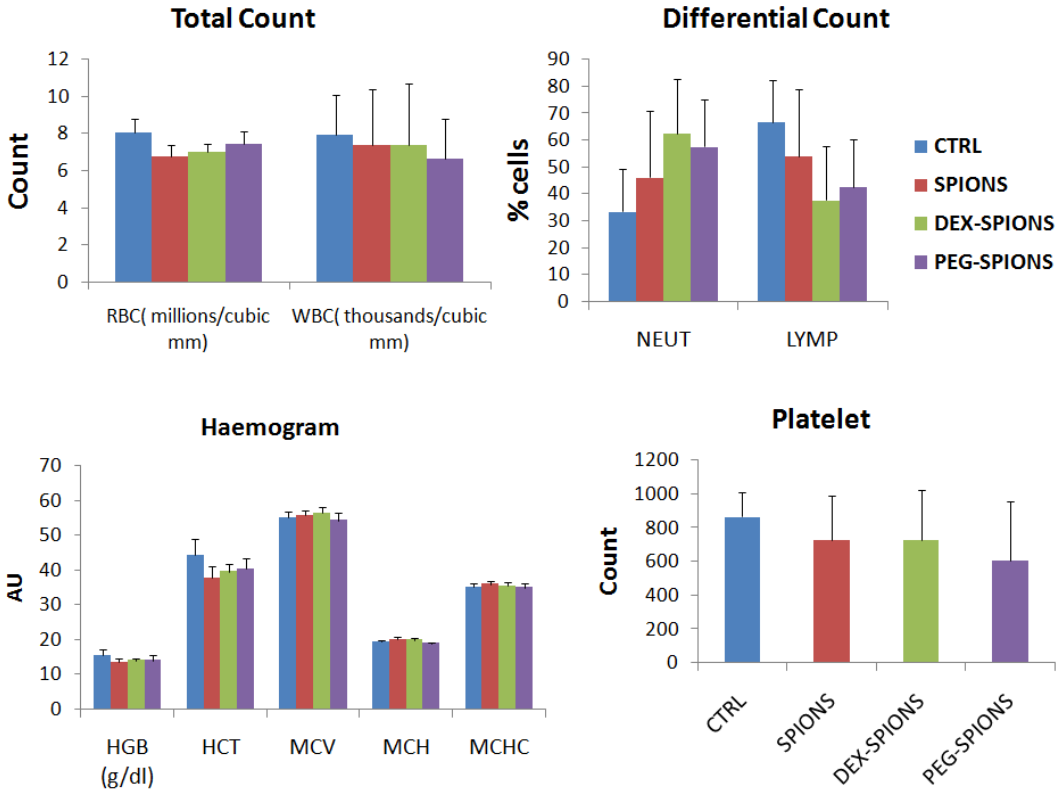

Figure 12. Haematology results of the SPIONS, DEX-SPIONS and PEG-SPIONS treated rat post 24 h of intravenous injection. White blood cells (WBC), Red blood cells (RBC), Hematocrit (HCT), Mean Corpuscular Volume (MCV), Hemoglobin (HGB), Platelets (PLT), Mean Corpuscular Hemoglobin (MCH), and Mean Corpuscular Hemoglobin Concentration (MCHC). Values represent means ± SD, *n* = 4 - 6.

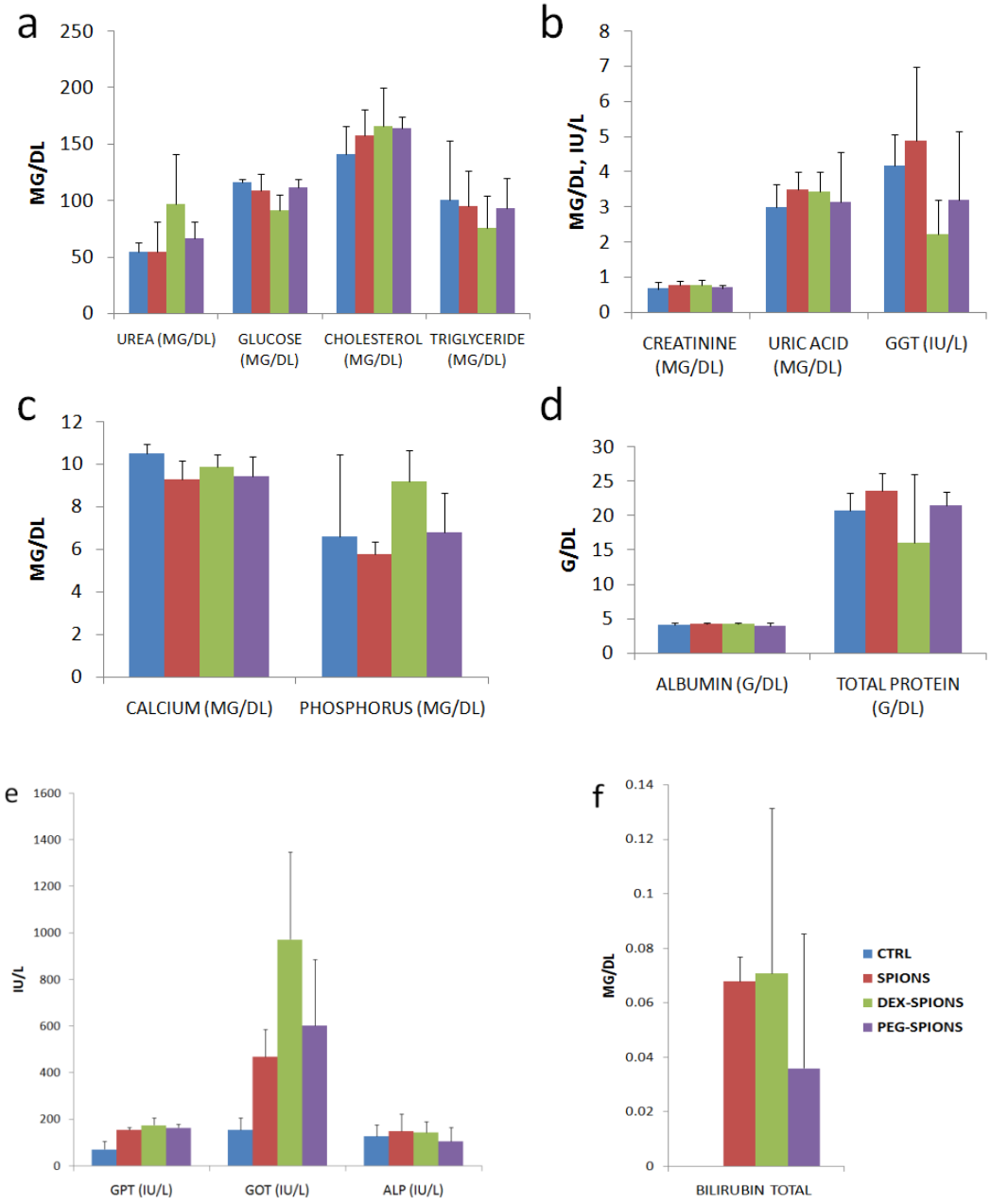

Figure 13. Blood biochemistry results of the SPIONS, DEX-SPIONS and PEG-SPIONS treated rat post 24 h of intravenous injection.**a-d)** Total Protein (TP), Glucose (GLU), Cholesterol (CHOL), Triglycerides (TGY), Alkaline phosphatase (ALP), Gamma Glutamyl Transferase (GGT), Albumin (ALB), Calcium (CAL), Phosperous (PHOS), Chlorides (CL), Urea (UR), Uric acid and Creatinine (CREA). Values represent means ± SD, *n* = 4-6. (**e)** Changes in serum SGOT and SGPT level (values represents mean ± SD, n=4 to 6, * - $p<0.05$ Control vs. DEX-SPIONS, PEG-SPIONS. # - $p<0.05$ SPIONS vs DEX-SPIONS). (**f)** Serum total bilirubin content.

GGT level (Fig. 13b) was significantly increased in SPIONS group when compared to control group. Bilirubin content (Fig 13c) was detected in the serum of treated groups and found to be within the normal range for this species but in the control group it is below the detectable limit.

4.13 *Flow cytometry*

The results of the Forward Scattering vs Side Scattering dot plot are given in the Fig 14. It was demonstrated that the granular cell populations of treated groups were significantly increased when compared to control group.

4.14 *Oxidative stress studies in tissues*

4.14.1 SOD activity

The level of SOD in liver, lung, spleen, kidney and heart tissue homogenates of SPIONS, DEX-SPIONS and PEG-SPIONS treated animals was decreased (Figure 15c) but not statistically significant when compared to control group. Within treated groups SOD level was low in SPIONS and PEG-SPIONS group when compared to DEX-SPIONS where it was slightly increased. There was an unpredictable variation between individual animals in control and treated groups.

4.14.2 Level of GSH

The level of reduced glutathione in liver, lung, spleen and kidney tissue homogenates of SPIONS, DEX-SPIONS and PEG-SPIONS treated animals was decreased (Figure 15b) significantly ($p<0.05$) except in pulmonary tissue of DEX-SPIONS when compared to control group. The reduced glutathione level was also decreased in heart among treated groups but there is no statistical significance when compared to control.

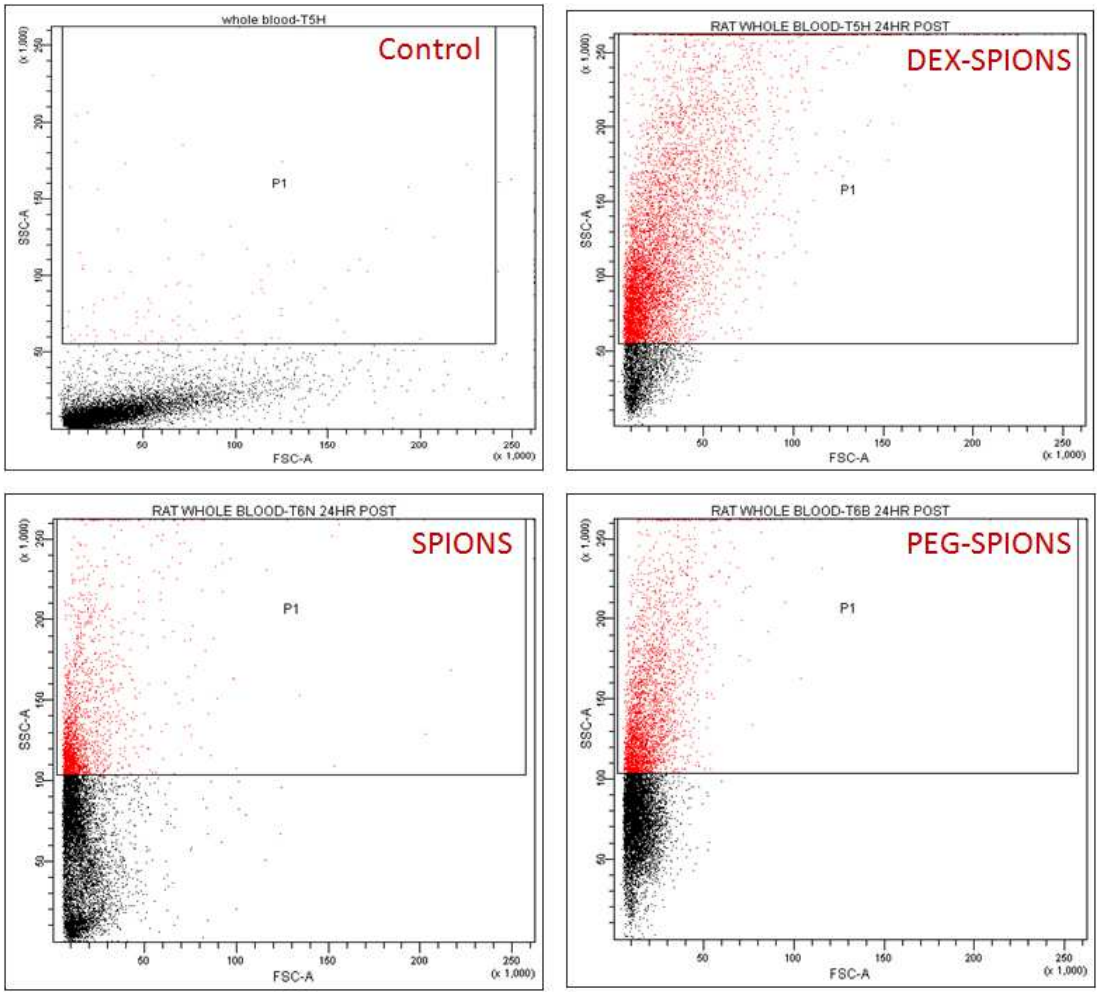

Figure 14. Flow Cytometry results of the SPIONS, DEX-SPIONS and PEG-SPIONS treated rat 24 h post intravenous injection.

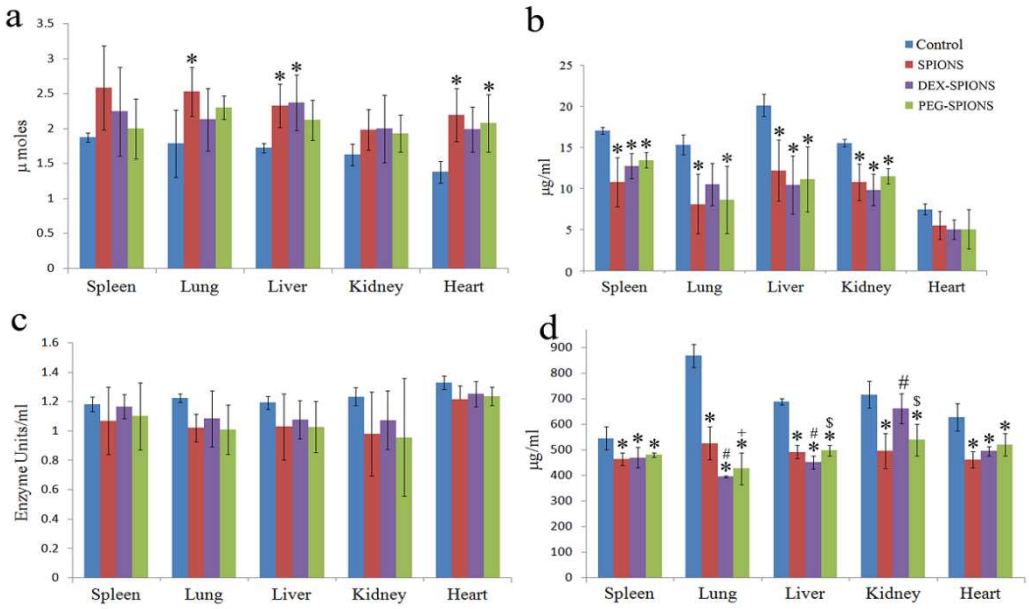

Figure 15. *In vivo* oxidative stress analysis in liver, spleen, kidney and lung tissues **(a)** Lipid peroxidation (LPO) * - p<0.05 Control vs SPIONS, DEX-SPIONS and PEG-SPIONS. **(b)** Glutothione sulf-hydryl (GSH). **(c)** Super oxide dismutase (SOD). **(d)** tissue nitrite (NO) level (Values represents mean ± SD, n=4 to 6, * - p<0.05 control vs SPIONS, DEX-SPIONS and PEG-SPIONS, # - p<0.05 SPIONS vs DEX-SPIONS, + - p<0.05 SPIONS vs PEG-SPIONS, $ - p<0.05 PEG-SPIONS vs DEX-SPIONS)

4.14.3 Lipid peroxidation

A significant (p<0.05) increase in lipid peroxides level in liver, lung and heart tissue homogenates of SPIONS treated animals was noted when compared with control groups (Figure 15a). There was a significant (p<0.05) increase in heart lipid peroxide level observed between control and PEG-SPIONS group. Significant (p<0.05) increase in liver lipid peroxide level was also noted between control and DEX-SPIONS group.

4.14.4 Nitrite level

The level of nitrite in liver, lung, spleen, kidney and heart tissue homogenates of SPIONS, DEX-SPIONS and PEG-SPIONS treated animals was decreased (Figure

15d) significantly ($p<0.05$) except in kidney tissue of PEG-SPIONS when compared to control group. There was a significant ($p<0.05$) decrease in nitrite level in kidney tissue of SPIONS as compared to DEX-SPIONS group, in liver tissue of DEX-SPIONS compared to SPIONS and PEG-SPIONS group, in pulmonary tissue of PEG-SPIONS compared to SPIONS group and in kidney tissue of PEG-SPIONS compared to DEX-SPIONS group.

4.15 *Histopathology*

The histopathological assessment was carried out on the following tissues namely salivary glands, pharynx, trachea, lung, heart, thymus, liver, spleen, kidneys, stomach, duodenum, jejunum, ileum, colon, caecum, rectum, ovary, fallopian tubes, uterus, vagina, accessory sex glands, skin, skeletal muscle (gluteus), eyes, cerebrum, cerebellum and spinal cord.

Figure16 shows the microscopic observations of the liver. Liver architecture was normal in all groups. In SPIONS group (Figure 16b), hepatocytes with discrete nucleus, moderate granular cytoplasmic degeneration and multi focal intra hepatocyte cholestasis were found compared to control group (Figure 16 a). In DEX-SPIONS group (Figure 16c), few polymorphonuclear cells and moderate proliferation of Kuppfer cells with brown-yellow cytoplasmic pigments were seen in the sinusoidal space. Hepatocytes with discrete nucleus and eosinophilic dark granular cytoplasm were observed. In PEG-SPIONS group (Figure 16d), very few Kuppfer cells with occasional brown-yellow cytoplasmic pigments were seen in the sinusoidal space and hepatocytes with discrete nucleus and granular cytoplasm was observed. Iron deposits stained blue with Prussian blue stain were present in the

cytoplasm of Kupffer cells in the SPIONS, DEX-SPIONS group and they were also seen in sinusoids and cytoplasm of hepatocytes in PEG-SPIONS group (Figure 16 e-h).

The histological micrographs of kidneys show normal architecture (Figures 17). In SPIONS group, glomeruli appeared normal in the cortex region. Protein casts were observed in the collecting tubular lumen. Tubular epithelial cells with enlarged nuclei, formation of prominent nucleoli and marked granular cytoplasm (Figure 17j) were observed. In DEX-SPIONS group (Figure 17k) focal tubular degeneration was seen with the tubular epithelium showing moderate granular cytoplasmic degeneration. In PEG-SPIONS group (Figure 17l) glomeruli architecture was normal. Protein casts were noted in the convoluted tubular lumen.

The pattern of SPIONS nanoparticles distribution in kidney tissues using Perl's Prussian blue staining revealed iron deposits in the cytoplasm of convoluted tubule cells in the SPIONS group, DEX-SPIONS group and PEG-SPIONS group. These deposits were also seen in the glomerular region in PEG-SPIONS group (Figure 17m-p).

Pulmonary architecture was preserved in all groups (Figures 18). In SPIONS (Figure 18b) group infiltration of macrophages in the alveolar septa was seen. In DEX-SPIONS (Figure18c) group, infiltration of macrophages in the alveolar septa and peribronchial region was seen. In PEG-SPIONS (Figure 18d) group, mild peribronchial infiltration of macrophages was noted. The pattern of SPIONS

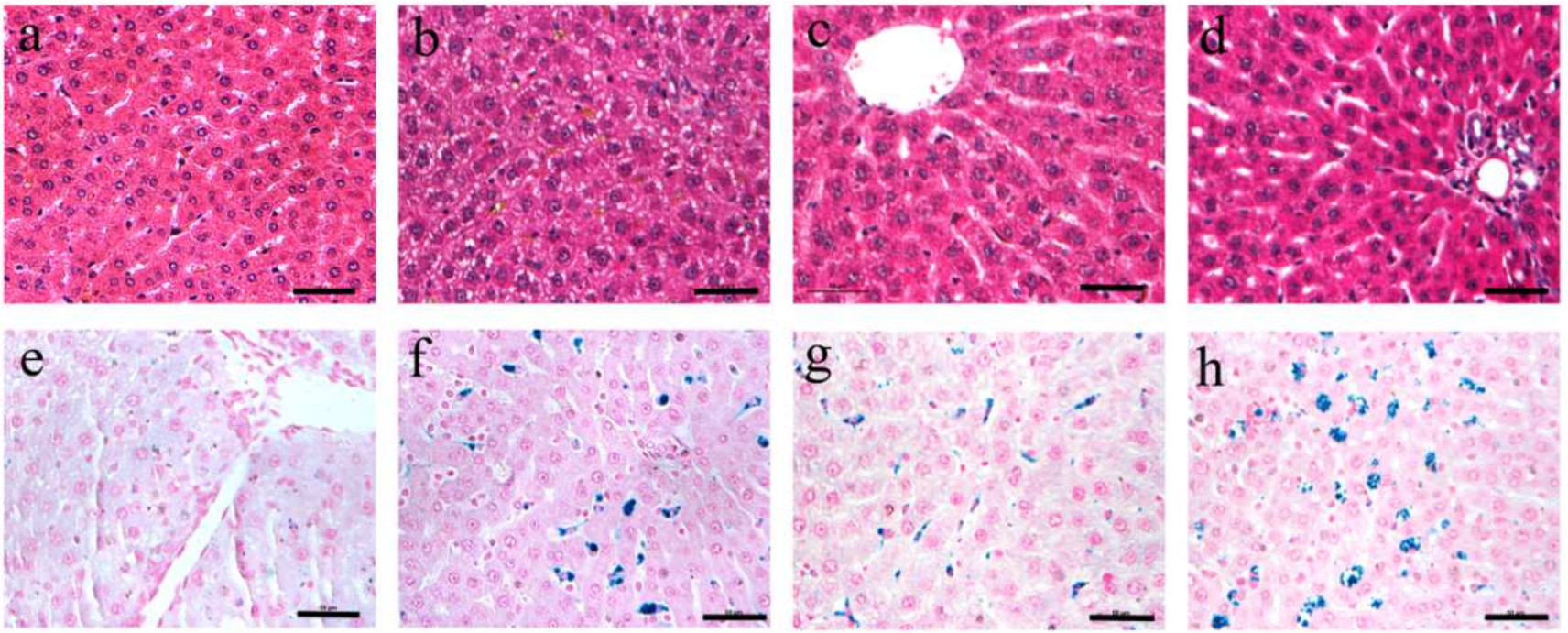

Figure 16. Haematoxylin and eosin staining of liver (**a)** Control (**b)** SPIONS group showing the bile pigments in the cytoplasm of hepatocytes. (**c)** DEX-SPIONS group showing Kupffer cells. (**d)** PEG-SPIONS group. Prussian blue staining of liver (**e)** Control (**f)** SPIONS group with iron laden Kupffer cells. (**g)** DEX-SPIONS group with iron laden Kupffer cells in the sinusoidal space. (**h)** PEG-SPIONS group with iron pigments in the hepatocyte and sinusoidal space. Scale bar 50µm.

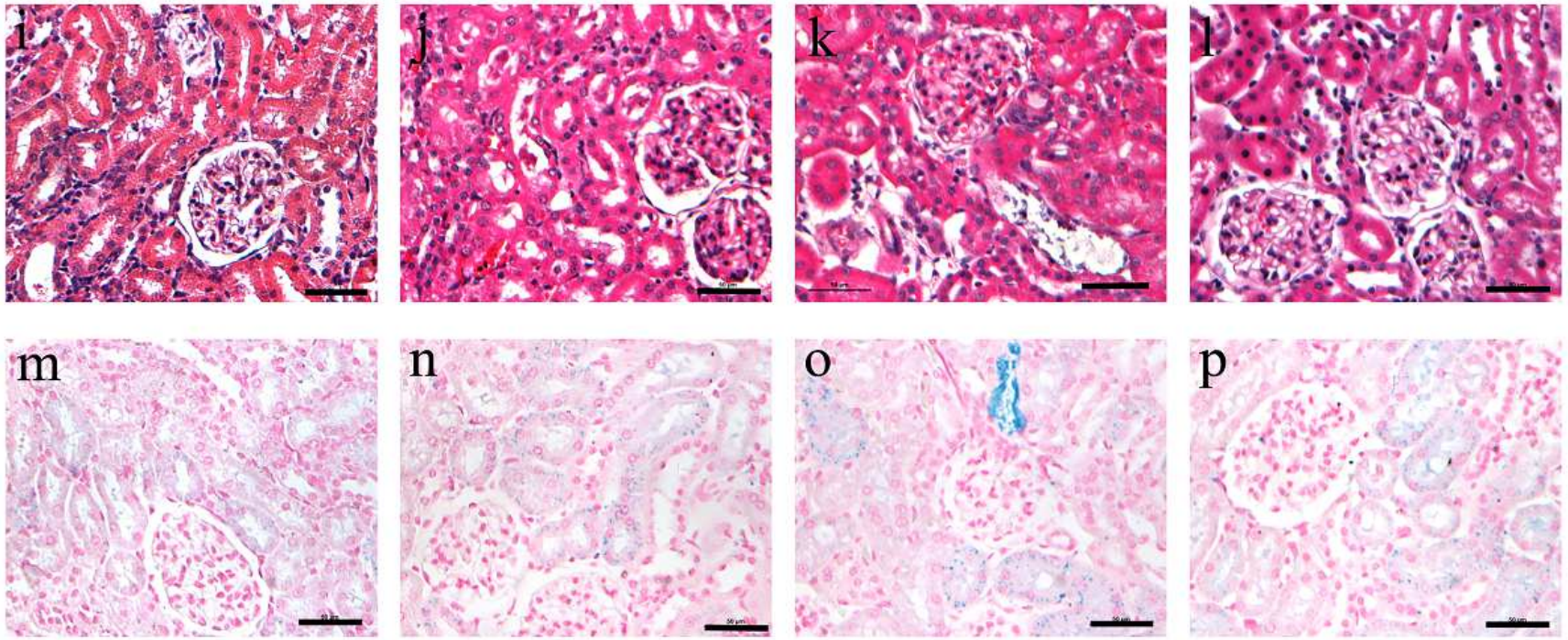

Figure 17. Haematoxylin and eosin staining of kidney (**i)** Control (**j)** SPIONS group showing protein casts in the lumen convoluted tubules. (**k)** DEX-SPIONS group showing the degenerated proximal convoluted tubule. (**l)** PEG-SPIONS group. Prussian blue staining of kidney (**m)** Control (**n)** SPIONS group showing iron pigments in the cytoplasm of convoluted tubule epithelium. (**o)** DEX-SPIONS group showing iron pigments in the cytoplasm of convoluted tubule epithelium. (**p)** PEG-SPIONS group showing iron pigments in the lumen of convoluted tubules. Scale bar 50µm.

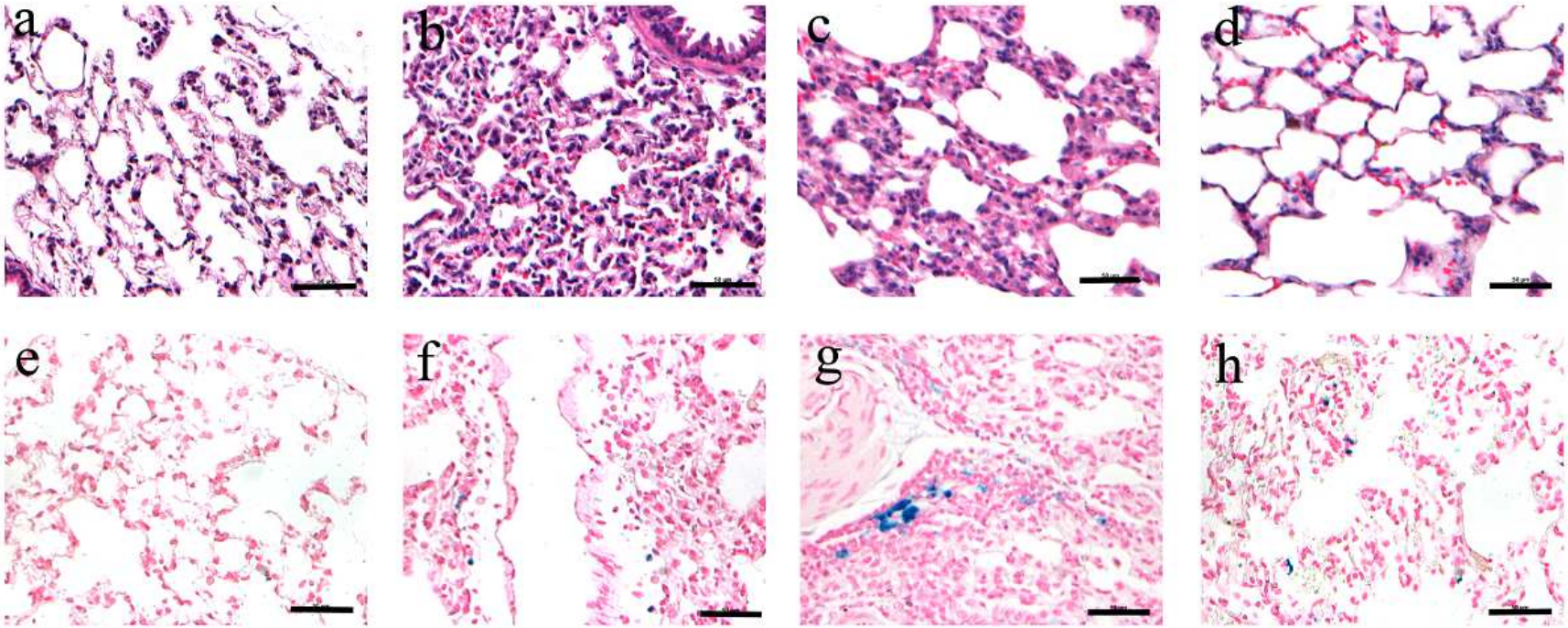

Figure 18. Haematoxylin and eosin staining of lung (**a)** Control (**b)** SPIONS group showing the mononuclear cell infiltration in alveolar region. (**c)** DEX-SPIONS group showing the thickening of alveolar septa with mononuclear cell infiltration. (**d)** PEG-SPIONS group. Prussian blue staining of lung (**e)** Control (**f)** SPIONS group with iron laden macrophages in the perivascular region. (**g)** DEX-SPIONS group with iron laden macrophages in the peribronchial region. (**h)** PEG-SPIONS group showing the diffuse presence of iron pigments in the alveolar region. Scale bar 50µm.

distribution in pulmonary tissues was further investigated using Perl's Prussian blue staining for the detection of iron. Iron deposits in the cytoplasm of macrophage cells were observed in the SPIONS group in the alveolar region, macrophages of peribronchial region in DEX-SPIONS group and perivascular region in PEG SPIONS group (Figure 18 e-h).

Spleenic architecture was normal in all groups (Figures 19). In SPIONS and DEX-SPIONS group (Figure 19 j,k), brown siderotic pigments were seen in the macrophages in spleenic red pulp. In PEG-SPIONS group (Figure 19l), relatively increased numbers of macrophages were observed in the spleenic red pulp. Perl's Prussian blue staining for the detection of iron showed blue pigment deposits in the cytoplasm of macrophage cells in the red pulp region in the SPIONS group, DEX-SPIONS group and PEG-SPIONS group (Figure 19 m-p) with more intensity in the later group. Mast cells were absent in DEX-SPIONS and SPIONS group and were scant in PEG-SPIONS group as compared to control group.

Histological sections of heart showed normal architecture (Figure 20 a-d). There were no changes in striations and no nuclear changes. Perl's Prussian blue staining showed iron deposits in the perivascular region in the SPIONS group, DEX-SPIONS group and PEG-SPIONS group (Figure 20 e-h).

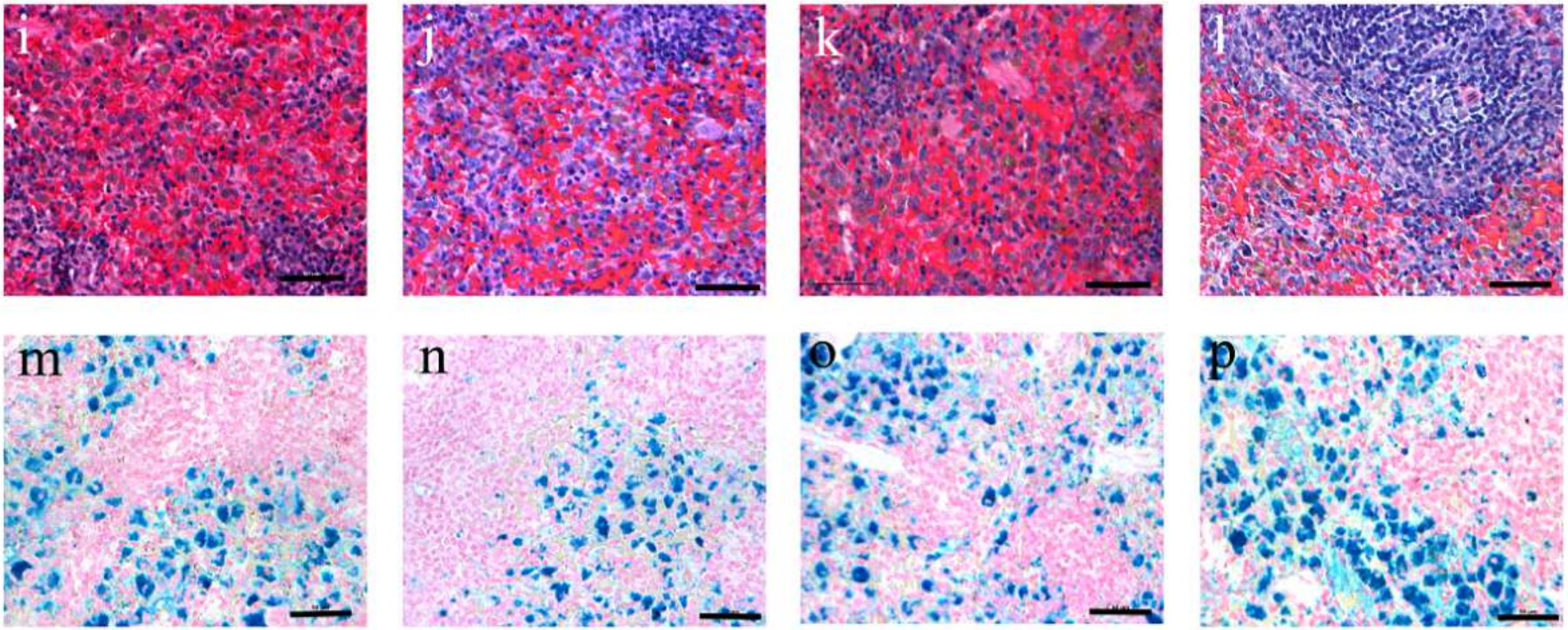

Figure 19. Haematoxylin and eosin staining of spleen (**i)** Control (**j)** SPIONS (**k)** DEX-SPIONS (**l)** PEG-SPIONS. Prussian blue staining of spleen (**m)** Control (**n)** SPIONS (**o)** DEX-SPIONS (**p)** PEG-SPIONS. Scale bar 50 µm.

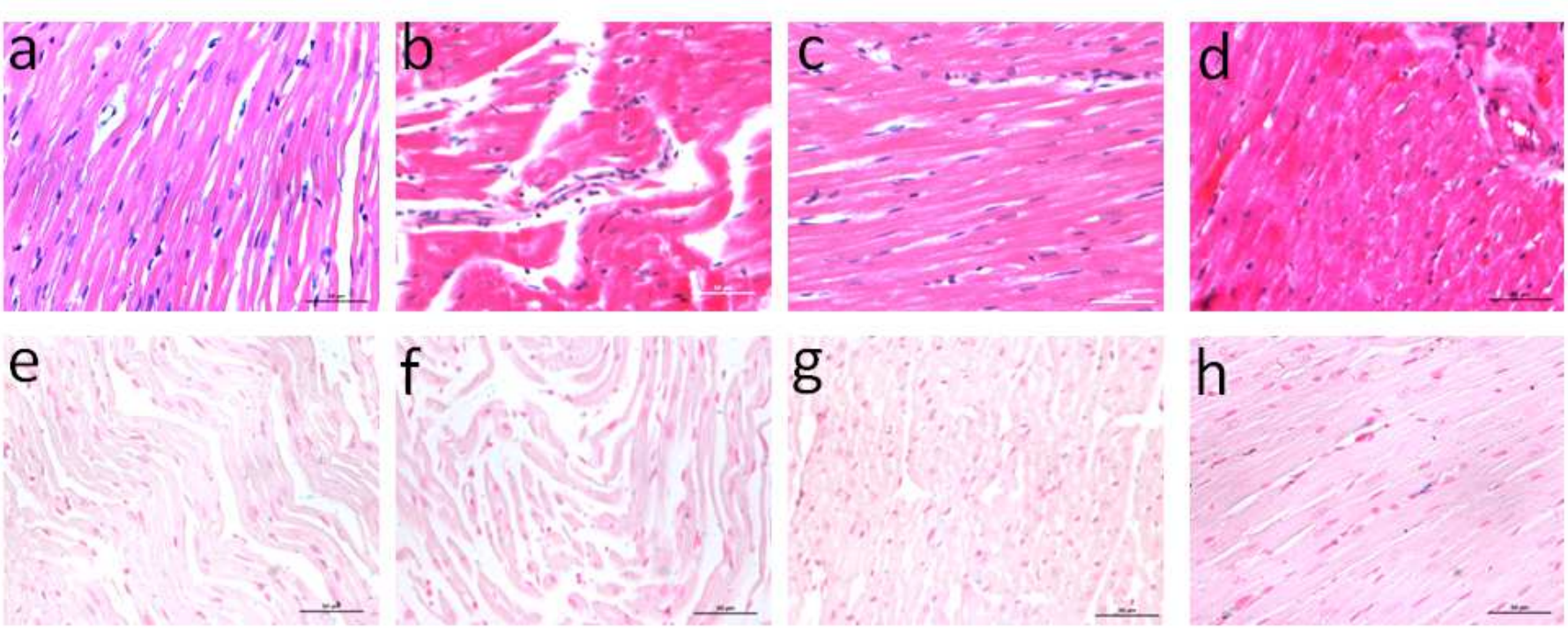

Figure 20. Haematoxylin and eosin staining of heart a) Control b) SPIONS c) DEX-SPIONS d) PEG-SPIONS. Prussian blue staining of heart e) Control f) SPIONS g) DEX-SPIONS h) PEG-SPIONS. Scale 50 µm.

Histological sections of cerebral cortex showed normal architecture in the SPIONS group, DEX-SPIONS group and PEG-SPIONS group (Figure 21 a-f). The outer pia mater, plexiform layer, pyramidal layer, granular layer and polymorphic cell layer showed normal architecture. Blood capillaries surrounded by a clear Virchow-Robin space were observed. Cresyl violet stained sections revealed Nissl bodies in the neurons present in the outer cortex region in the SPIONS group, DEX-SPIONS group and PEG-SPIONS group (Figure 22 a-f).

Histological sections of cerebellum showed normal architecture (Figure 23 a-f). The outer molecular layer and inner granular layer were appeared normal. Purkinje cells were appeared normal. Granule cells were appeared normal in the inner granular layer.

Sections from salivary glands, pharynx, trachea, thymus, stomach, duodenum, jejunum, ileum, colon, caecum, rectum, ovary, fallopian tubes, uterus, vagina, accessory sex glands, skin, skeletal muscle (gluteus), eyes and spinal cord appeared histologically normal.

4.15.1 Histomorphometry for mast cells

In liver, mast cells were observed more in DEX-SPIONS but not statistically significant and almost similar in SPIONS and PEG-SPIONS group, when compared to control group (Figure 25). Mast Cells were mostly distributed in the periportal region in all groups (Figure 24a-d).

In, kidney, mast cells were absent in the renal cortex in all three groups and control group. They were mostly present in the hilus and medulla region in all groups.

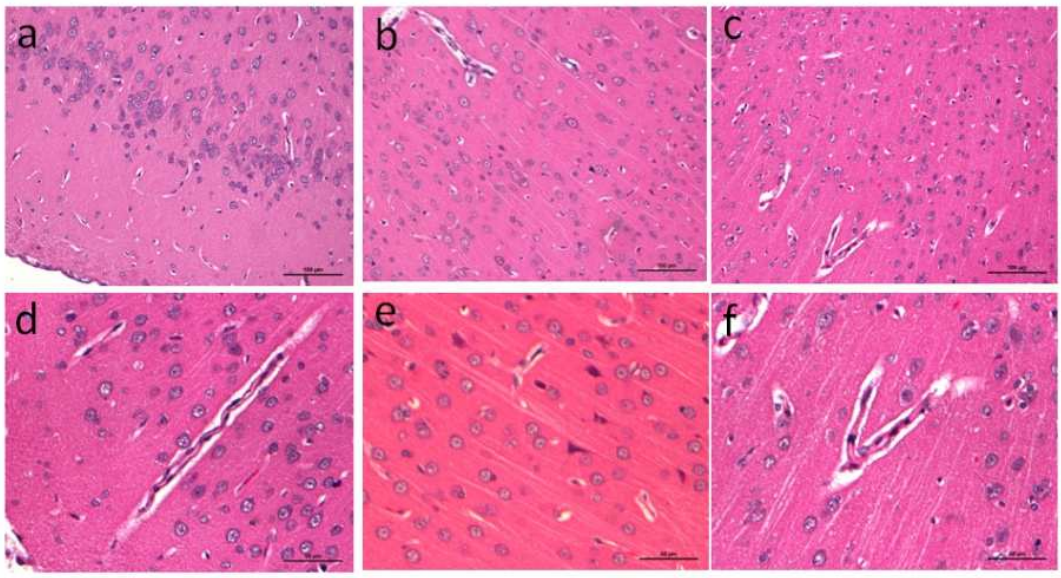

Figure 21. Haematoxylin and eosin staining of cerebrum a&d) SPIONS, b&e) DEX-SPIONS c&f) PEG-SPIONS.

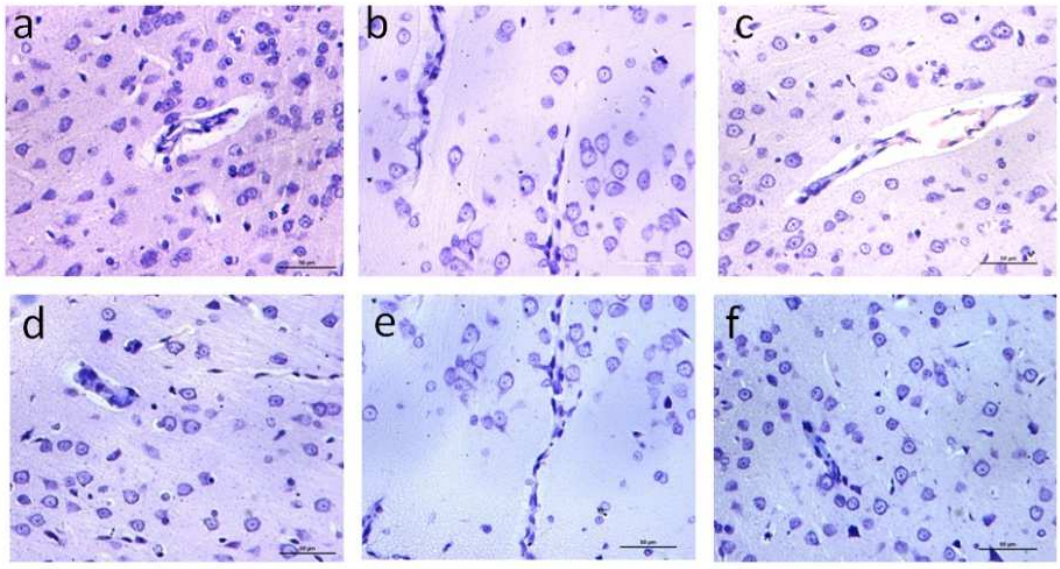

Figure 22. Cresyl violet staining of cerebrum a&d) SPIONS b&e) DEX-SPIONS and c&f) PEG-SPIONS.

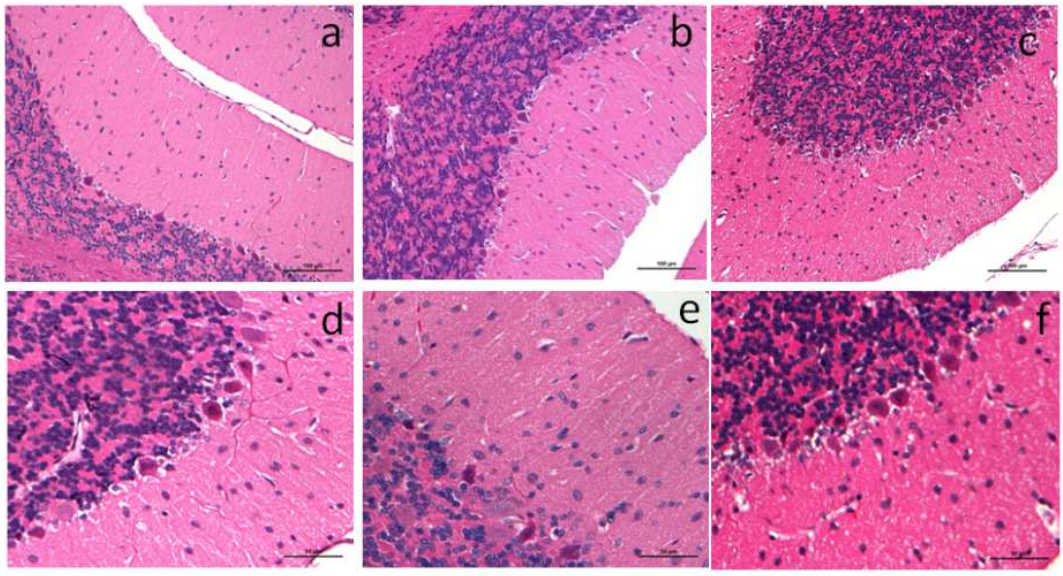

Figure 23. Haematoxylin and eosin staining of cerebellum a&d) SPIONS b&e) DEX-SPIONS c&f) PEG-SPIONS.

In the lung, mast cells were observed to be significantly ($p<0.05$) more in DEX-SPIONS and SPIONS group. Numerous mast cells were also present in PEG-SPIONS group, though not statistically significant as compared to control group (Figure 25). They were mostly distributed in the alveolar region in all groups (Figure 24e-h).

In spleen, mast cells were absent in DEX-SPIONS and SPIONS group and occasional mast cell was observed in PEG-SPIONS group compared to control group.

In heart, mast cells were observed significantly ($p<0.05$) more in PEG-SPIONS and followed by DEX- SPIONS and SPIONS groups as compared to control group (Figure 25). They were mostly distributed in the peri vascular region in all groups and additionally in the sub endocardial region of SPIONS group (Figure 24i-l).

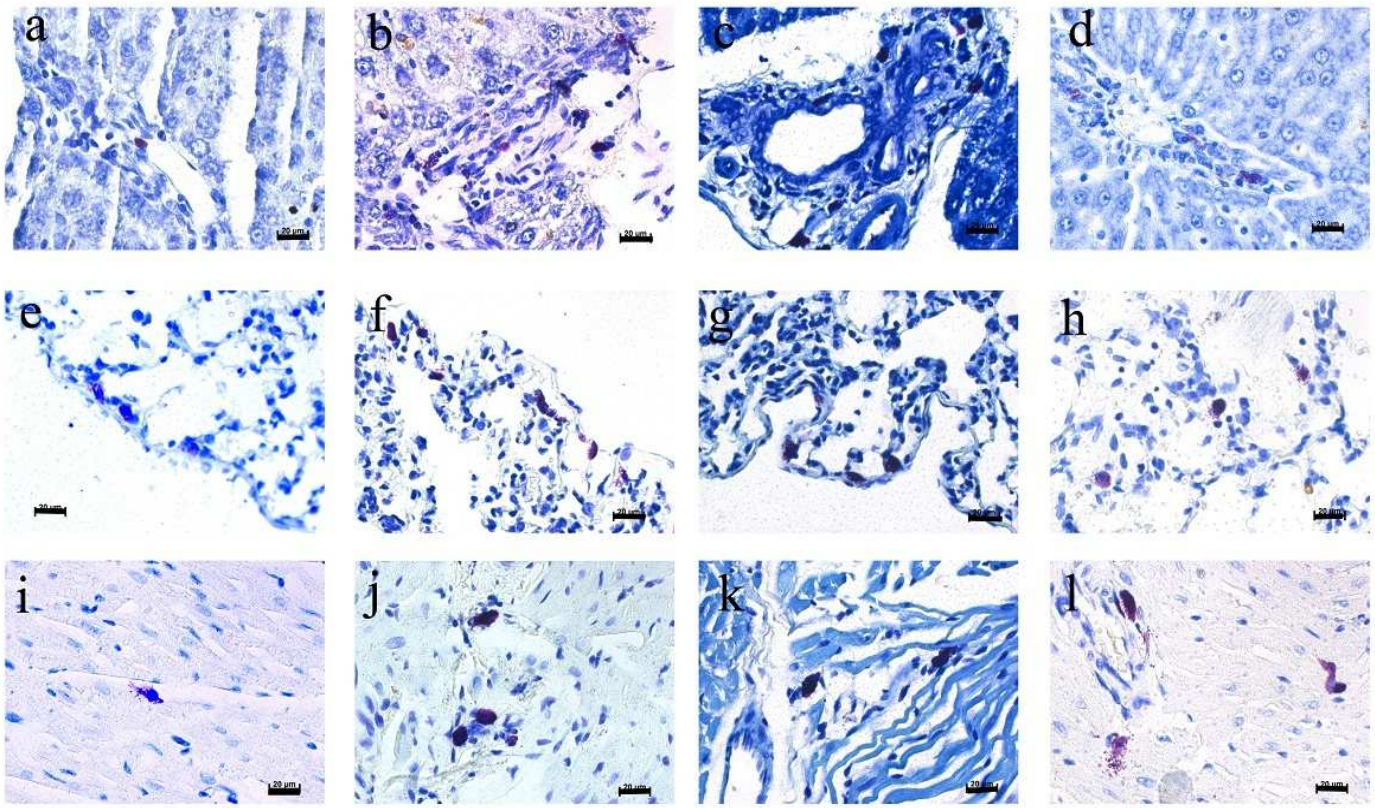

Figure 24. Toluidine blue staining showing the presence of mast cells in liver (**a)** Control (**b)** SPIONS group periportal region. (**c)** DEX-SPIONS group periportal region. (**d)** PEG-SPIONS group periportal region. Lung (**e)** Control alveolar region. (**f)** SPIONS group alveolar region. (**g)** DEX-SPIONS group alveolar region. (**h)** PEG-SPIONS group alveolar region. Heart (**i)** Control group perivascular region (**j)** SPIONS group perivascular region (**k)** DEX-SPIONS group perivascular region (**l)** PEG-SPIONS group perivascular region. Scale bar 20 µm.

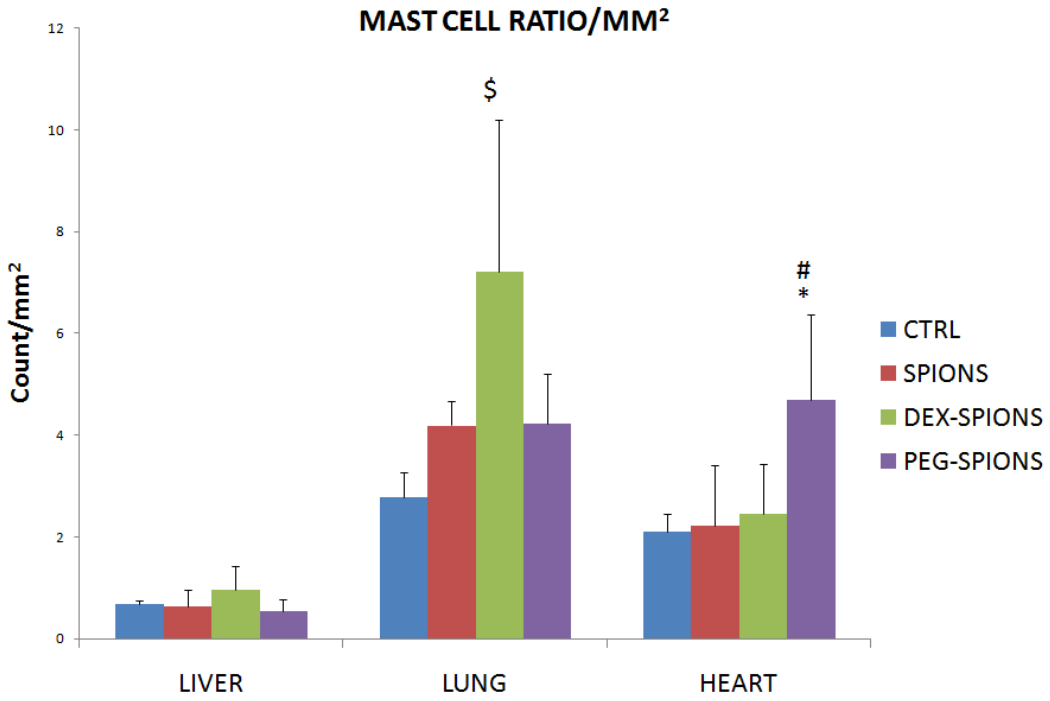

Figure 25. *In vivo* histomorphometry analysis of mast cell count (values represents mean ± SD, n=4 to 5, $ - $p<0.05$ Control vs. DEX-SPIONS, * -$p<0.05$ Control vs PEG-SPIONS, # - $p<0.05$ SPIONS vs PEG-SPIONS).

4.16 *Transmission electron microscopy study of liver*

The ultrastructural images of liver injected with DEX-SPIONS, PEG-SPIONS and SPIONS are shown in fig 26. In SPIONS (Figure 26 a,b), DEX-SPIONS (Figure 26 c,d) groups, Kuppfer cells with aggregates of iron particles were seen in the cytoplasm but were not in PEG-SPIONS group (Figure 26 e,f). The few Kuppfer cells in reflect the absence in TEM. The absence is correlated with the few Kuppfer cells observed in H&E stained semi-thin sections.

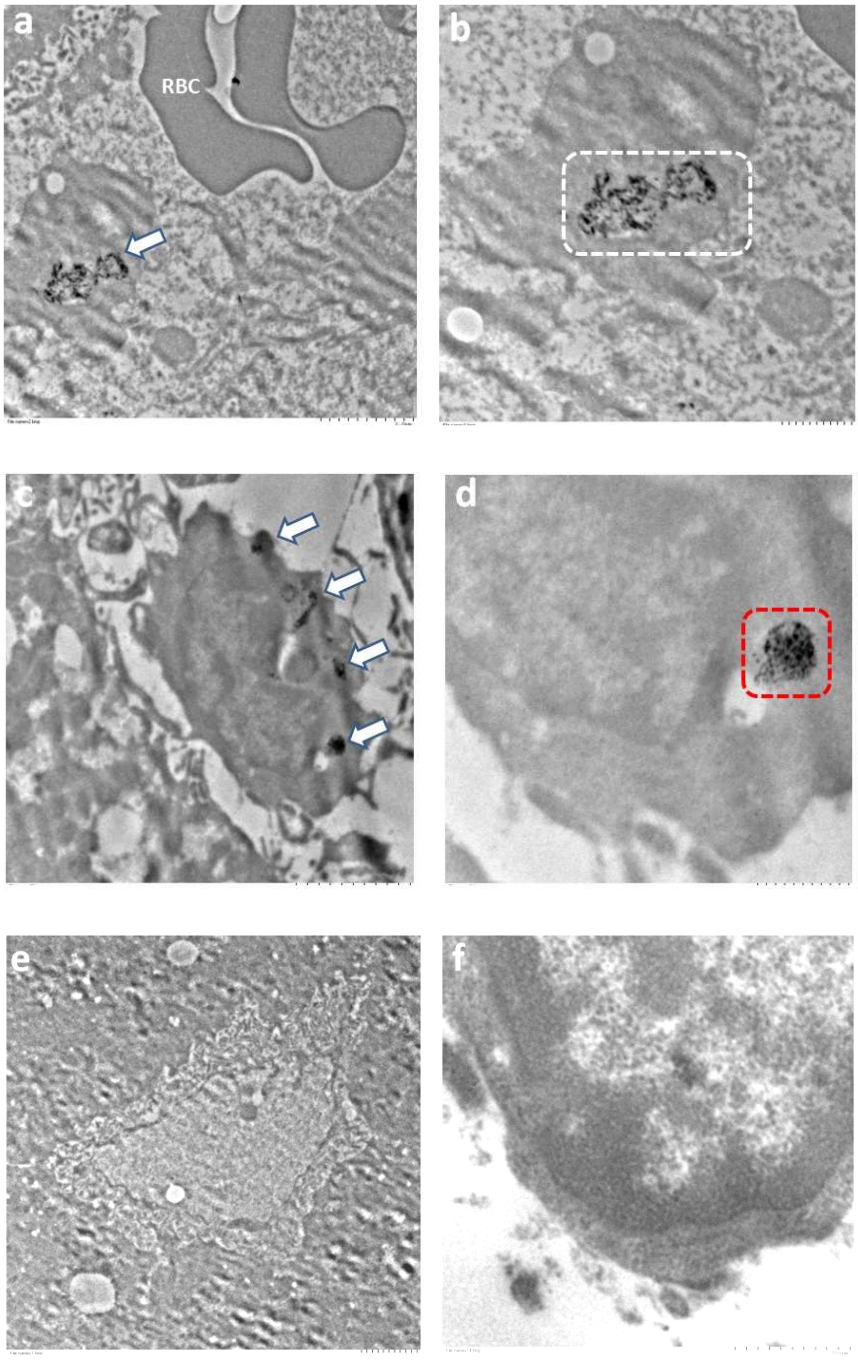

Figure 26. Ultrastructural image of Kuppfer cell in liver (**a)** SPIONS group with nanoparticles (arrow) in cytoplasm. (**b)** DEX-SPIONS group with nanoparticles (arrow) in cytoplasm. (**c)** PEG-SPIONS group with no nanoparticles seen in cytoplasm. Scale bar100 nm.

4.17 *Gene expression studies*

4.17.1 Haemoxygenase-1 (HO-1)

In liver, HO-1 gene was up regulated 4 fold in DEX-SPIONS and 3 fold in PEG-SPIONS group when compared to control group (Figure 27a).

4.17.2 Heat Shock Protein-70 (HSP-70)

In liver, HSP-70 gene was up regulated 20 fold in DEX-SPIONS group and 0.3 fold in PEG-SPIONS group when compared to control group (Figure 27b).

4.17.3 Transferrin

In liver, three and fifteen fold increase in the expression of Transferrin was observed in DEX-SPIONS and PEG-SPIONS group respectively when compared to control group (Figure 27c).

4.17.4 Ceruloplasmin

In liver, eleven and three fold increase in the Ceruloplasmin gene expression was observed in DEX-SPIONS and PEG-SPIONS group respectively when compared to control group (Figure 27d).

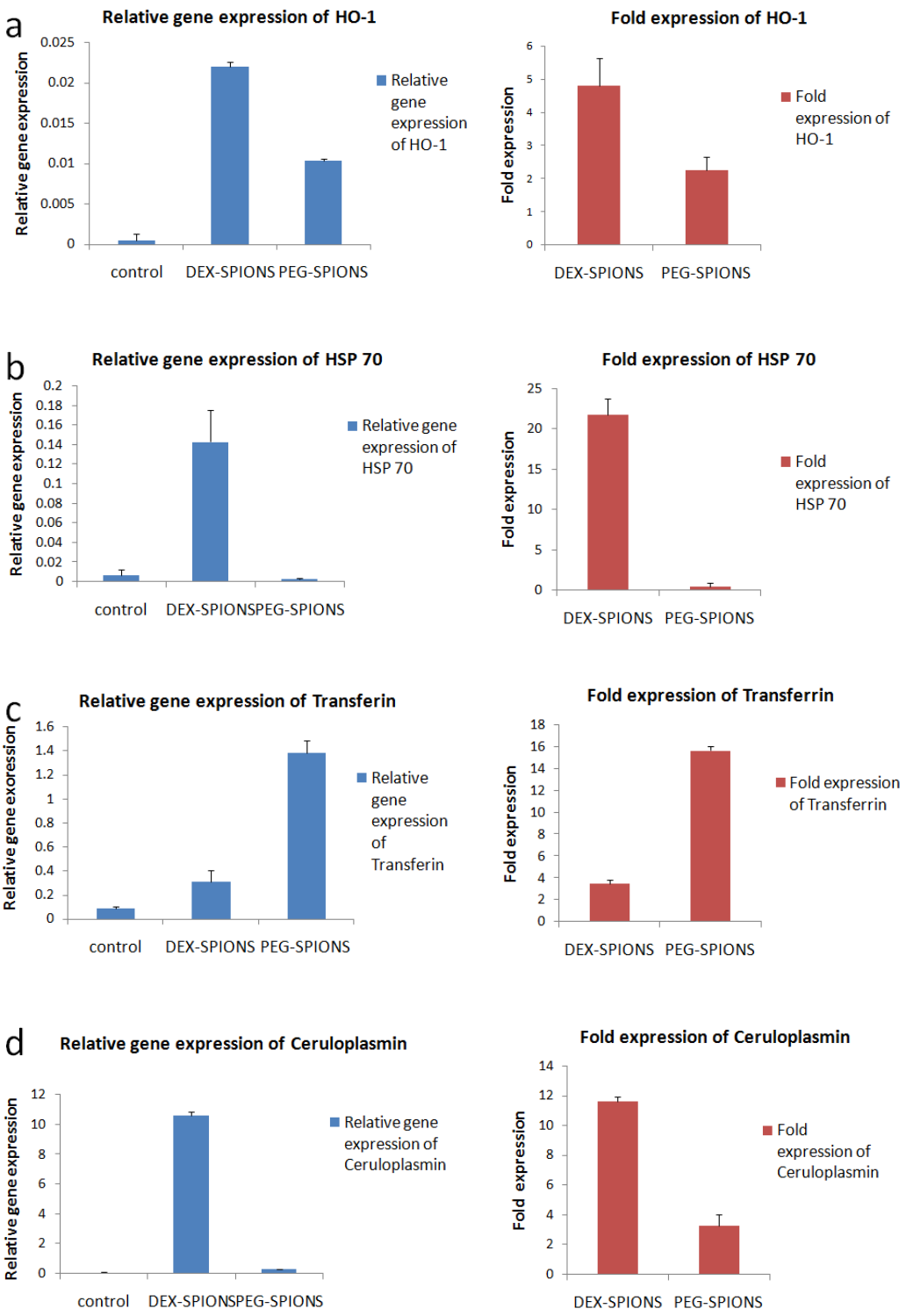

Figure 27. Relative and fold expression of genes, a) Haemoxygenase-1 b) Heat shock protein-70 c) Transferrin d) Ceruloplasmin using real-time PCR.

4.18 *Results of ICP-OES Elemental analysis*

Elemental distribution of Fe, Cu, Zn, Mg and Mn in liver, spleen and kidney are shown in figure 28.

The iron content was increased significantly in liver and spleen of SPIONS, DEX-SPIONS and PEG-SPIONS groups when compared to control (figure 28a) and within treated group was increased significantly in DEX-SPIONS group.

Copper content was significantly increased in liver and kidney of SPIONS group alone when compared to control (figure 28b).

Zinc level was significantly increased in liver, kidney and spleen of SPIONS group when compared to control group. Within treated groups, was increased significantly in DEX-SPIONS group in liver and spleen and SPIONS group in kidney (figure 28c).

Magnesium level was significantly increased in spleen of DEX-SPIONS group when compared to control group (figure 28d).

Manganese was significantly increased in liver and spleen of SPIONS, PEG-SPIONS and DEX-SPIONS group and significantly decreased in kidney of SPIONS, DEX-SPIONS group when compared to control group (figure 28e).

Co, Cr, Mo, Ni, Se, Sr and V were present but below the detectable limit.

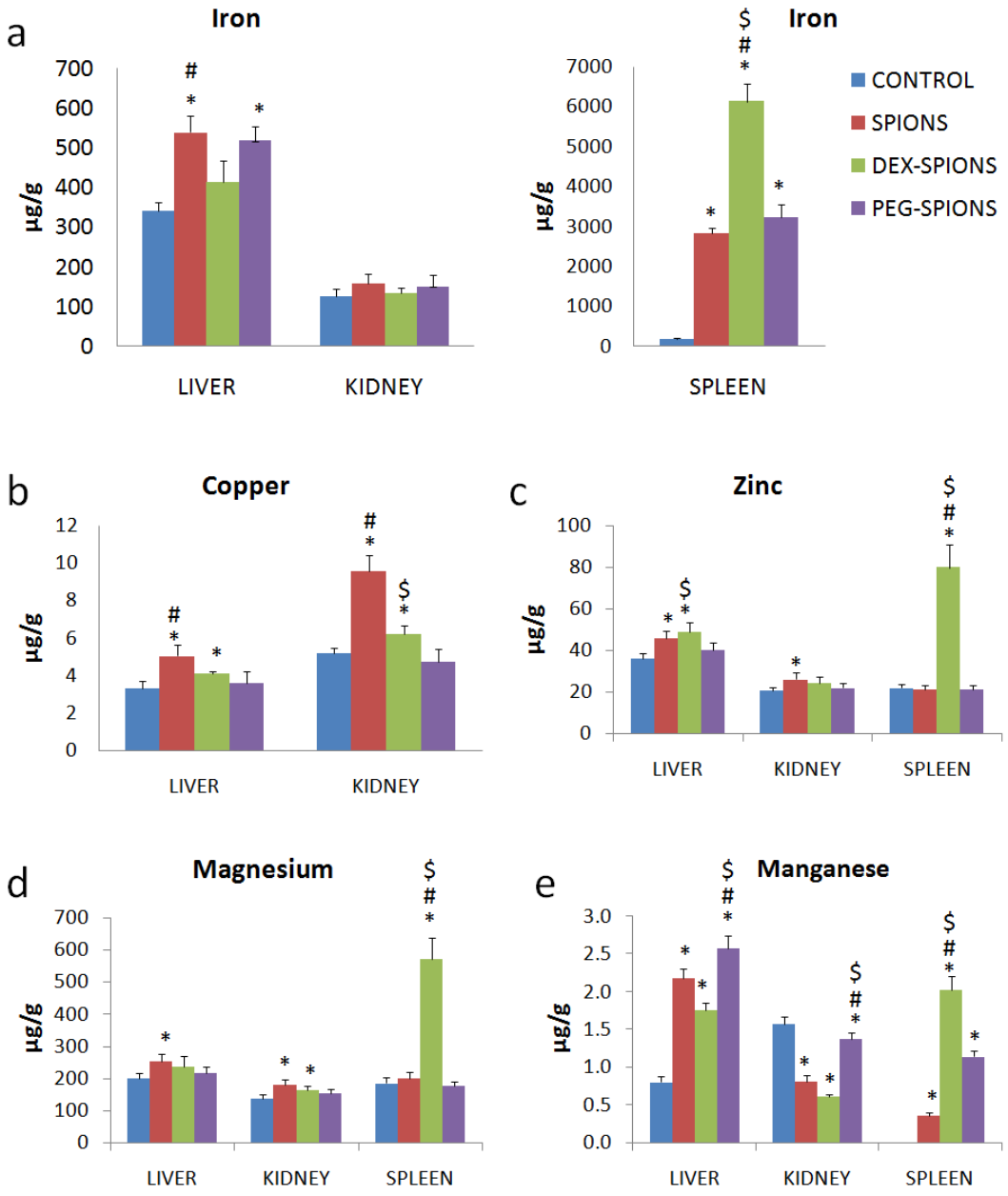

Figure 28. ICP-OES elemental analysis in liver, kidney and spleen a) Iron b) Copper c) Zinc d) Magnesium e) Manganese. $p<0.05$ * - Control vs SPIONS, DEX-SPIONS and PEG-SPIONS, # - SPIONS vs DEX-SPIONS and PEG-SPIONS, $ - DEX-SPIONS vs PEG-SPIONS. Values are represented as mean ± S.D. with n = 3.

Discussion

5 DISCUSSION

5.1 *PHASE-I: Synthesis and surface modification of SPIONS*

Superparamagnetic Iron oxide nanoparticles were prepared by the standard chemical co-precipitation method. The most common method for production of magnetic nanoparticle populations involves synthesis via the co-precipitation of ferrous and ferric salts in an alkaline medium (Massart, 1981) (Gupta and Gupta, 2005). Shortcoming of co-precipitation method is polydispersity with wide range of particle diameter. Hence, a wide variety of factors (temperature, stirring rate, solution pH, drop size) have been adjusted during the synthesis of the iron oxide nanoparticles in order to control size, magnetic characteristics, stability in solution, surface properties, and coatings. It is reported that Fe_3O_4 nanoparticles can be produced in the sizes range from 8 to 20 nm by changing the operational parameters like concentration of sodium oleate, reaction temperature, solution pH, and stirring rate (Sun et al., 2007). The obtained nanoparticles were uniform in size with average diameter of 10.3 nm and similar results were reported by Kang et al, (1996) and Cheng et al, (2005).

Stabilization of magnetic iron oxide nanoparticles for a long time without agglomeration is crucial for several applications. Especially Fe_3O_4 nanoparticles are not very stable under ambient conditions and can be easily oxidized to γ-Fe_2O_3. In order to avoid possible oxidation in the air, the synthesis of Fe_3O_4 nanoparticles must

be done in anaerobic conditions (Binh et al., 1998) hence, synthesis was carried out in nitrogen atmosphere.

The main reason for the agglomeration of magnetic iron oxide nanoparticles is the large surface area-to-volume ratio. In the absence of any proper surface coating, the magnetic nanoparticles try to minimize their surface energy by forming agglomerations. The clustering process takes place through attractive interaction between hydrophobic surfaces of the nanoparticles. Bare SPIONS can subsequently be coated in monomers and polymers through non-specific adsorption following their purification to make them less agglomerative so as to be more suited for biomedical applications (Petri-Fink et al., 2005).

The SPIONS were stabilized in aqueous condition by the surface modification through polymeric molecules. Two types of polymers were used for surface modification of SPIONS namely dextran and polyethylene glycol. Dextran (DEX), a natural branched polysaccharide, which is nontoxic, biodegradable and hydrophilic was chosen to facilitate the intra cellular uptake of dextran coated SPIONS (Mehvar, 2000). Moreover, DEX enables optimum polar interactions with iron oxide surfaces, improves the blood circulation time, stability, and biocompatibility (Carmen Bautista et al., 2005).

Polyethylene glycol (PEG), a synthetic polyether compound has the ability to provide a steric barrier to protein adsorption and it protects surfaces from interacting with immune cells which results in reduced uptake by macrophages of the reticulo endothelial system and increased blood circulation time (Schellekens et al., 2013). PEG was chosen as it enhances the hydrophilicity and water-solublility, which

improves the biocompatibility and blood circulation times (Mondini et al., 2008). Gupta and Wells, (2004a) have used a microemulsion polymerization process to prepare a poly (ethyleneglycol) modified superparamagnetic iron oxide nanoparticles with magnetic core and hydrophilic polymeric shell.

The different surface modifications of SPIONS could strongly influence their biodistribution and cellular interactions (Lee et al., 2006) (Fruijtier-Pölloth, 2005). Hence, two types of surface modified SPIONS were used in the present study.

5.2 *Physico-chemical Characterisation of nanoparticles*

5.2.1 Transmission electron microscopy

The size of the particle core was determined by TEM images. It provided details on the size distribution and the shape. Cheng et al, (2005) reported that the average particle diameter of iron oxide synthesised by chemical co-precipitation was found to be 9.1±2.1 nm and Sun et al, (2007) reported that Fe_3O_4 nanoparticles can be produced in the sizes ranging from 8 to 20 nm which correlate very well with the SPIONS synthesised in the present study.

5.2.2 Dynamic light scattering and Zeta potential

The hydrodynamic diameter of SPIONS is smaller followed by PEG-SPIONS and DEX-SPIONS which could be due to the coating material. Both dextran and PEG are hydrophilic and moreover dextran being a high molecular weight polymer, the hydrodynamic diameter is largest among the three SPIONS. In the literature, the average size of the PEG-modified nanoparticles was reported to be around 40–50 nm with narrow size distribution (Gupta and Wells, 2004a). However, the higher

hydrodynamic diameter of PEG-SPIONS could be due to the higher molecular weight (8000 da) of PEG polymer used for coating.

5.2.3 X-Ray Diffraction analysis

X-ray diffraction (XRD) method was used to characterize the crystal structure and analysed the particular phase of the in house synthesised nanoparticles. The XRD pattern of synthesised SPIONS, DEX-SPIONS and PEG-SPIONS demonstrated that the surface modification did not interfere with the phase purity of the crystals. The results are well supported by the findings of (Sun et al., 2007) (Saraswathy et al., 2014) (Beeran et al., 2015).

5.2.4 Vibrational sample magnetometry

The VSM analysis showed there was a reduction in magnetization saturation in coated nanoparticles when compared to bare nanoparticles. Coating effect of dextran and polyethyleneglycol over the magnetic particles would have caused the reduction in the magnetization value. The results were well supported by the findings of (Sun et al., 2007) (Saraswathy et al., 2014). Superparamagnetic property exhibited by the particles indicated the single domain existence and the absence of aggregation.

Experimental value for magnetization saturation in magnetic iron oxide nanoparticles have been reported to span the 30–80 emu/g range, lower than the bulk magnetic value 100 emu/g. In addition, Fe_3O_4 nanoparticles are not very stable under ambient conditions and are easily oxidised to Fe_2O_3 or dissolved in an acidic medium (Binh et al., 1998).

5.2.5 Fourier Transform –Infra Red spectra

Fourier Transform infrared spectroscopy (FTIR) technique was used to determine the chemical functional groups especially dextran and polyetheylene glycol in the surface of synthesised nanoparticles.

SPIONS showed prominent peak of Fe-O vibration at ~570 cm^{-1} corresponding to the magnetite phase (Beeran et al., 2015). The peak at ~3382 cm^{-1} is attributed to the stretching vibrations of -OH, which is also assigned to OH^- absorbed by Fe_3O_4 nanoparticles (Sun et al., 2007). The distinct peaks around 2932, 1018 cm^{-1} corresponding to the C-H and C-O deformations of dextran, confirmed the presence of surface attached dextran molecule in the DEX-SPIONS (Saraswathy et al., 2014). Similarly, the PEG-SPIONS peaks at 2912 cm^{-1} and 955 cm^{-1} corresponded to $–CH_2$ stretching and out of plane bending vibrations. Also the ether group peaks around 1105 cm^{-1} corresponded to C-O-C stretching and peak around 1344 cm^{-1} coming from C-H bending vibrations. The presence of stretching and bending peaks of PEG confirmed the successful modification of SPIONS surfaces with PEG polymeric molecules (Larsen et al., 2009).

5.2.6 Thermo Gravimetric Analysis

TGA was done to estimate the amount of coating material present in order to calculate the dose during in vivo experiment. TGA plot of DEX-SPIONS shows four distinct stages of thermal decompositions around 126.56^oC, 200.74^oC, 413.07 ^oC and 794.74^oC corresponding to the total weight loss of 1.08%, 12.59%, 24.75%, and 28.25 % due to elimination of bound water, exothermic phase transition, endothermic phase transition and linear degradation respectively. These phase

transitions indicates the step by step degradation due to the dissociation of dextran-Fe bonds. The shift observed in the decomposition temperature of DEX-SPIONS from that of pure dextran is due to the effect of catalytic behaviour of iron oxide nanoparticles in the system (Saraswathy et al., 2014). The high temperature of around 800^{o}C required to eliminate the total weight of 28.25% of dextran shows the strong binding of the same to the material. TGA plot of PEG-SPIONS also shows four similar stages of decomposition around 119.81^{o}C, 218.24^{o}C, 270.91^{o}C, 519.27 ^{o}C and 794.51^{o} C corresponding to the total weight loss of 0.69%, 7.61%, 18.31%, 23.08% and 24.72%. Significant weight loss for PEG-SPIONS was noticed between 270^{o}C - 800^{o}C which could be due to decomposition of PEG polymers which absorbed on the surface of SPIONS (Gupta and Gupta, 2005).

5.3 *PHASE-II: In vitro Cell culture and Phase contrast microscopic studies*

It should be noted that *in vitro* tests that produce specific and quantitative toxicity results are particularly convenient for the initial evaluation of toxicity and biocompatibility of SPIONS. In the present study, murine L929 fibroblasts cells and RAW264.7 macrophages were incubated with bare and coated SPIONS at varying concentrations. Phase contrast images revealed the close association of bare and coated SPIONS along the cellular margins on the dorsal surface of the fibroblasts and macrophages. The binding of bare and coated SPIONS did not induce any drastic changes in cellular morphology relative to the controls. This suggests that interaction of bare and coated SPIONS did not affect the adherence property of the cells. Our results are in agreement with earlier reports (Gupta and Wells, 2004a),

who reported that after incubation with immortalized fibroblasts, PEG-coated SPIONS did not affect cell adhesion behavior or morphology (Gupta and Curtis, 2004). Laurent et al, (2008) reported the sedimentation of magnetic nanoparticles, as this phenomenon effectively leads to an apparent increase in magnetic nanoparticle concentration at the cell surface and so should be taken into account when performing toxicity assays.

Phase contrast microscopic studies revealed morphologically that there were no deleterious changes due to SPIONS but to study the functional changes, further investigative studies employing the MTT assay and live and dead assay were undertaken.

5.4 *MTT assay*

The MTT (3- (4,5-Dimethylthiazol-2-yl)-2,5-diphenyltetrazolium bromide) and PI (Propidium Iodide) live/dead assay are most commonly used *in vitro* tests for nanoparticle mediated toxicity and cell viability. These assays are aimed at investigating vital cellular activity such as cell death and cell viability.

The proliferation/viability of fibroblasts was measured by MTT assay after culturing for 24 h and showed that cell proliferation and metabolic activity was more favorable in case of coated particles than with uncoated ones. Many toxic effects caused by magnetic nanoparticle may stop mitochondrial activity which is measured by assays such as MTT (Mosmann, 1983). In the present study, cytotoxicity evaluation was carried out using two types of immortalised cell lines, namely fibroblast and macrophage since, the degree of toxicity has been known to vary with

cell type, magnetic nanoparticles, and a combination of these two factors (Bulte, 2009).

In the present study, the data suggests that the surface modified nanoparticles did not affect the viability and metabolic activity drastically but the bare SPIONS have cytotoxic effect at higher concentration. For instance, it has been reported that uncoated SPIONS caused significant cell death in dermal fibroblasts while lung cells appeared not to be affected (Mahmoudi et al., 2012). This specifies the importance of cell type and magnetic nanoparticle relationship. Mahmoudi et al, (2011a) also showed that uncoated and coated SPIONS were less toxic as previously thought and induced toxicity in various cell lines at greater doses than permitted for humans.

Cytotoxicity tests for human glia, human breast cancer and normal cell lines exhibited almost nontoxicity and reveal biocompatibility of Fe_3O_4 nanoparticles in the concentration range of 0.1–10 µg / ml, while accountable cytotoxicity had been noted at 100 µg/ml (Ankamwar et al., 2010). At higher concentrations more particles tend to sediment enhancing the cytotoxic effect and could be the reason for the cytotoxic effect (Laurent et al., 2012).

5.5 *Live and dead assay*

Toxic cellular effects are translated into impaired mitochondrial activity, membrane leakage and morphological changes. This can have adverse effects on cell viability, proliferation and metabolic activity (Yang et al., 2009). From the present study it can be noticed that surface modified SPIONS minimally affected the cell viability or proliferation capacity. In DEX-SPIONS and PEG-SPIONS challenged group, more than 95 percentage cells remain viable. The results indicated the

biocompatible nature of the coatings and confirm low toxicity of surface modified nanoparticles. Similar results were reported earlier also by Gupta and Wells, (2004a). Similarly, dextran-coated SPION labeled with the Tat-internalizing peptide showed no significant effects on cell viability (Lewin et al., 2000).

5.6 *In vitro Oxidative stress analysis*

Oxidative stress arises when there is an imbalance between damaging oxidants also referred to as reactive oxygen species (ROS) such as hydrogen peroxide, hydroxyl radicals, and the protective antioxidants such as superoxide dismutase, catalase and glutathione sulf-hydryl. ROS are primarily formed by the incomplete reduction of oxygen. It has been reported that dissociated iron oxide magnetic nanoparticle can promote the formation of ROS and hydroxyl radicals, and as a result may lead to cellular toxicity along with impaired cell metabolism and increases in apoptosis (Yang et al., 2009). In the present experiment ROS would have generated from the surface of magnetic nanoparticle, the leaching of metal iron ions from the core, or release of oxidants by enzymatic degradation of the magnetic nanoparticle. It is reported that elevation of low molecular weight iron species due to magnetic nanoparticle biodegradation may be implicated in tissue damage via oxidative stress (Crichton et al., 2002).

In the present study, SOD, GSH, LPO and tissue nitrite level were found to be significantly altered post nanoparticle exposure in HepG2 cells. It has been reported that cell proliferation, mitochondrial activity, or cell viability were not affected when human skin fibroblasts were treated with $AgNO_3$. However, Ag^+ strongly increased the production of reactive oxygen species, including superoxide anion radicals.

These effects correspond to a strong decrease in intracellular reduced glutathione and to an increased susceptibility to H_2O_2-induced cell death (Cortese-Krott et al., 2009).

Studies using C10 lung epithelial cells have shown that the large and small agglomerates of carboxylated SPIONS have similar inherent potency for the generation of ROS, induction of stress-related genes and eventual cytotoxicity. It is also suggested that reactive moieties on the agglomerate surface are more efficient in catalysing cellular ROS production than molecules buried within the agglomerate core (Sharma et al., 2013).

Another study reported that SPIONS induced oxidative stress in two human cell lines; skin epithelial A431 and lung epithelial A549. Prepared SPIONS were polygonal in shape with a smooth surface and had an average diameter of 25 nm. SPIONS were found to induce oxidative stress in a dose-dependent manner, evident by depletion of glutathione and induction of reactive oxygen species (ROS) and lipid peroxidation (Ahamed et al., 2013).

5.7 *Raman chemical mapping of L929 and RAW cells treated with SPIONS, DEX-SPIONS and PEG-SPIONS*

A nanocarrier can be internalized simply because of its physical proximity to the membrane or because of interactions with specific receptors, originating via a number of different internalization paths. Interpretation of toxicity results depends upon an understanding of how nanoparticles and the living systems interact. To understand the toxicity of nanoparticles, we need to accurately measure how they are distributed in the cell after exposure, and how they interact with specific organells. The most common method for studying biodistribution in cells exposed to

nanoparticles at high magnification is transmission electron microscopy (TEM). TEM analysis is intrusive and requires extensive sample preparation and manual inspection to distinguish nanoparticles from naturally occurring cell structures. Fluorescence microscopy and confocal light microscopy are powerful techniques for studying biodistribution, but they require intrinsically fluorescent nanoparticles or fluorescence-labeled nanoparticles and the cells are usually stained. These methods often require extensive sample preparation and labeling is intrusive in the sense that it intrinsically modifies the surface properties of the nanoparticles, which may lead to biased results. Similarly, attaching labeling molecules to the surfaces of nanoparticles may alter their surface chemical properties, agglomeration state, etc., and hence alter their intrinsic bio-response (Marquis et al., 2009). It is therefore necessary to develop new, label-free techniques that complement these well-established methods. Raman micro spectroscopy is a label-free technique that has the potential to be used for nanoparticle-uptake studies. For the present experiment, Raman spectroscopy a label free technique was used to study the nanoparticle uptake using L929 fibroblast cells and RAW 264.7 macrophages. The fibroblasts were used as it is reported to have phagocytic activity (Arora et al., 2013) (Arbi et al., 2015). Raman spectroscopy was used as a tool as Raman z-scans can prove the intracellular distribution and colocalization of the nanoparticles with different intracellular environments (Estrela-Lopis et al., 2011b).

Another study, Raman spectroscopic mapping of the cells in combination with K-means cluster analysis was used to clearly identify and localise the polystyrene nanoparticles in exposed cells, based on their characteristic spectroscopic signatures. Principal component analysis identifies the local environment as rich in lipidic

signatures which are associated with localisation of the polystyrene nanoparticles of 50 nm or 100 nm in the endoplasmic reticulum (Dorney et al., 2012).

Shah et al, (2011) used confocal Raman spectroscopy to visualize polyethylene-coated gold nanoparticles in cells. They studied two to three cells exposed to nanoparticles for 2 h, 12 h, and 24 h. The cell nucleus as well as the nucleoli could be resolved in the images, which were constructed by integrating the CH stretching band at 2800–3050 cm^{-1}. They found that nanoparticles reached the perinuclear region after 24 h of exposure. Lamprecht et al, (2012) used the CH stretching mode to identify organelles in cells. Using Raman spectroscopy, they were able to localize functionalized carbon nanotubes inside cells, primarily accumulated around the nucleus but not inside the nucleus.

Results of the present study show uptake of SPIONS, DEX-SPIONS and PEG-SPIONS into the cytoplasm of fibroblasts and macrophages after 24 h, correlate with those in literature.

5.8 *Haemocompatibility studies*

Heamocompatibility tests were included in this study as it is reported that study of haematological change caused by newly synthesised SPIONS is of importance and should be included in the toxicity and compatibility tests to be made in the development of these particles (Mayer et al., 2009).

5.8.1 Haematology

The test results of haematological parameters studied, indicated that 50 µg/ml concentrations of SPIONS DEX-SPIONS and PEG-SPIONS under test, the

difference in percentage change in haematological parameters evaluated is less than 10% which is well within the acceptable limit prescribed by standard ISO10993-4.

Similarly, it has been reported that studied bioferrofluids coated with poly (4-vinyl pyridine) (P4VP) and polyethylene glycol (PEG) have no effect on the complete blood count (erythrocytes, Leucocytes, Platelets, Hemoglobin and hematocrit) and neither they show in vitro hemolytic effect on blood (Ali et al., 2013).

5.8.2 Hemolysis assay

Nanoparticles can potentially damage the cell membrane and even the cytoplasm since they can penetrate inside cells. They can cause hemolysis by acting on the membrane of red blood cells. If hemolysis is severe the number of red cells decreases and haemoglobin in plasma can be detected with the naked eye. If hemolysis is subtle it can only be detected by a laboratory test for free hemoglobin in plasma (Rugal et al., 2007) (Ostomel et al., 2007) (Simberg et al., 2009).

The hemolysis rates were lower than 5%, which lie within the recommended value in ISO 10993–4 standard. Furthermore, It has been shown that these nanoparticles do not have any observable adverse effect on erythrocytes, leukocytes, platelets, hemoglobin and hematocrit at the concentration tested (50 µg/ml).

These findings showed that the synthesised SPIONS satisfied the requirements of hemolysis test on medical materials. Synthesised SPIONS have no effect on the complete blood count neither they show hemolytic effect on blood *in vitro.* Further experiments using small animals *in vivo* also did not show any adverse effect on

erythrocytes, leukocytes, platelets, hemoglobin level and hematocrit values indicating the haemocompatible nature of the synthesised nanoparticles.

In the present study, PEG showed insignificant increase in hemolysis compared to SPIONS and DEX-SPIONS due to hydrophilic nature of polymer. It has been reported that PEGylated poly (*N*-isopropylacrylamide) nanoparticles are hemocompatible with insignificant toxicity (Gulati et al., 2010).

5.9 *Genocompatibility study by comet assay*

The direct interactionn of the metal oxide NPs with the DNA and protein may alter their structure and function. Additionally, if these NPs agglomerate within the cell and cannot gain access to the nucleus, there are possibilities for their direct contact with DNA during the process of mitosis when the nuclear membrane breaks down. The Comet assay or single cell electrophoresis is a sensitive and rapid technique for quantifying and analyzing DNA damage in individual cells for the evaluation of genotoxicity (Widziewicz et al., 2012). This assay can be used to detect DNA damage caused by double strand breaks, single strand breaks, alkali labile sites, oxidative base damage and DNA cross-linking with DNA or protein. The Comet assay gains special significance in the field of nanomaterials research due to the short period between exposure to genotoxic agent and genetic effect (s) becoming apparent. In the present investigation, the time (24 h) elapsed between exposures and measuring of the DNA damage is adequate for the repair of the possible lesions and enables to detect whether or not the chemical is able to produce the DNA damage. As per the assay the SPIONS, DEX-SPIONS and PEG-SPIONS did not evoke a significant effect on DNA migration on the electric field at the

applied concentrations and were found to be non-genotoxic. From the assay it is clear that the neither iron oxide nanoparticle nor the degradation products leaching from them affect the genomic integrity of the genetic materials.

In a study, the human lung epithelial cell line A549 was exposed to the iron oxide particles. DNA damage was determined using the comet assay and for iron oxide particles (Fe_3O_4, Fe_2O_3), no or low toxicity was observed (Karlsson et al., 2008).

Comet assay revealed that level of DNA damage was observed only with higher concentration of SPIONS (100 μg) in skin epithelial A431 and lung epithelial A549cells (Ahamed et al., 2013). Similarly, no genotoxicity was observed due to exposure of human lymphocytes to MSA- or DMSA-MNPs (Lima et al., 2013).The non genotoxic results in the present studies indicate the safety of the nanoparticles in tested concentration.

5.10 *Phase-III: Animal experiment*

It is pertinent to evaluate the acute systemic effect of synthesised SPIONS in a suitable animal model. Female Wistar rats were alone used in this study because it is reported that iron is distributed differently in male and female rats (Ben-Assa et al., 2009) (Kong et al., 2014). Also the issue of sex influence on the biodistribution and toxicity of nanoparticles is debated, with reports of differences between males and females (Chen et al., 2013). A dose of 5 mg Fe/kg body wt. was fixed for this study since it was the highest dose tested in the clinical Phase II studies for MRI imaging (Wang et al., 2001).

The various interactions of NPs with fluids, cells, and tissues need to be considered from the route of entry through the wide range of possible pathways ending at potential target organs. The systemic administration of nanoparticles by intravenous route was selected since it is the most preferred route of administration of MRI contrast agents as well as drug delivery agents. Acute changes in the blood and histological changes in the tissues and organs were also evaluated. Schlachter et al, (2011) administered magnetic nanoparticles systemically to validate toxicity which included histology on injection sites and major metabolic sites (liver, pancreas, kidneys and brain) to look for signs of spreading and accumulation of MNP.

5.11 *Haematology and Flow cytometry*

To quantify the toxicity analysis of synthesised nanoparticles, the important step is an assessment of standard hematological and biochemical parameters of the target organs (liver, kidney and spleen) of SPION. When SPIONS are intravenously administered, the first physiological system they interact with is the blood and blood components.

The hematology results showed the blood counts to be within the normal range although there was a slight increase in the percentage of mixed cells in all three treated groups. This could be expected on an acute immune response to the foreign materials (nanoparticles). This is well supported by the literature (Xu et al., 2013) (Varma HK, 2014).

Flow cytometry results showed that the granular cell populations of treated groups were significantly increased when compared to control values. It was

reported that Ni nanoparticles significantly increased the WBC count in all dose groups and no significant changes were observed in the other hematological parameters measured (Magaye et al., 2014). This particular experiment was attempted to find out if there was any difference in the scatter pattern in dot plot. The results obtained were complementary and substantiated the finding of routine haematology.

5.12 *Biochemical assays*

In the rat, serum glutamic-pyruvic transaminase (SGPT) is specific for cellular damage in the liver. Serum glutamic oxaloacetic transaminase (SGOT) is also useful but not as specific. Reduction in liver function and cholestasis can be assessed by substances produced by the liver, including albumin, globulin, total protein, alkaline phosphatase (ALP), and total bilirubin. Indicators of kidney function include creatinine and urea, although these are not as specific or sensitive. Results did not indicate significant toxicity compared to control animals and reflected normal variation present in populations of animals (James, 1993).

Blood chemistry showed increase in SGOT and SGPT enzyme level in treated groups. These enzymes are mainly associated with the hepatocytes (Zimmerman, 1999). The altered SGOT and SGPT level in treated group is due to damage caused by the sudden increase in Fe ions which has more avidity towards the mitochondria (Walter et al., 2002). Higher and more prolonged oxidative stress levels, cellular perturbation and disarray result in decrease in mitochondrial membrane potential, leading to cell death (Fariss et al., 2005). Since, the nanoparticles are first taken up in the Kupffer cells in the liver, it is suggested that the increase of SGOT and SGPT

levels is due to slow transfer of presumably toxic degradation products of the surface modified SPIONS from the macrophages to the hepatocytes (Singh et al., 2010). This was observed by the increased number of Kupffer cells present in the DEX-SPIONS group correlating with statistically significant increase in SGOT level in DEX-SPIONS group. Liver is one of the major target organs and a dominant site of accumulation of nanoparticles (Patlolla et al., 2011) (Yang et al., 2008). Kumari et al, (2013) have reported that SGPT and SGOT activity increased significantly in serum at the 1,000 and 2,000 mg/kg doses of Fe_2O_3 nanoparticles in female wistar rats in an acute oral toxicity study. Another study showed that increased serum level of SGOT 24 h after Fe_2O_3 MNP formulation injection in male Sprague- Dawley rats; however, there was slight transient increase in the serum SGPT level also (Jain et al., 2008). Similar results were shown in a previous study with large pluronic-coated SPIONS nanocomposites tested in rats, where increased levels of SGOT and SGPT was observed up to 3 days post-injection (Gu et al., 2012).

Serum determination of gamma-glutamyl transferase activity is considered to be an index of hepatobiliary dysfunction and recent epidemiology and pathology studies have suggested its independent role in the pathogenesis and clinical evolution of cardiovascular diseases. GGT is the enzyme responsible for the extracellular catabolism of glutathione (GSH, gamma-glutamyl-cisteinyl-glycine), the main thiol intracellular antioxidant agent in mammalian cells. It is present, linked through a small lipophilic sequence of its larger subunit, on the cell surface membrane of most cell type. Although the same protein is produced in all tissues, differences in the sugar moieties allow that only the liver GGT is detectable in serum.

Increased GGT level in SPIONS group may be due to the oxidative stress caused by the iron. Experimental studies have indicated that higher intake of iron may lead to elevated level of GGT in serum (Lee et al., 2004).

In *in-vivo* experiments, it has been shown that GGT activity directly related to the oxidative events, playing role in the evolution of atheromatous plaque and induces LDL oxidation in the presence of iron ions (Paolicchi et al., 1999). Regarding the possible association between GGT and inflammatory process, it should also be considered that GGT has a key role in the interconversion of the glutathione containing inflammatory mediator leukotriene C4 into leukotriene D4 (Ulus et al., 2007).

The association of GGT to lipoproteins suggests that LDL lipoproteins can carry GGT activity in the tissues where free iron is also present. In the extracellular milieu, GGT is the only enzyme responsible for GSH catabolism by hydrolysis of its gamma-glutamyl bond between glutamate and cysteine. This reaction produces cysteinyl-glycine moieties, which are usually taken within intracellular milieu by the action of membrane dipeptidases, as precursors for GSH resynthesis (Whitfield, 2001). Cysteinyl-glycine is a powerful reducer of Fe^{3+} in the extracellular milieu that is able to simultaneously generate Fe^{2+} and a free thiyl radical. Subsequent reactions lead to the formation of superoxide anion radical and hydrogen peroxide (Pompella et al., 2004). These GGT-mediated reactions have been shown to catalyze the oxidation of LDL lipoproteins, likely contributing to oxidative events (Pang et al., 1996). Because of the iron dependence of GGT mediated reactions, the described association between increased body iron stores and excess risk of acute myocardial

infarction suggests that iron metabolism could influence the predictive value of serum GGT (Tuomainen et al., 1998).

The present study indicates that the oxidative stress mediated by GGT could have played a relevant role in the SPIONS induced cytotoxicity.

There is a substantial increase in bilirubin content in blood in all three treated groups which correlates with the cholestasis noted in liver histology. It has been reported that the iron is excreted through bile in conjugated form through Hemeoxygenase-1 mediated heme degradation in the cells (Maines, 2000). Hemin-mediated increase in HO-1 protein expression and haemoxygenase activity is associated with augmented bilirubin levels and protection against oxidative stress in bovine smooth muscle cells (Clark et al., 2000).

5.13 *Oxidative stress*

Nanoparticles with their small size and large surface area have been reported to interact with proteins and enzymes within mammalian cells and to generate ROS. When the depletion of the antioxidant defense mechanism occurs and ROS accumulate, an inflammatory response can be initiated leading to the disturbance and destruction of the mitochondria resulting in eventual cell death (You et al., 2005). Levy et al, (2011) reported that SPIONS can be degraded in a simulated lysosomal acidic environment. Inside the cells, the iron oxide nanoparticles will degrade in lysosomes and endosomes and release free iron ions (Fe^{2+}, Fe^{3+}) (Singh et al., 2012). The iron ions are then available for Haber–Weiss–Fenton reactions and are associated with increases in ROS generation (Emerit et al., 2001). The Haber–Weiss reaction is the main pathway when antigens crosslink the IgE on mast cells, resulting

in Fe^{3+} accumulation in the intracellular region. Oxidative stress and trace elements kinetics are potential factors related to the pathogenesis of asthma and other allergies (Nakashima et al., 2005).

The present investigation has shown that exposure to SPIONS had significant effects on rat organs, suggesting that reactive oxygen species (ROS) were generated under the experimental conditions employed. A significant increase was observed in lipid peroxidation level in the SPIONS treated group. The change in activities of antioxidant enzymes and lipid peroxidation levels in present study was regarded as evidence of increased ROS production during the exposure period and may reflect the pathological process of the exposure.

SOD is a specific antioxidant enzyme which dismutates O^{-2} and forms H_2O_2 as a result, which is scavenged by peroxisomal CAT or GSH-Px. It protects the cells against toxic effect of superoxide radicals (Scherz-Shouval and Elazar, 2011) (Apel and Hirt, 2004). In the present study, the association between increase in MDA level and decrease in SOD activities and GSH level indicates that there is oxidant-induced tissue damage in liver, kidney, lung, heart and spleen. Srinivas et al, (2012) have reported that SPIONS increase the plasma malondialdehyde (MDA) level as an indicator of lipid peroxidation and lower the activity of blood superoxide dismutase (SOD) level and decrease the intracellular glutathione (GSH). The present study indicates that SPIONS exhibits its toxicity by increasing lipid peroxidation and surface coating using dextran and PEG substantially reduced the lipid peroxidation in the organs examined. This could be due to better clearance from the system. Studies indicated nano ceria-induced hepatic injury and oxidative stress,

respectively. It has been been observed that a single vascular infusion of nano ceria could lead to persistent hepatic retention of particles (Tseng et al., 2012). Similarly, several studies with Ag NPs have demonstrated toxicity through an oxidative stress pathway. Decreased GSH levels and an up-regulation of oxidative stress and inflammatory genes were observed (Hussain et al., 2005) (Schrand et al., 2008).

Increased production of nitric oxide may protect the cells from oxidative stress and this explain the elevated levels of nitrite in control group compared to SPIONS, DEX-SPIONS and PEG-SPIONS.

5.14 *Histopathology*

Studies have shown that SPIO surface properties can influence uptake of nanoparticles by phagocytic cells. For example, carboxydextran-coated SPIO (of equal or even smaller sizes) appear to be internalized by macrophages to a greater extent than dextran-coated SPIO (Matuszewski et al., 2005). Yet another study reported an increase in liver uptake with an increase in hydrodynamic diameter from 33 to 90 nm of dextran-coated magnetite nanoparticles (Chouly et al., 1996).

In the present study, the hydrodynamic diameter of DEX-SPIONS nanoparticle was 89 nm and this group showed more Kupffer cells in the liver followed by SPIONS group. In general, in vivo cellular uptake increases with hydrodynamic size, suggesting larger nanoparticles are more susceptible to opsonization an immune response that adsorbs a class of proteins called opsonins to foreign materials. Mono nuclear phagocytic system cells, such as the Kupffer cells in the liver, readily recognize opsonin-labeled nanoparticles for rapid removal through phagocytic

processes (Metz et al., 2004b) (Owens and Peppas, 2006) (Alexis et al., 2008) (Aggarwal et al., 2009).

Macrophages remove large foreign particles through endophagocytic pathways. For example, SPIONS that are hydrophobic, aggregating, cationic or tagged with specific proteins called opsonins are quickly recognized and taken up by MPS cells (Almeida et al., 2011).

Furthermore, Fang et al, (2006) showed that protein adsorption to nanoparticles coated with the same 5,000 Da PEG, but different hydrodynamic diameters – 80 and 243 nm – increased from 6% to 34%, respectively. Aminated, cross-linked starch and aminosilane coated MNPs were modified with 5 kDa or 20 kDa polyethylene glycol chains. These modified PEG-MNPs were studied in RES simulations in vitro using RAW264.7 macrophages in cell culture medium at 37 °C and a 7 to 10 fold less uptake in RAW264.7 macrophages when compared to unmodified starch MNPs was observed (Cole et al., 2011). The above results were very well correlated with our observation of low uptake by Kupffer cells in the liver PEG –SPIONS group and more uptakes seen in the DEX-SPIONS group.

Histology sections were also examined by Prussian blue staining (iron) to observe the degradation and clearance of the nanoparticles accumulated in the liver and spleen. Particularly, in the liver, most of the nanoparticles were found in the Kupffer cells located in the linings of the sinusoids, not in the hepatocytes. This was substantiated in the magnified images of transmission electron micrographs, where iron particles were observed in cytoplasm of Kupffer cells in SPIONS and DEX-SPIONS groups. Concerning iron oxide nanoparticle clearance, it is known that they

are primarily phagocytosed by the Kupffer cells in the liver (Sadauskas et al., 2007). TEM micrographs indicated that Kupffer cells exhibit uptake patterns and metabolism of the iron oxide nanoparticles found in cytoplasm of SPIONS and DEX-SPIONS groups. In addition, the relatively inefficient uptake or no uptake in Kupffer cells of PEG-SPIONS group indicated that these nanoparticles might not have been taken up by adsorptive or receptor-mediated endocytosis which could be attributed to the non immunogenic nature of PEG (Schellekens et al., 2013). In PEG-SPIONS group, the accumulation of iron was not appreciated in the Kuppfer cells.

In spleen also iron staining was similar to that of control group. In another study, the results showed that the residence time was doubled for PEG coated nanoparticles and consequently particle accumulation in liver and spleen was reduced. Post-mortem histological analyses showed no alterations in the liver and confirm heterogeneous distribution of NPs in the organ, in agreement with magnetic measurements and iron analysis (Ruiz et al., 2013).

The kidney in DEX-SPIONS group showed occasional convoluted tubule damage which was not seen in PEG-SPIONS group. This may be due to the fact that PEG is amphiphilic and easily excreted through the kidney when compared to dextran which has a higher molecular weight and cannot be easily excreted by kidney tubules. It was also described that polyvinyl alcohol coated SPION were first excreted within the primary urine through glomerular filtration system of the kidneys and then reabsorbed in the proximal tubuli (Neuberger et al., 2005). Studies have shown that the ferric nitrilotriacetate that is filtered by the renal tubules is rapidly reduced, and the resulting Fe^{2+} initiates lipid peroxidation in the lumen. Peroxidation

of polyunsaturated fattyacids occurs, followed by acute renal tubular necrosis (Deiana et al., 2001). It has been reported that uncoated iron oxide nanoparticles may have harmful effects in the liver, kidney, and lungs when administered by a single intravenous injection (Hanini et al., 2011).

An earlier report has shown the presence of clustered SPION microbubbles predominantly in the lungs as early as 10 minutes post injection. The frequency of microbubbles declined in the pulmonary vasculature and increased in pulmonary, hepatic, and splenic macrophages over time, resulting in a relative shift from the lungs to the spleen and liver. Meanwhile, macrophages showed increasing signs of cytoplasmic iron accumulation, initially in the lungs and then followed by other organs (Barrefelt et al., 2013). In the present study, the observation also well correlated with the literature.

In the present study large number of macrophages in the red pulp region took up the iron particles in treated groups were observed. Hemosiderin was also stained blue in the spleen by Prusian blue stain but the difference in staining intensity was more in treated groups when compared to control. In the spleen, PVA coated SPIONs were found clearly accumulated in the macrophages located in the red pulp, the primary site of splenic filtration but not in the white pulp (Neuberger et al., 2005). In a study carried out following systemic administration of 138 mM Poly Ampholyte coated MNPs, (Wang et al., 2015) have reported normal histological structures of heart, liver and kidney which were similar to that of normal control mice, with the exception of slight proliferation, haemorrhage and infiltration of inflammatory corpuscles at the germinal center of the mouse spleen. Numerous

alveoli, alveolar ducts and alveolar sacs could be seen, and the alveolar space was filled with gas without any sign of edema. Alveolar interval showed mild broadening, and alveolar epithelial cells were seen. The lung also showed slight congestion and a little infiltration of inflammatory corpuscles.

5.14.1 Histomorphometry for mast cells

In cases where the MNPs are incorporated into the therapy and transplanted within the body, the risk of MNPs migrating through the organism, entering and accumulating within organs is a constant concern. This could trigger an immunological or an inflammatory response by the body. To my knowledge, this is the first report on the effects of surface modified SPIONS on mast cell distribution in major organs.

In a recent study (Zhao et al., 2014), it has been reported that oxidative stress and mast cells interact with each other and promote intestinal ischemia-reperfusion induced acute lung injuries.

The decrease in NO induces mast cells which we can appreciate in all treated groups. Increased circulatory availability of nanoparticles might have reduced NO level in organs examined, which in turn could have induced the mast cells in the major organs examined compared to control.It has been reported that NO regulates mast cell function (Brooks et al., 1999) (Coleman, 2002) (Gilchrist et al., 2004). It is apparent that NO is important in both allergic and non-allergic functions of mast cell (Metzger et al., 2006).

Dextrans are known to elicit IgG and IgE antibody-mediated reactions and this could be correlated to the increased mast cells in DEX-SPIONS group in lungs.

Santosh et al, (2010), reported adverse reaction to an iron oxide with a carbohydrate shell composed of modified dextran clinically consistent with anaphylaxis, with markedly elevated serum tryptase level.

The results of the present investigative study clearly show that oxidative stress induced mast cells in all treated groups. Previous studies have demonstrated that activation of the intracellular oxidative burst was an important regulatory mechanism of mast cell responses (Suzuki et al., 2009) (Suzuki et al., 2003).

5.15 *Transmission electron microscopy studies of Liver*

It is reported that following internalization, SPION generally accumulate in lysosomes where the iron oxide core is broken down to iron ions through low pH exposure and these ions are incorporated into the hemoglobin pool (Weissleder et al., 1995). Intracellular dextranase further assist with the degradation process by cleaving the dextran moiety.

SPIONS uptake depends on the surface aspects of materials, which may be described according to their chemistry, hydrophilic/hydrophobic characteristics, or surface energy (Nel et al., 2006) (Lunov et al., 2011). These surface characteristics determine how the nanoparticles adsorb to the cell surface and more particularly, determine the cell behavior on contact. In SPIONS group, because of large surface area to volume ratio, the magnetic nanoparticles tend to agglomerate and adsorb plasma proteins (Nel et al., 2009). The variation of the protein corona composition can define the amount and fate of particles inside the cells, which strongly affect the toxicity behavior of particles (Mahmoudi et al., 2011b). The body's reticulo endothelial system (RES), mainly the Kupffer cells in the liver, usually takes up

these nanoparticles due to the hydrophobic surface. The low toxicity of nanoparticles coated with PEG may be attributed to the fact that PEG is hydrophilic, and it protects surfaces from interacting with cells or proteins. It has been demonstrated that PEG-modified nanoparticles can interact with cell membranes, resulting in enhanced cellular response, as these coatings on the nanoparticles are biocompatible, non-immunogenic, and non-antigenic (Liu et al., 2011) (Soenen et al., 2011). The initial biodistribution of SPIONS into the cells of the RES is dependent upon the half-life in the blood, the coating material and the size of the SPIONS administered (Chouly et al., 1996). Generally, SPIONS that exhibit long blood half-lives will have limited distribution into the sinusoidal cells of the liver (comprising mainly endothelial and Kupffer cells) with significant uptake into the RES cells of other organs such as the spleen, lymph nodes and bone marrow (Réty et al., 2000). However, sinusoidal liver cells will take up the majority (>70%) of the injected dose of particulate materials exhibiting relatively short blood half-lives (Briley-Saebo et al., 2004). SPIONS with smaller particle diameters are known to circulate for longer duration than particles with larger diameters. The coating material used to stabilise the particles may influence both the pharmacokinetics and biodistribution of the particles into liver cells (Weissleder et al., 1995) (Varma HK, 2014) (Weissleder et al., 1989). Ferumoxtran-10 an ultra small superparamagnetic iron oxide nanoparticle was taken up by macrophages, mostly in liver, spleen, and lymph nodes, within 24 hours after bolus injection and underwent progressive metabolism (Bourrinet et al., 2006).

5.16 *Gene expression studies*

Gene expression studies of few iron handling genes were studied, namely transferrin and ceruloplasmin and the cytoprotective genes HO-1 and HSP70 in liver which is the major organ involved in the metabolism of SPIONS. These genes are also associated with oxidative stress.

The major means of metal detoxification in cells is induction of antioxidant proteins, metal transporters, and metallothionein. Heavy metals activate the nuclear factor erythroid-derived 2-like 2 (Nrf2) and induce the expression of phase II antioxidant genes, including NADPH-quinone oxidoreductase, glutathione S-transferase Ya subunit, haemeoxygenase 1, and both subunits (catalytic and modifying) of glutamate cysteine ligase (GCL) an essential enzyme involved in the synthesis of GSH (Leonard et al., 2004).

In addition to in vitro and in vivo studies, gene-expression analysis is an important factor in molecular studies, with real-time reverse transcription (RT) polymerase chain reaction (PCR) becoming the method of choice for high throughput and accurate expression profiling of selected genes under single experiment conditions. Quantitative real-time RT PCR analysis provides substantial microarray like information on nanotoxicity-related changes in a host of gene expressions, which can be assayed simultaneously with high sensitivity and specificity, offering multiple gene expression profiling.

5.16.1 Haemoxygenase -1

The inducible isoform of haemoxygenase (HO-1) has been proposed as an effective system to counteract oxidant-induced cell injury. The cytoprotective effect

has been attributed to increased generation of the antioxidant bilirubin during haem degradation by HO-1. The results in the present study has shown that the HO-1 gene expression was upregulated 4 folds and 3 folds in DEX-SPIONS and PEG-SPIONS group respectively in liver tissue, oxidative stress was observed and more noticeably bilirubin content also was increased in those treated groups.

Clark et al, (2000) have reported that after stimulation of vascular smooth-muscle cells with hemin which is a prooxidant and potent inducer of the HO-1 gene, it was found that hemin-mediated increase in HO-1 protein expression and haemoxygenase activity was associated with increased bilirubin levels. The majority of bilirubin production occurred early after exposure of cells to hemin. It was also observed that this protective effect was manifested only when cells were actively producing bilirubin as a consequence of increased haem availability and utilization by HO-1.

In another study when PEG-35 was used as a rinse solution, reducion in hepatic injury and improvement in liver function were noted after reperfusion. The PEG-35 rinse solution prevented oxidative stress, mitochondrial damage and liver autophagy. Further, it increased the expression of cytoprotective heat shock proteins such as HO-1 and HSP70, activated AMPK, and contributed to the restoration of cytoskeleton integrity after ischemic reperfusion injury in Sprague dawley rat (Zaouali et al., 2014). This correlated with expression of HO-1 and HSP70 in liver tissue of PEG-SPIONS group in the present study.

HO-1 can be induced by a variety of seemingly disparate stimuli, most of which are linked by their ability to provoke oxidative stress. Although constitutive

expression of HO-1 in the liver is restricted to Kupffer cells, the gene is inducible in nonparenchymal as well as in parenchymal liver cells. HO-1 induction potentially confers protection against oxidative stress in a variety of experimental models, such as liver ischemia/reperfusion secondary to transplantation or hemorrhage/resuscitation. Induction of HO-1 may protect the cell against oxidative injury by (a) controlling intracellular levels of "free" heme (a prooxidant), (b) producing biliverdin (an antioxidant), (c) improving nutritive perfusion via CO release, and (d) fostering the synthesis of the Fe-binding protein ferritin. Although protective effects of up-regulation of the HO pathway presumably through production of bile pigments and CO-have been reported for a variety of cells and tissues, including the liver, evidence suggests that the protective action might be restricted to a rather narrow threshold of over expression.

5.16.2 Heat shock protein -70

In liver, HSP-70 gene was upregulated in DEX-SPIONS group when compared to control group which could be due to oxidative stress induced by the excessive load of transitional metal ions. In PEG-SPIONS group, the up regulation of HSP-70 was very minimal.

In response to many metabolic disturbances and injuries, the cell mounts a stress response with induction of a variety of proteins, most notably the 70 kDa heat shock protein (HSP-70). Heat shock proteins (HSPs) are induced by stressful stimuli and are thought to assist in the maintenance of cellular integrity and viability. HSPs consist of both stress-inducible and constitutive family members, as well as members

that are associated with specific organelles. Constitutively synthesised HSPs perform housekeeping functions.

They function as molecular chaperones by helping nascent polypeptides assume their proper conformation by binding to nascent proteins via their C-terminal domain. HSPs are also involved in antigen presentation, steroid receptor function, intracellular trafficking, nuclear receptor binding and apoptosis (Sharp et al., 1999).

However, many HSPs are up regulated by stress which in the present study is the oxidative stress caused by the coated SPIONS. The up regulation of HSP-70 may prevent protein unfolding or aggregation and enhance cell survival in the present study.

5.16.3 Transferrin

Iron is an essential metal for almost all living organisms due to its involvement in a large number of iron-containing enzymes and proteins. Cellular iron homeostasis involving the iron regulatory proteins IRP1 and IRP2 and their interactions with the iron regulatory elements, affecting either mRNA translation (ferritin and erythroid cell δ-aminolaevulinate synthase) or mRNA stability (transferrin receptor) are important. If iron were free within the cell, the element can catalyze the conversion of hydrogen peroxide into free radicals that cause damage to cellular structures. To prevent that kind of damage, living organisms bind iron atoms to different proteins such as heme, ferritin, and transferrin that allow use of the benefits of iron (Walker et al., 2001) (Wallander et al., 2006). In liver, the high levels of cytoprotective enzymes and low antioxidants, indicates that to observe toxic effects substantial

levels of iron loading are required. In reticuloendothelial cells, such as macrophages, relatively small increases in cellular iron (2–3 fold) could affect cellular signalling.

In the present study, the results have shown that the upregulation of transferrin gene expression along with cytoprotective genes like HSP-70 and HO-1 could be due oxidative stress in the cells caused by the coated iron oxide nanoparticle degradation. Soenen et al, (2010a) reported that the citrate-coated particles induced the highest level of ROS and the greatest increase in transferrin receptor 1 up regulation and interfered cell functionality intensely.

5.16.4 Ceruloplasmin

Ceruloplasmin is a ferroxidase that oxidizes toxic ferrous iron to its nontoxic ferric form. Studies in a ceruloplasmin gene-deficient ($Cp^{-/-}$) mouse has shown increased iron deposition in several regions of the CNS such as the cerebellum and brainstem. Increased lipid peroxidation was also seen in some CNS regions. Cerebellar cells from neonatal $Cp^{-/-}$ mice were also more susceptible to oxidative stress. The authors reported that ceruloplasmin plays an important role in maintaining iron homeostasis in the CNS and in protecting the CNS from iron-mediated free radical injury (Patel et al., 2002). In the present study, the elevated level of expression of ceruloplasmin in DEX-SPIONS and PEG-SPIONS group could have important implications in protecting cells from iron induced toxicity.

5.17 *ICP-OES Elemental analysis*

Fe, Cu, Zn, Mg, and Mn elemental distribution in liver, spleen and kidney were found to be disturbed in treated groups.

In mammals and man, a trace element is defined as one that makes up less than 0.01% of the body's mass. Together, the 50 or more trace elements found in the body, both normal and abnormal, make up less than 0.2% of the total weight of the body. Iron, fluorine, and zinc, the most abundant trace elements, comprise 0.006%, 0.0037%, and 0.0033% of the body, respectively. By comparison, the least abundant bulk elements, magnesium and silicon, make up 0.027% and 0.026%, respectively, of the body. There are two general classes of abnormalities associated with trace elements: specific deficiency-from dietary inadequacies, imbalances, or secondary to other diseases and accumulation of innately toxic trace elements from the environment, which can either displace essential elements from their metabolically active sites and cause conditional deficiency, or act directly as cellular toxins.

Manganese is essential for glucose and lipid metabolism, oxidative phosphorylation and a number of other basic biochemical processes and it is essential that human beings have adequate amounts.

Both kinds of abnormalities can be diagnosed by analyses of trace elements in plasma or serum, red blood cells, and urine. Furthermore, secondary changes occur as a result of systemic disease; they are not yet under stood.

SPIONS accumulation / distribution should be studied to understand the cellular toxicity concerns. So, the present study evaluated the distribution of iron in liver, kidney and spleen. Simultaneously, the study checked the alterations in some of the divalent metal cations also in those organs.

The effects of trace element are heavily dependent on one another. Thus, high intakes of zinc, cadmium or copper interfere with the utilization and tissue storage of

iron. Low concentrations of dietary iron enhance the absorption of not only dietary iron, but also of lead, zinc, cadmium cobalt and manganese (Tapiero et al., 2003).

Inductively coupled plasma optical emission spectroscopy (ICP-OES) is one of the most commonly used techniques for elemental ion quantification. However, it must be pointed out that this technique determines total tissue iron. In addition to the exogenous iron, animal tissues are also rich in endogenous iron in the form of iron-containing proteins (e.g., hemoglobin, transferrin, and ferritin). In experimental condition the control tissues which did not receive any SPIONS may be considered to be base line values.

A study by Cortese-Krott et al, (2009) showed that human skin fibroblasts treated with concentrations of $AgNO_3$ induced oxidative stress. Furthermore Ag+ induced a transient intracellular zinc release and increased the mRNA and protein expression of the zinc-binding protein metallothionein by activating the metal-responsive transcription factor 1and affecting intracellular zinc homeostasis in the fibroblasts.

6 SUMMARY

6.1 *Summary*

Nanoparticles have the potential to be used in different biological and medical applications as tools for noninvasive imaging, drug delivery and recently as theranostic agents. Properties present only at nanoscale level, like the switchable magnetic properties of superparamagnetic iron oxide (SPIONS) nanoparticles, make these materials unique and useful for applications in biomedical field of MRI imaging, magnetic hyperthermia and drug delivery. In order to prevent the agglomeration, to improve the biocompatibility and to increase functionalisation, the surfaces of the SPIONS are modified with inorganic materials and organic materials including polysaccharides and polymers. Many studies have demonstrated that though SPIONS have various applications, they also have the potential to cause adverse effects to the system.

The present study was carried out in three phases with the objective to understand the adverse events caused by different surface modification of SPIONS at cellular and molecular level. In phase I, SPIONS nanoparticle was synthesised by chemical co-precipitation method and average particle diameter was 10.3 nm. The surfaces were modified with Dextran (DEX-SPIONS) and Polyethyleneglycol (PEG-SPIONS). The hydrodynamic diameter of SPIONS, DEX-SPIONS and PEG-SPIONS were 45, 89 and 67 nm respectively and zeta potentials were -11.00, + 7.67, + 6.07 mV respectively. XRD results have shown that the synthesised particles were magneteite and FT-IR indicated the presence of characteristic peaks for Dextran and

PEG specific molecules over the surface of SPIONS. VSM results have demonstrated the superparamagnetic property of synthesised particles.

In phase II, the nanoparticles were tested for cytocompatibility and haemocompatibility. The cytotoxicity results have shown that the synthesised SPIONS, DEX-SPIONS, PEG SPIONs were non cytotoxic to L929 and RAW 264.7 cells after 24 h exposure. In vitro cytocompatibility with fibroblasts and RAW 264.7 cells showed more favourable cell proliferation and metabolic activity in coated particles than uncoated ones. SPIONS nanoparticle affected the metabolic activity in concentration dependent manner when they were added in the concentration range of 50-12.25µg to the cells. It was observed that the cell proliferation/viability decreased when the concentration of SPIONS increased.

Live and dead assay also indicated that more than 95% cell viability in coated as well as uncoated nanoparticle groups but substantial increase in viability was observed in coated group compared to uncoated group. Haemocompatibility results have shown that the haematological parameters and hemolysis % of SPIONS, DEX-SPIONS and PEG-SPIONS were well within the acceptable limit.

The confocal Raman microscopic studies demonstrated the uptake of nanoparticles by L929 fibroblast cells and RAW 264.7 macrophages. The nanoparticles were mostly distributed in the cytoplasm.

Oxidative stress results in HepG2 cells showed significant increase in lipid peroxides level in cell lysates of SPIONS treated cells when compared with control. The level of reduced glutathione, superoxide dismutase and nitrite level in cell

lysates of SPIONS, DEX-SPIONS and PEG-SPIONS treated cells were decreased significantly when compared to control.

Intravenous administration of the SPIONS, DEX-SPIONS and PEG-SPIONs in rats in phase III of the study did not result in any adverse signs and symptoms. The results of haematological and biochemical parameters shows that in haematology, the mixed cell populations of treated groups were significantly increased when compared to control values which, could be expected from an acute immune response to foreign materials, here SPIONs. The biochemical parameters, namely SGOT level was significantly increased in DEX-SPIONS group, GGT level was significantly increased in SPIONS group when compared to control group. Bilirubin content was detected in the serum of treated groups and found to be within the normal range for this species but in the control group it is below the detectable limit.

Oxidative stress results showed significant increase in lipid peroxides level in liver, lung and heart tissue homogenates of SPIONS treated animals when compared to control groups. The level of reduced glutathione in liver, lung, spleen and kidney tissue homogenates of SPIONS, DEX-SPIONS and PEG-SPIONS treated animals were decreased significantly except lung of DEX-SPIONS when compared to control group. The level of SOD in liver, lung, spleen, kidney and heart tissue homogenates of SPIONS, DEX-SPIONS and PEG-SPIONS treated animals were decreased but not statistically significant when compared to control group. The level of nitrite in liver, lung, spleen, kidneys and heart tissue homogenates of SPIONS, DEX-SPIONS

and PEG-SPIONS treated animals were decreased significantly except kidney of PEG-SPIONS when compared to control group.

Liver architecture was normal in all groups. In SPIONS group, hepatocytes with discreet nucleus, moderate granular cytoplasmic degeneration and multi focal intra hepatocyte cholestasis were found compared to control group. In DEX-SPIONS group, few polymorphonuclear cells and moderate proliferation of Kuppfer cells with brown-yellow cytoplasmic pigments were seen in the sinusoidal space. Hepatocytes with discrete nucleus and eosinophilic dark granular cytoplasm were observed. In PEG-SPIONS group, very few Kuppfer cells with occasional brown-yellow cytoplasmic pigments were seen in the sinusoidal space and hepatocytes with discrete nucleus and granular cytoplasm was observed. Iron deposits in the cytoplasm of Kupffer cells were observed in the SPIONS, DEX-SPIONS group and iron deposits were also seen in sinusoids and cytoplasm of hepatocytes in PEG-SPIONS group. Mast cells were observed more in DEX-SPIONS but not statistically significant and also in SPIONS and PEG-SPIONS group compared to control group. Mast Cells were mostly distributed in the periportal region in all groups.

The histological micrographs of kidneys show normal architecture. In SPIONS group, glomeruli appeared normal in the cortex region. Protein casts were observed in the collecting tubular lumen. Tubular epithelial cells with enlarged nuclei, formation of prominent nucleoli and marked granular cytoplasm were observed. In DEX-SPIONS group, focal tubular degeneration was seen with the tubular epithelium showing moderate granular cytoplasmic degeneration. In PEG-SPIONS group, glomeruli architecture was normal; Protein casts were noted in the convoluted

tubular lumen. Iron deposits in the cytoplasm of convoluted tubule cells were observed in the SPIONS group, DEX-SPIONS group and PEG SPIONS group. These deposits were also seen in the glomerular region in PEG-SPIONS group. Mast cells were absent in the cortex region in all three groups and control group. They were mostly distributed in the hilus and medulla region in all groups.

Pulmonary architecture was preserved in all groups. In SPIONS group, infiltration of macrophages in the alveolar septa was seen. In DEX-SPIONS group, infiltration of macrophages in the alveolar septa and peribronchial region was seen. In PEG-SPIONS group, mild peribronchial infiltration of macrophages was noted. Iron deposits in the cytoplasm of macrophage cells were observed in the SPIONS group in the alveolar region, macrophages of peribronchial region in DEX-SPIONS group and perivascular region in PEG-SPIONS group. Mast cells were observed significantly more in DEX-SPIONS group and in SPIONS, PEG-SPIONS group it was more but not statistically significant compared to control group. Mast Cells were mostly distributed in the peribronchial and alveolar region in DEX-SPIONS group and in the ventral border of alveolar region in PEG-SPIONS and SPIONS group.

Spleenic architecture was normal in all groups. In SPIONS and DEX-SPIONS group, brown siderotic pigments were seen in the macrophages in the spleenic red pulp. In PEG-SPIONS group, there was relatively increased number of macrophages were observed in the spleenic red pulp area. Iron deposits were observed in the cytoplasm of macrophage cells in the red pulp region in the SPIONS group, DEX-SPIONS group and PEG-SPIONS group with more intensity in the later group. Mast

cells were absent in DEX-SPIONS and SPIONS group and were scant in PEG-SPIONS group as compared to control group.

Histological sections of heart show normal architecture. There were no changes in striations and no nuclear changes. Iron deposits in the perivascular region were observed in the SPIONS group, DEX-SPIONS group and PEG-SPIONS group. Mast Cells were mostly distributed in the peri vascular region in all groups and in addition in the sub endocardial region of SPIONS group. Mast cells were observed significantly more in PEG-SPIONS and followed by DEX- SPIONS group and SPIONS group compared to control group.

The ultrastructural images of liver injected with DEX-SPIONS, PEG-SPIONS and SPIONS shown aggregates of iron particles in the cytoplasm of Kuppfer cells in SPIONS, DEX-SPIONS group. Particles could not be identified in the cytoplasm of Kupffer cells in PEG-SPIONS group. The absence is correlates with few Kuppfer cells seen in H&E section.

Gene expression studies revealed that transferrin and ceruloplasmin genes were up regulated in coated groups when compared to control group which could be due to iron over load. Similarly HSP-70 and HO-1 genes were also up regulated when compared to control group which could be due to oxidative stress induced by the excessive load of transitional metal ions.

Elemental analysis showed that iron content was increased significantly in spleen of treated groups when compared to control. Copper content was significantly increased in SPIONs group alone when compared to control. Calcium level was significantly increased in kidney of PEG-SPIONS group and spleen of DEX-

SPIONS group when compared to control group. Magnesium and Zinc level was significantly increased in spleen of DEX-SPIONS group. Manganese was significantly increased in liver and spleen of SPIONS, PEG-SPIONS and DEX-SPIONS group and significantly decreased in kidney of SPIONS, DEX-SPIONS group when compared to control group.

6.2 *Conclusion*

In conclusion, results of this short term investigation into cellular effects of superparamagnetic iron oxide nanoparticles and surface modified nanoparticles show evidence of intracellular oxidative stress and iron accumulation. Though the SPIONS as well as Dextran and PEG coated nanoparticles are cytocompatible in vitro, twenty four hours posts intravenous administration in rats does give rise to adverse intracellular effects. This suggests that exposure of the cell mileu to SPIONS either as bare nanoparticles or surface modified nanoparticles, makes the cell more sensitive to oxidative stress. Degradation of the coatings wit release of SPIONS into the cytoplasm may have lead to the cytotoxic changes observed. The resultant iron overload, leads to induction of cytoprotective gene expression. This iron over load in major organs including liver and kidney also leads to altered elemental distribution in the body. Furthermore, the increased mast cells in these organs are important in reference to the coatings used for improving the biocompatibility of iron oxide nanoparticles.

The present in depth investigative study of intracellular effects of one time administration of superparamagnetic nanoparticles, as used as contrast agents in MRI and theranostics, advocates caution.

6.3 *Future direction*

Future, investigations should focus on elucidation of the long term effect of SPIONS on divalent metal cation homeostasis. There is a need to study gene expression associated to the iron transport and other divalent metal cation transport using specific knock out models.

BIBLIOGRAPHY

Abraham SN, John ALS (2010) Mast cell-orchestrated immunity to pathogens. Nat. Rev. Immunol. **10**: 440–452.

Aggarwal P, Hall JB, McLeland CB, Dobrovolskaia MA, McNeil SE (2009) Nanoparticle interaction with plasma proteins as it relates to particle biodistribution, biocompatibility and therapeutic efficacy. Adv. Drug Deliv. Rev. **61**: 428–437. doi:10.1016/j.addr.2009.03.009.

Ahamed M, Alhadlaq HA, Alam J, Khan MAM, Ali D, Alarafi S (2013) Iron oxide nanoparticle-induced oxidative stress and genotoxicity in human skin epithelial and lung epithelial cell lines. Curr. Pharm. Des. **19**: 6681–6690.

Albanese A, Tang PS, Chan WC (2012) The effect of nanoparticle size, shape, and surface chemistry on biological systems. Annu. Rev. Biomed. Eng. **14**: 1–16.

Alcalá MD, Real C (2006) Synthesis based on the wet impregnation method and characterization of iron and iron oxide-silica nanocomposites. Solid State Ion. **177**: 955–960. doi:10.1016/j.ssi.2006.01.019.

Alderton WK, Cooper CE, Knowles RG (2001) Nitric oxide synthases: structure, function and inhibition. Biochem. J. **357**: 593–615.

Alexis F, Pridgen E, Molnar LK, Farokhzad OC (2008) Factors Affecting the Clearance and Biodistribution of Polymeric Nanoparticles. Mol. Pharm. **5**: 505–515. doi:10.1021/mp800051m.

Ali LMA, Gutiérrez M, Cornudella R, Moreno JA, Piñol R, Gabilondo L, Millán A, Palacio F (2013) Hemostasis disorders caused by polymer coated iron oxide nanoparticles. J. Biomed. Nanotechnol. **9**: 1272–1285.

Almeida JPM, Chen AL, Foster A, Drezek R (2011) In vivo biodistribution of nanoparticles. Nanomed. **6**: 815–835.

Alvarim LT, Nucci LP, Mamani JB, Marti LC, Aguiar MF, Silva HR, Silva GS, Nucci-da-Silva MP, DelBel EA, Gamarra LF (2014) Therapeutics with SPION-labeled stem cells for the main diseases related to brain aging: a systematic review. Int. J. Nanomedicine **9**: 3749.

Anderson KA (1999) Analytical Techniques for Inorganic Contaminants, AOAC International. AOAC International, Gaithersberg, MD, USA.

Ankamwar B, Lai TC, Huang JH, Liu RS, Hsiao M, Chen CH, Hwu YK (2010) Biocompatibility of Fe(3)O(4) nanoparticles evaluated by in vitro cytotoxicity assays using normal, glia and breast cancer cells. Nanotechnology **21**: 75102. doi:10.1088/0957-4484/21/7/075102.

AOAC International (2006) AOAC Official Methods of Analysis No.990.08, 18th Ed (Revised). AOAC International, Gaithersberg, MD, USA.

Apel K, Hirt H (2004) Reactive oxygen species: metabolism, oxidative stress, and signal transduction. Annu. Rev. Plant Biol. **55**: 373–399. doi:10.1146/annurev.arplant.55.031903.141701.

Arbab AS, Wilson LB, Ashari P, Jordan EK, Lewis BK, Frank JA (2005) A model of lysosomal metabolism of dextran coated superparamagnetic iron oxide (SPIO) nanoparticles: implications for cellular magnetic resonance imaging. NMR Biomed. **18**: 383–389. doi:10.1002/nbm.970.

Arbi S, Eksteen EC, Oberholzer HM, Taute H, Bester MJ (2015) Premature Collagen Fibril Formation, Fibroblast-Mast Cell Interactions and Mast Cell-Mediated Phagocytosis of Collagen in Keloids. Ultrastruct. Pathol.: 1–9. doi:10.3109/01913123.2014.981326.

Arora PD, Wang Y, Bresnick A, Dawson J, Janmey PA, McCulloch CA (2013) Collagen remodeling by phagocytosis is determined by collagen substrate topology and calcium-dependent interactions of gelsolin with nonmuscle myosin IIA in cell adhesions. Mol. Biol. Cell **24**: 734–747. doi:10.1091/mbc.E12-10-0754.

Ben-Assa E, Youngster I, Kozer E, Abu-Kishk I, Bar-Haim A, Bar-Oz B, Berkovitch M (2009) Changes in serum hepcidin levels in acute iron intoxication in a rat model. Toxicol. Lett. **189**: 242–247. doi:10.1016/j.toxlet.2009.06.848.

Babes L, Tanguy G, Le Jeune JJ, Jallet P, others (1999) Synthesis of iron oxide nanoparticles used as MRI contrast agents: a parametric study. J. Colloid Interface Sci. **212**: 474–482.

Bačić G, Spasojević I, Šećerov B, Mojović M (2008) Spin-trapping of oxygen free radicals in chemical and biological systems: New traps, radicals and possibilities. Spectrochim. Acta. A. Mol. Biomol. Spectrosc. **69**. Selected papers from the 10th EMARDIS Meeting 10th EMARDIS: 1354–1366. doi:10.1016/j.saa.2007.09.047.

Balasubramanian SK, Jittiwat J, Manikandan J, Ong C-N, Yu LE, Ong W-Y (2010) Biodistribution of gold nanoparticles and gene expression changes in the liver and spleen after intravenous administration in rats. Biomaterials **31**: 2034–2042. doi:10.1016/j.biomaterials.2009.11.079.

Barratt GM (2000) Therapeutic applications of colloidal drug carriers. Pharm. Sci. Technol. Today **3**: 163–171. doi:10.1016/S1461-5347(00)00255-8.

Barrefelt Å, Saghafian M, Kuiper R, Ye F, Egri G, Klickermann M, Brismar TB, Aspelin P, Muhammed M, Dähne L, Hassan M (2013) Biodistribution, kinetics, and biological fate of SPION microbubbles in the rat. Int. J. Nanomedicine **8**: 3241–3254. doi:10.2147/IJN.S49948.

Beeran AE, Nazeer SS, Fernandez FB, Muvvala KS, Wunderlich W, Anil S, Vellappally S, Rao MSR, John A, Jayasree RS, Varma PRH (2015) An aqueous method for the controlled manganese (Mn2+) substitution in superparamagnetic iron oxide nanoparticles for contrast enhancement in MRI. Phys. Chem. Chem. Phys. **17**: 4609–4619. doi:10.1039/C4CP05122J.

Benzie IF (1996) Lipid peroxidation: a review of causes, consequences, measurement and dietary influences. Int. J. Food Sci. Nutr. **47**: 233–261.

Bergamini CM, Gambetti S, Dondi A, Cervellati C (2004) Oxygen, reactive oxygen species and tissue damage. Curr. Pharm. Des. **10**: 1611–1626.

Berry CC, Wells S, Charles S, Curtis ASG (2003) Dextran and albumin derivatised iron oxide nanoparticles: influence on fibroblasts in vitro. Biomaterials **24**: 4551–4557.

Binh VT, Purcell ST, Semet V, Feschet F (1998) Nanotips and nanomagnetism. Appl. Surf. Sci. **130–132**: 803–814. doi:10.1016/S0169-4332(98)00158-5.

Bourrinet P, Bengele HH, Bonnemain B, Dencausse A, Idee J-M, Jacobs PM, Lewis JM (2006) Preclinical safety and pharmacokinetic profile of ferumoxtran-10, an ultrasmall superparamagnetic iron oxide magnetic resonance contrast agent. Invest. Radiol. **41**: 313–324. doi:10.1097/01.rli.0000197669.80475.dd.

Briley-Saebo K, Bjørnerud A, Grant D, Ahlstrom H, Berg T, Kindberg GM (2004) Hepatic cellular distribution and degradation of iron oxide nanoparticles following single intravenous injection in rats: implications for magnetic resonance imaging. Cell Tissue Res. **316**: 315–323. doi:10.1007/s00441-004-0884-8.

Brooks AC, Whelan CJ, Purcell WM (1999) Reactive oxygen species generation and histamine release by activated mast cells: modulation by nitric oxide synthase inhibition. Br. J. Pharmacol. **128**: 585–590. doi:10.1038/sj.bjp.0702838.

Brunner TJ, Wick P, Manser P, Spohn P, Grass RN, Limbach LK, Bruinink A, Stark WJ (2006) In Vitro Cytotoxicity of Oxide Nanoparticles: Comparison to Asbestos, Silica, and the Effect of Particle Solubility †. Environ. Sci. Technol. **40**: 4374–4381. doi:10.1021/es052069i.

Bulte JWM (2009) In vivo MRI cell tracking: clinical studies. AJR Am. J. Roentgenol. **193**: 314–325. doi:10.2214/AJR.09.3107.

Bulte JW, Douglas T, Witwer B, Zhang SC, Strable E, Lewis BK, Zywicke H, Miller B, van Gelderen P, Moskowitz BM, Duncan ID, Frank JA (2001) Magnetodendrimers allow endosomal magnetic labeling and in vivo tracking of stem cells. Nat. Biotechnol. **19**: 1141–1147. doi:10.1038/nbt1201-1141.

Cabuil V, Dubois E, Neveu S, Bacri J-C, Hasmonay E, Perzynski R (1995) Phase separation in aqueous magnetic colloidal solutions. In Trends Colloid Interface Sci. IX, 23–29. Springer. http://link.springer.com/chapter/10.1007/BFb0115201.

Calvin S, Carpenter EE, Harris VG (2003) Characterization of passivated iron nanoparticles by x-ray absorption spectroscopy. Phys. Rev. B **68**: 033411.

Canesi L, Ciacci C, Betti M, Fabbri R, Canonico B, Fantinati A, Marcomini A, Pojana G (2008) Immunotoxicity of carbon black nanoparticles to blue mussel hemocytes. Environ. Int. **34**: 1114–1119. doi:10.1016/j.envint.2008.04.002.

Carmen Bautista M, Bomati-Miguel O, del Puerto Morales M, Serna CJ, Veintemillas-Verdaguer S (2005) Surface characterisation of dextran-coated iron oxide nanoparticles prepared by laser pyrolysis and coprecipitation. J. Magn. Magn. Mater. **293**. Proceedings of the Fifth International Conference on Scientific and Clinical Apllications of Magnetic Carriers: 20–27. doi:10.1016/j.jmmm.2005.01.038.

Cheng F-Y, Su C-H, Yang Y-S, Yeh C-S, Tsai C-Y, Wu C-L, Wu M-T, Shieh D-B (2005) Characterization of aqueous dispersions of Fe 3 O 4 nanoparticles and their biomedical applications. Biomaterials **26**: 729–738.

Chen J, Xiu Z, Lowry GV, Alvarez PJJ (2011) Effect of natural organic matter on toxicity and reactivity of nano-scale zero-valent iron. Water Res. **45**: 1995–2001. doi:10.1016/j.watres.2010.11.036.

Chen J, Wang H, Long W, Shen X, Wu D, Song S-S, Sun Y-M, Liu P-X, Fan S, Fan F, Zhang X-D (2013) Sex differences in the toxicity of polyethylene glycol-coated gold nanoparticles in mice. Int. J. Nanomedicine **8**: 2409–2419. doi:10.2147/IJN.S46376.

Chen Q, Rondinone AJ, C. Chakoumakos B, John Zhang Z (1999) Synthesis of superparamagnetic MgFe2O4 nanoparticles by coprecipitation. J. Magn. Magn. Mater. **194**: 1–7. doi:10.1016/S0304-8853(98)00585-X.

Chnari E, Nikitczuk JS, Uhrich KE, Moghe PV (2006) Nanoscale anionic macromolecules can inhibit cellular uptake of differentially oxidized LDL. Biomacromolecules **7**: 597–603. doi:10.1021/bm0506905.

Choi JY, Lee SH, Na HB, An K, Hyeon T, Seo TS (2010) In vitro cytotoxicity screening of water-dispersible metal oxide nanoparticles in human cell lines. Bioprocess Biosyst. Eng. **33**: 21–30.

Chouly C, Pouliquen D, Lucet I, Jeune JJ, Jallet P (1996) Development of superparamagnetic nanoparticles for MRI: effect of particle size, charge and surface nature on biodistribution. J. Microencapsul. **13**: 245–255. doi:10.3109/02652049609026013.

Cho W-S, Cho M, Jeong J, Choi M, Cho H-Y, Han BS, Kim SH, Kim HO, Lim YT, Chung BH, Jeong J (2009) Acute toxicity and pharmacokinetics of 13 nm-sized PEG-coated gold nanoparticles. Toxicol. Appl. Pharmacol. **236**: 16–24. doi:10.1016/j.taap.2008.12.023.

Clark JE, Foresti R, Green CJ, Motterlini R (2000) Dynamics of haem oxygenase-1 expression and bilirubin production in cellular protection against oxidative stress. Biochem. J. **348**: 615–619.

Coccini T (2014) Gene Expression Changes in Rat Liver and Testes after Lung Instillation of a Low Dose of Silver Nanoparticles. J. Nanomedicine Nanotechnol. **05**. doi:10.4172/2157-7439.1000227.

Cole AJ, David AE, Wang J, Galbán CJ, Hill HL, Yang VC (2011) Polyethylene glycol modified, cross-linked starch-coated iron oxide nanoparticles for enhanced magnetic tumor targeting. Biomaterials **32**: 2183–2193.

Coleman JW (2002) Nitric oxide: a regulator of mast cell activation and mast cell-mediated inflammation. Clin. Exp. Immunol. **129**: 4–10.

Cortese-Krott MM, Münchow M, Pirev E, Hessner F, Bozkurt A, Uciechowski P, Pallua N, Kröncke K-D, Suschek CV (2009) Silver ions induce oxidative stress and intracellular zinc release in human skin fibroblasts. Free Radic. Biol. Med. **47**: 1570–1577. doi:10.1016/j.freeradbiomed.2009.08.023.

Crichton RR, Wilmet S, Legssyer R, Ward RJ (2002) Molecular and cellular mechanisms of iron homeostasis and toxicity in mammalian cells. J. Inorg. Biochem. **91**: 9–18.

Cui Y, Liu H, Ze Y, Zengli Z, Hu Y, Cheng Z, Cheng J, Hu R, Gao G, Wang L, Tang M, Hong F (2012) Gene Expression in Liver Injury Caused by Long-term Exposure to Titanium Dioxide Nanoparticles in Mice. Toxicol. Sci. **128**: 171–185. doi:10.1093/toxsci/kfs153.

Deiana M, Aruoma OI, Rosa A, Crobu V, Casu V, Piga R, Dessi MA (2001) The effect of ferric-nitrilotriacetic acid on the profile of polyunsaturated fatty acids in the kidney and liver of rats. Toxicol. Lett. **123**: 125–133.

Devalapally H, Duan Z, Seiden MV, Amiji MM (2008) Modulation of Drug Resistance in Ovarian Adenocarcinoma by Enhancing Intracellular Ceramide Using Tamoxifen-Loaded Biodegradable Polymeric Nanoparticles. Clin. Cancer Res. **14**: 3193–3203. doi:10.1158/1078-0432.CCR-07-4973.

Devasagayam TPA, Tilak JC, Boloor KK, Sane KS, Ghaskadbi SS, Lele RD (2004) Free radicals and antioxidants in human health: current status and future prospects. J. Assoc. Physicians India **52**: 794–804.

Diem M, Miljkovi, Milonovik, Bird B, Chernenko T, Schubert J, Marcsisin E, Mazur A, Kingston E, Zuser E, Papamarkakis K, Laver N (2012) Applications of Infrared and Raman Microspectroscopy of Cells and Tissue in Medical Diagnostics: Present Status and Future Promises. J. Spectrosc. **27**: 463–496.

Dorney J, Bonnier F, Garcia A, Casey A, Chambers G, Byrne HJ (2012) Identifying and localizing intracellular nanoparticles using Raman spectroscopy. The Analyst **137**: 1111–1119. doi:10.1039/c2an15977e.

Dumortier H, Lacotte S, Pastorin G, Marega R, Wu W, Bonifazi D, Briand J-P, Prato M, Muller S, Bianco A (2006) Functionalized carbon nanotubes are non-cytotoxic and preserve the functionality of primary immune cells. Nano Lett. **6**: 1522–1528.

Dykman LA, Khlebtsov NG (2014) Uptake of Engineered Gold Nanoparticles into Mammalian Cells. Chem. Rev. **114**: 1258–1288. doi:10.1021/cr300441a.

Emerit J, Beaumont C, Trivin F (2001) Iron metabolism, free radicals, and oxidative injury. Biomed. Pharmacother. Bioméd. Pharmacothérapie **55**: 333–339.

Enamorado-Bais, Ez SM, Abril JM, mez-Guzmais, N JM (2013) Determination of 25 Trace Element Concentrations in Biological Reference Materials by ICP-MS following Different Microwave-Assisted Acid Digestion Methods Based on Scaling Masses of Digested Samples. Int. Sch. Res. Not. **2013**: e851713. doi:10.1155/2013/851713.

Estrela-Lopis I, Romero G, Rojas E, Moya SE, Donath E (2011a) Nanoparticle uptake and their co-localization with cell compartments – a confocal Raman microscopy study at single cell level. J. Phys. Conf. Ser. **304**: 012017. doi:10.1088/1742-6596/304/1/012017.

Estrela-Lopis I, Romero G, Rojas E, Moya SE, Donath E (2011b) Nanoparticle uptake and their co-localization with cell compartments – a confocal Raman microscopy study at single cell level. J. Phys. Conf. Ser. **304**: 012017. doi:10.1088/1742-6596/304/1/012017.

Fang C, Shi B, Pei Y-Y, Hong M-H, Wu J, Chen H-Z (2006) In vivo tumor targeting of tumor necrosis factor-alpha-loaded stealth nanoparticles: effect of MePEG molecular weight and particle size. Eur. J. Pharm. Sci. Off. J. Eur. Fed. Pharm. Sci. **27**: 27–36. doi:10.1016/j.ejps.2005.08.002.

Fariss MW, Chan CB, Patel M, Van Houten B, Orrenius S (2005) Role of mitochondria in toxic oxidative stress. Mol. Interv. **5**: 94–111. doi:10.1124/mi.5.2.7.

Fischer HC, Chan WC (2007) Nanotoxicity: the growing need for in vivo study. Curr. Opin. Biotechnol. **18**. Chemical biotechnology / Pharmaceutical biotechnology: 565–571. doi:10.1016/j.copbio.2007.11.008.

Frossi B, De Carli M, Daniel KC, Rivera J, Pucillo C (2003) Oxidative stress stimulates IL-4 and IL-6 production in mast cells by an APE/Ref-1-dependent pathway. Eur. J. Immunol. **33**: 2168–2177. doi:10.1002/eji.200323995.

Fruijtier-Pölloth C (2005) Safety assessment on polyethylene glycols (PEGs) and their derivatives as used in cosmetic products. Toxicology **214**: 1–38. doi:10.1016/j.tox.2005.06.001.

Galli SJ, Grimbaldeston M, Tsai M (2008) Immunomodulatory mast cells: negative, as well as positive, regulators of innate and acquired immunity. Nat. Rev. Immunol. **8**: 478–486. doi:10.1038/nri2327.

Gannon CJ, Cherukuri P, Yakobson BI, Cognet L, Kanzius JS, Kittrell C, Weisman RB, Pasquali M, Schmidt HK, Smalley RE, Curley SA (2007) Carbon nanotube-enhanced thermal destruction of cancer cells in a noninvasive radiofrequency field. Cancer **110**: 2654–2665. doi:10.1002/cncr.23155.

Gierlinger N, Keplinger T, Harrington M (2012) Imaging of plant cell walls by confocal Raman microscopy. Nat. Protoc. **7**: 1694–1708. doi:10.1038/nprot.2012.092.

Gilchrist M, McCauley SD, Befus AD (2004) Expression, localization, and regulation of NOS in human mast cell lines: effects on leukotriene production. Blood **104**: 462–469. doi:10.1182/blood-2003-08-2990.

Giljohann DA, Seferos DS, Patel PC, Millstone JE, Rosi NL, Mirkin CA (2007) Oligonucleotide loading determines cellular uptake of DNA-modified gold nanoparticles. Nano Lett. **7**: 3818–3821. doi:10.1021/nl072471q.

Goodman CM, McCusker CD, Yilmaz T, Rotello VM (2004) Toxicity of gold nanoparticles functionalized with cationic and anionic side chains. Bioconjug. Chem. **15**: 897–900.

Greish K (2010) Enhanced permeability and retention (EPR) effect for anticancer nanomedicine drug targeting. In Cancer Nanotechnol., 25–37. Springer. http://link.springer.com/protocol/10.1007/978-1-60761-609-2_3.

Gulati N, Rastogi R, Dinda AK, Saxena R, Koul V (2010) Characterization and cell material interactions of PEGylated PNIPAAM nanoparticles. Colloids Surf. B Biointerfaces **79**: 164–173. doi:10.1016/j.colsurfb.2010.03.049.

Gu L, Fang RH, Sailor MJ, Park J-H (2012) In Vivo Clearance and Toxicity of Monodisperse Iron Oxide Nanocrystals. ACS Nano **6**: 4947–4954. doi:10.1021/nn300456z.

Gupta AK, Curtis ASG (2004) Surface modified superparamagnetic nanoparticles for drug delivery: Interaction studies with human fibroblasts in culture. J. Mater. Sci. Mater. Med. **15**: 493–496. doi:10.1023/B:JMSM.0000021126.32934.20.

Gupta AK, Gupta M (2005) Synthesis and surface engineering of iron oxide nanoparticles for biomedical applications. Biomaterials **26**: 3995–4021. doi:10.1016/j.biomaterials.2004.10.012.

Gupta AK, Naregalkar RR, Vaidya VD, Gupta M (2007) Recent advances on surface engineering of magnetic iron oxide nanoparticles and their biomedical applications. Nanomed. **2**: 23–39. doi:10.2217/17435889.2.1.23.

Gupta AK, Wells S (2004a) Surface-modified superparamagnetic nanoparticles for drug delivery: preparation, characterization, and cytotoxicity studies. IEEE Trans. NanoBioscience **3**: 66–73. doi:10.1109/TNB.2003.820277.

Gupta AK, Wells S (2004b) Surface-modified superparamagnetic nanoparticles for drug delivery: preparation, characterization, and cytotoxicity studies. IEEE Trans. NanoBioscience **3**: 66–73. doi:10.1109/TNB.2003.820277.

Häfeli UO, Riffle JS, Harris-Shekhawat L, Carmichael-Baranauskas A, Mark F, Dailey JP, Bardenstein D (2009) Cell uptake and in vitro toxicity of magnetic nanoparticles suitable for drug delivery. Mol. Pharm. **6**: 1417–1428. doi:10.1021/mp900083m.

Hanini A, Schmitt A, Kacem K, Chau F, Ammar S, Gavard J (2011) Evaluation of iron oxide nanoparticle biocompatibility. Int. J. Nanomedicine **6**: 787–794. doi:10.2147/IJN.S17574.

Harris ZL, Durley AP, Man TK, Gitlin JD (1999) Targeted gene disruption reveals an essential role for ceruloplasmin in cellular iron efflux. Proc. Natl. Acad. Sci. U. S. A. **96**: 10812–10817.

Hellman NE, Gitlin JD (2002) Ceruloplasmin metabolism and function. Annu. Rev. Nutr. **22**: 439–458. doi:10.1146/annurev.nutr.22.012502.114457.

Huang G, Diakur J, Xu Z, Wiebe LI (2008) Asialoglycoprotein receptor-targeted superparamagnetic iron oxide nanoparticles. Int. J. Pharm. **360**: 197–203. doi:10.1016/j.ijpharm.2008.04.029.

Hubbs AF, Sargent LM, Porter DW, Sager TM, Chen BT, Frazer DG, Castranova V, Sriram K, Nurkiewicz TR, Reynolds SH, Battelli LA, Schwegler-Berry D, McKinney W, Fluharty KL, Mercer RR (2013) Nanotechnology: toxicologic pathology. Toxicol. Pathol. **41**: 395–409. doi:10.1177/0192623312467403.

Hume DA, Ross IL, Himes SR, Sasmono RT, Wells CA, Ravasi T (2002) The mononuclear phagocyte system revisited. J. Leukoc. Biol. **72**: 621–627.

Hu, Neoh KG, Cen L, Kang E-T (2006) Cellular Response to Magnetic Nanoparticles “PEGylated” via Surface-Initiated Atom Transfer Radical Polymerization. Biomacromolecules **7**: 809–816. doi:10.1021/bm050870e.

Hussain SM, Hess KL, Gearhart JM, Geiss KT, Schlager JJ (2005) In vitro toxicity of nanoparticles in BRL 3A rat liver cells. Toxicol. In Vitro **19**. Thirteenth International Workshop on In Vitro Toxicology Thirteenth International Workshop on In Vitro Toxicology: 975–983. doi:10.1016/j.tiv.2005.06.034.

ISO 10993-4:2002:Biological evaluation of medical devices -- Part 4: Selection of tests for interactions with blood. ISO.

Jain TK, Reddy MK, Morales MA, Leslie-Pelecky DL, Labhasetwar V (2008) Biodistribution, clearance, and biocompatibility of iron oxide magnetic nanoparticles in rats. Mol. Pharm. **5**: 316–327. doi:10.1021/mp7001285.

Al-Jamal WT, Al-Jamal KT, Tian B, Lacerda L, Bomans PH, Frederik PM, Kostarelos K (2008) Lipid−Quantum Dot Bilayer Vesicles Enhance Tumor Cell Uptake and Retention *in Vitro* and *in Vivo*. ACS Nano **2**: 408–418. doi:10.1021/nn700176a.

James RW (1993) The relevance of clinical pathology to toxicology studies. Comp. Haematol. Int. **3**: 190–195. doi:10.1007/BF02341965.

Jia G, Zhuang Z (2010) [Safety needs for nano-technology promoted the development of nano-toxicology]. Zhonghua Yu Fang Yi Xue Za Zhi **44**: 773–774.

Jokerst JV, Lobovkina T, Zare RN, Gambhir SS (2011) Nanoparticle PEGylation for imaging and therapy. Nanomed. **6**: 715–728. doi:10.2217/nnm.11.19.

Kang YS, Risbud S, Rabolt JF, Stroeve P (1996) Synthesis and Characterization of Nanometer-Size Fe3O4 and γ-Fe2O3 Particles. Chem. Mater. **8**: 2209–2211. doi:10.1021/cm960157j.

Karlsson HL, Cronholm P, Gustafsson J, Möller L (2008) Copper Oxide Nanoparticles Are Highly Toxic: A Comparison between Metal Oxide Nanoparticles and Carbon Nanotubes. Chem. Res. Toxicol. **21**: 1726–1732.

Kermanizadeh A, Chauché C, Balharry D, Brown DM, Kanase N, Boczkowski J, Lanone S, Stone V (2013) The role of Kupffer cells in the hepatic response to silver nanoparticles. Nanotoxicology **8**: 149–154. doi:10.3109/17435390.2013.866284.

Kim DK, Mikhaylova M, Zhang Y, Muhammed M (2003) Protective Coating of Superparamagnetic Iron Oxide Nanoparticles. Chem. Mater. **15**: 1617–1627. doi:10.1021/cm021349j.

Kim JS, Yoon T-J, Yu KN, Kim BG, Park SJ, Kim HW, Lee KH, Park SB, Lee J-K, Cho MH (2006) Toxicity and tissue distribution of magnetic nanoparticles in mice. Toxicol. Sci. **89**: 338–347.

Kojouri GA, Jahanabadi S, Shakibaie M, Ahadi AM, Shahverdi AR (2012) Effect of selenium supplementation with sodium selenite and selenium nanoparticles on iron homeostasis and transferrin gene expression in sheep: A preliminary study. Res. Vet. Sci. **93**: 275–278. doi:10.1016/j.rvsc.2011.07.029.

Kong W-N, Niu Q-M, Ge L, Zhang N, Yan S-F, Chen W-B, Chang Y-Z, Zhao S-E (2014) Sex differences in iron status and hepcidin expression in rats. Biol. Trace Elem. Res. **160**: 258–267. doi:10.1007/s12011-014-0051-3.

Kregel KC (2002) Heat shock proteins: modifying factors in physiological stress responses and acquired thermotolerance. J. Appl. Physiol. Bethesda Md 1985 **92**: 2177–2186. doi:10.1152/japplphysiol.01267.2001.

Kumari M, Rajak S, Singh SP, Murty USN, Mahboob M, Grover P, Rahman MF (2013) Biochemical alterations induced by acute oral doses of iron oxide nanoparticles in Wistar rats. Drug Chem. Toxicol. **36**: 296–305.

Kunzmann A, Andersson B, Thurnherr T, Krug H, Scheynius A, Fadeel B (2011) Toxicology of engineered nanomaterials: focus on biocompatibility, biodistribution and biodegradation. Biochim. Biophys. Acta **1810**: 361–373.

Kyung OY, Grabinski CM, Schrand AM, Murdock RC, Wang W, Gu B, Schlager JJ, Hussain SM (2009) Toxicity of amorphous silica nanoparticles in mouse keratinocytes. J. Nanoparticle Res. **11**: 15–24.

Lamprecht C, Gierlinger N, Heister E, Unterauer B, Plochberger B, Brameshuber M, Hinterdorfer P, Hild S, Ebner A (2012) Mapping the intracellular distribution of carbon nanotubes after targeted delivery to carcinoma cells using confocal Raman imaging as a label-free technique. J. Phys. Condens. Matter Inst. Phys. J. **24**: 164206. doi:10.1088/0953-8984/24/16/164206.

Larsen EKU, Nielsen T, Wittenborn T, Birkedal H, Vorup-Jensen T, Jakobsen MH, Østergaard L, Horsman MR, Besenbacher F, Howard KA, Kjems J (2009) Size-Dependent Accumulation of PEGylated Silane-Coated Magnetic Iron Oxide Nanoparticles in Murine Tumors. ACS Nano **3**: 1947–1951.

Laurent S, Burtea C, Thirifays C, Häfeli UO, Mahmoudi M (2012) Crucial Ignored Parameters on Nanotoxicology: The Importance of Toxicity Assay Modifications and "Cell Vision." PLoS ONE **7**: e29997. doi:10.1371/journal.pone.0029997.

Laurent S, Dutz S, Häfeli UO, Mahmoudi M (2011) Magnetic fluid hyperthermia: Focus on superparamagnetic iron oxide nanoparticles. Adv. Colloid Interface Sci. **166**: 8–23. doi:10.1016/j.cis.2011.04.003.

Laurent S, Forge D, Port M, Roch A, Robic C, Vander Elst L, Muller RN (2008) Magnetic Iron Oxide Nanoparticles: Synthesis, Stabilization, Vectorization, Physicochemical Characterizations, and Biological Applications. Chem. Rev. **108**: 2064–2110. doi:10.1021/cr068445e.

Laurent S, Saei AA, Behzadi S, Panahifar A, Mahmoudi M (2014) Superparamagnetic iron oxide nanoparticles for delivery of therapeutic agents: opportunities and challenges. Expert Opin. Drug Deliv. **11**: 1449–1470. doi:10.1517/17425247.2014.924501.

Lee D-H, Blomhoff R, Jacobs DR (2004) Is serum gamma glutamyltransferase a marker of oxidative stress? Free Radic. Res. **38**: 535–539.

Lee H, Lee E, Kim DK, Jang NK, Jeong YY, Jon S (2006) Antibiofouling polymer-coated superparamagnetic iron oxide nanoparticles as potential magnetic resonance contrast agents for in vivo cancer imaging. J. Am. Chem. Soc. **128**: 7383–7389. doi:10.1021/ja061529k.

Lemarchand C, Gref R, Lesieur S, Hommel H, Vacher B, Besheer A, Maeder K, Couvreur P (2005) Physico-chemical characterization of polysaccharide-coated nanoparticles. J. Controlled Release **108**: 97–111.

Leonard SS, Harris GK, Shi X (2004) Metal-induced oxidative stress and signal transduction. Free Radic. Biol. Med. **37**: 1921–1942.

Lepoivre M, Chenais B, Yapo A, Lemaire G, Thelander L, Tenu JP (1990) Alterations of ribonucleotide reductase activity following induction of the nitrite-generating pathway in adenocarcinoma cells. J. Biol. Chem. **265**: 14143–14149.

Levy M, Luciani N, Alloyeau D, Elgrabli D, Deveaux V, Pechoux C, Chat S, Wang G, Vats N, Gendron F, Factor C, Lotersztajn S, Luciani A, Wilhelm C, Gazeau F (2011) Long term in vivo biotransformation of iron oxide nanoparticles. Biomaterials **32**: 3988–3999.

Lewin M, Carlesso N, Tung CH, Tang XW, Cory D, Scadden DT, Weissleder R (2000) Tat peptide-derivatized magnetic nanoparticles allow in vivo tracking and recovery of progenitor cells. Nat. Biotechnol. **18**: 410–414. doi:10.1038/74464.

Lima R de, Oliveira JL, Murakami PSK, Molina M a. M, Itri R, Haddad P, Seabra AB (2013) Iron oxide nanoparticles show no toxicity in the comet assay in lymphocytes: A promising vehicle as a nitric oxide releasing nanocarrier in biomedical applications. J. Phys. Conf. Ser. **429**: 012021. doi:10.1088/1742-6596/429/1/012021.

Li S-Q, Zhu R-R, Zhu H, Xue M, Sun X-Y, Yao S-D, Wang S-L (2008) Nanotoxicity of TiO 2 nanoparticles to erythrocyte in vitro. Food Chem. Toxicol. **46**: 3626–3631.

Liu Q, Shao X, Chen J, Shen Y, Feng C, Gao X, Zhao Y, Li J, Zhang Q, Jiang X (2011) In vivo toxicity and immunogenicity of wheat germ agglutinin conjugated poly(ethylene glycol)-poly(lactic acid) nanoparticles for intranasal delivery to the brain. Toxicol. Appl. Pharmacol. **251**: 79–84. doi:10.1016/j.taap.2010.12.003.

Lunov O, Zablotskii V, Syrovets T, Röcker C, Tron K, Nienhaus GU, Simmet T (2011) Modeling receptor-mediated endocytosis of polymer-functionalized iron oxide nanoparticles by human macrophages. Biomaterials **32**: 547–555. doi:10.1016/j.biomaterials.2010.08.111.

Lynch I, Dawson KA (2008) Protein-nanoparticle interactions. Nano Today **3**: 40–47.

Macedo MF, de Sousa M (2008) Transferrin and the transferrin receptor: of magic bullets and other concerns. Inflamm. Allergy Drug Targets **7**: 41–52.

Mackenzie EL, Iwasaki K, Tsuji Y (2008) Intracellular Iron Transport and Storage: From Molecular Mechanisms to Health Implications. Antioxid. Redox Signal. **10**: 997–1030. doi:10.1089/ars.2007.1893.

Magaye RR, Yue X, Zou B, Shi H, Yu H, Liu K, Lin X, Xu J, Yang C, Wu A, Zhao J (2014) Acute toxicity of nickel nanoparticles in rats after intravenous injection. Int. J. Nanomedicine **9**: 1393–1402. doi:10.2147/IJN.S56212.

Mahmoudi M, Hofmann H, Rothen-Rutishauser B, Petri-Fink A (2012) Assessing the in vitro and in vivo toxicity of superparamagnetic iron oxide nanoparticles. Chem. Rev. **112**: 2323–2338. doi:10.1021/cr2002596.

Mahmoudi M, Hosseinkhani H, Hosseinkhani M, Boutry S, Simchi A, Journeay WS, Subramani K, Laurent S (2011a) Magnetic resonance imaging tracking of stem cells in vivo using iron oxide nanoparticles as a tool for the advancement of clinical regenerative medicine. Chem. Rev. **111**: 253–280. doi:10.1021/cr1001832.

Mahmoudi M, Sant S, Wang B, Laurent S, Sen T (2011b) Superparamagnetic iron oxide nanoparticles (SPIONs): development, surface modification and applications in chemotherapy. Adv. Drug Deliv. Rev. **63**: 24–46. doi:10.1016/j.addr.2010.05.006.

Mahmoudi M, Simchi A, Imani M (2009a) Cytotoxicity of Uncoated and Polyvinyl Alcohol Coated Superparamagnetic Iron Oxide Nanoparticles. J. Phys. Chem. C **113**: 9573–9580. doi:10.1021/jp9001516.

Mahmoudi M, Simchi A, Milani AS, Stroeve P (2009b) Cell toxicity of superparamagnetic iron oxide nanoparticles. J. Colloid Interface Sci. **336**: 510–518. doi:10.1016/j.jcis.2009.04.046.

Maines MD (1997) The heme oxygenase system: a regulator of second messenger gases. Annu. Rev. Pharmacol. Toxicol. **37**: 517–554. doi:10.1146/annurev.pharmtox.37.1.517.

Maines MD (2000) The heme oxygenase system and its functions in the brain. Cell. Mol. Biol. Noisy--Gd. Fr. **46**: 573–585.

Ma P, Luo Q, Chen J, Gan Y, Du J, Ding S, Xi Z, Yang X (2012) Intraperitoneal injection of magnetic Fe3O4-nanoparticle induces hepatic and renal tissue injury via oxidative stress in mice. Int. J. Nanomedicine **7**: 4809.

Marquis BJ, Love SA, Braun KL, Haynes CL (2009) Analytical methods to assess nanoparticle toxicity. The Analyst **134**: 425–439. doi:10.1039/b818082b.

Massart R (1981) Preparation of aqueous magnetic liquids in alkaline and acidic media. IEEE Trans. Magn. **17**: 1247–1248. doi:10.1109/TMAG.1981.1061188.

Massart R, Dubois E, Cabuil V, Hasmonay E (1995) Preparation and properties of monodisperse magnetic fluids. J. Magn. Magn. Mater. **149**. Proceedings of the Seventh International Conference on Magnetic Fluids: 1–5. doi:10.1016/0304-8853(95)00316-9.

Matthäus C, Chernenko T, Newmark JA, Warner CM, Diem M (2007) Label-free detection of mitochondrial distribution in cells by nonresonant Raman microspectroscopy. Biophys. J. **93**: 668–673. doi:10.1529/biophysj.106.102061.

Matuszewski L, Persigehl T, Wall A, Schwindt W, Tombach B, Fobker M, Poremba C, Ebert W, Heindel W, Bremer C (2005) Cell tagging with clinically approved iron oxides: feasibility and effect of lipofection, particle size, and surface coating on labeling efficiency. Radiology **235**: 155–161. doi:10.1148/radiol.2351040094.

Maurer-Jones MA, Bantz KC, Love SA, Marquis BJ, Haynes CL (2009) Toxicity of therapeutic nanoparticles. Nanomed. **4**: 219–241. doi:10.2217/17435889.4.2.219.

Mayer A, Vadon M, Rinner B, Novak A, Wintersteiger R, Fröhlich E (2009) The role of nanoparticle size in hemocompatibility. Toxicology **258**: 139–147. doi:10.1016/j.tox.2009.01.015.

McCord JM, Fridovich I (1969) Superoxide Dismutase AN ENZYMIC FUNCTION FOR ERYTHROCUPREIN (HEMOCUPREIN). J. Biol. Chem. **244**: 6049–6055.

Mehvar R (2000) Dextrans for targeted and sustained delivery of therapeutic and imaging agents. J. Control. Release Off. J. Control. Release Soc. **69**: 1–25.

Metzger IF, Sertorio JTC, Tanus-Santos JE (2006) Relationship between systemic nitric oxide metabolites and cyclic GMP in healthy male volunteers. Acta Physiol. Oxf. Engl. **188**: 123–127. doi:10.1111/j.1748-1716.2006.01612.x.

Metz S, Bonaterra G, Rudelius M, Settles M, Rummeny EJ, Daldrup-Link HE (2004a) Capacity of human monocytes to phagocytose approved iron oxide MR contrast agents in vitro. Eur. Radiol. **14**: 1851–1858.

Metz S, Bonaterra G, Rudelius M, Settles M, Rummeny EJ, Daldrup-Link HE (2004b) Capacity of human monocytes to phagocytose approved iron oxide MR contrast agents in vitro. Eur. Radiol. **14**: 1851–1858. doi:10.1007/s00330-004-2405-2.

Misra HP, Fridovich I (1972) The role of superoxide anion in the autoxidation of epinephrine and a simple assay for superoxide dismutase. J. Biol. Chem. **247**: 3170–3175.

Moghimi SM, Hunter AC, Murray JC (2001) Long-circulating and target-specific nanoparticles: theory to practice. Pharmacol. Rev. **53**: 283–318.

Mohapatra M, Anand S (2010) Synthesis and applications of nano-structured iron oxides/hydroxides–a review. Int. J. Eng. Sci. Technol. **2**. http://www.ajol.info/index.php/ijest/article/view/63846.

Mondini S, Cenedese S, Marinoni G, Molteni G, Santo N, Bianchi CL, Ponti A (2008) One-step synthesis and functionalization of hydroxyl-decorated magnetite nanoparticles. J. Colloid Interface Sci. **322**: 173–179. doi:10.1016/j.jcis.2008.03.008.

Morano KA (2007) New tricks for an old dog: the evolving world of Hsp70. Ann. N. Y. Acad. Sci. **1113**: 1–14. doi:10.1196/annals.1391.018.

Mornet S, Vasseur S, Grasset F, Duguet E (2004) Magnetic nanoparticle design for medical diagnosis and therapy. J. Mater. Chem. **14**: 2161–2175. doi:10.1039/B402025A.

Moron MS, Depierre JW, Mannervik B (1979) Levels of glutathione, glutathione reductase and glutathione S-transferase activities in rat lung and liver. Biochim. Biophys. Acta **582**: 67–78.

Mosmann T (1983) Rapid colorimetric assay for cellular growth and survival: application to proliferation and cytotoxicity assays. J. Immunol. Methods **65**: 55–63.

Murdock RC, Braydich-Stolle L, Schrand AM, Schlager JJ, Hussain SM (2008) Characterization of Nanomaterial Dispersion in Solution Prior to In Vitro Exposure Using Dynamic Light Scattering Technique. Toxicol. Sci. **101**: 239–253. doi:10.1093/toxsci/kfm240.

Nakashima K, Takeuchi T, Shirakawa T (2005) Differentiation, distribution, and chemical state of intracellular trace elements in LAD2 mast cell line. Biol. Trace Elem. Res. **108**: 105–114. doi:10.1385/BTER:108:1-3:105.

Nel AE, Mädler L, Velegol D, Xia T, Hoek EMV, Somasundaran P, Klaessig F, Castranova V, Thompson M (2009) Understanding biophysicochemical interactions at the nano–bio interface. Nat. Mater. **8**: 543–557. doi:10.1038/nmat2442.

Nel A, Xia T, Mädler L, Li N (2006) Toxic potential of materials at the nanolevel. Science **311**: 622–627. doi:10.1126/science.1114397.

Neuberger T, Schöpf B, Hofmann H, Hofmann M, Von Rechenberg B (2005) Superparamagnetic nanoparticles for biomedical applications: possibilities and limitations of a new drug delivery system. J. Magn. Magn. Mater. **293**: 483–496.

Oberdörster G, Maynard A, Donaldson K, Castranova V, Fitzpatrick J, Ausman K, Carter J, Karn B, Kreyling W, Lai D, Olin S, Monteiro-Riviere N, Warheit D, Yang H, $author.lastName $author firstName (2005) Principles for characterizing the potential human health effects from exposure to nanomaterials: elements of a screening strategy. Part. Fibre Toxicol. **2**: 8. doi:10.1186/1743-8977-2-8.

Ohkawa H, Ohishi N, Yagi K (1979) Assay for lipid peroxides in animal tissues by thiobarbituric acid reaction. Anal. Biochem. **95**: 351–358.

Ostomel TA, Shi Q, Stoimenov PK, Stucky GD (2007) Metal Oxide Surface Charge Mediated Hemostasis. Langmuir **23**: 11233–11238. doi:10.1021/la701281t.

Owens DE, Peppas NA (2006) Opsonization, biodistribution, and pharmacokinetics of polymeric nanoparticles. Int. J. Pharm. **307**: 93–102. doi:10.1016/j.ijpharm.2005.10.010.

Pang JH, Jiang MJ, Chen YL, Wang FW, Wang DL, Chu SH, Chau LY (1996) Increased ferritin gene expression in atherosclerotic lesions. J. Clin. Invest. **97**: 2204–2212. doi:10.1172/JCI118661.

Panyam J, Sahoo SK, Prabha S, Bargar T, Labhasetwar V (2003) Fluorescence and electron microscopy probes for cellular and tissue uptake of poly (D, L-lactide-co-glycolide) nanoparticles. Int. J. Pharm. **262**: 1–11.

Paolicchi A, Minotti G, Tonarelli P, Tongiani R, De Cesare D, Mezzetti A, Dominici S, Comporti M, Pompella A (1999) Gamma-glutamyl transpeptidase-dependent iron reduction and LDL oxidation--a potential mechanism in atherosclerosis. J. Investig. Med. Off. Publ. Am. Fed. Clin. Res. **47**: 151–160.

Pardoe H, Chua-anusorn W, St. Pierre TG, Dobson J (2001) Structural and magnetic properties of nanoscale iron oxide particles synthesized in the presence of dextran or polyvinyl alcohol. J. Magn. Magn. Mater. **225**. Proceedings of the Third International Conference on Scientific and Clinical Applications of Magnetic Carriers: 41–46. doi:10.1016/S0304-8853(00)01226-9.

Patel BN, Dunn RJ, Jeong SY, Zhu Q, Julien J-P, David S (2002) Ceruloplasmin Regulates Iron Levels in the CNS and Prevents Free Radical Injury. J. Neurosci. **22**: 6578–6586.

Patlolla A, McGinnis B, Tchounwou P (2011) Biochemical and histopathological evaluation of functionalized single-walled carbon nanotubes in Swiss-Webster mice. J. Appl. Toxicol. JAT **31**: 75–83. doi:10.1002/jat.1579.

Petri-Fink A, Chastellain M, Juillerat-Jeanneret L, Ferrari A, Hofmann H (2005) Development of functionalized superparamagnetic iron oxide nanoparticles for interaction with human cancer cells. Biomaterials **26**: 2685–2694. doi:10.1016/j.biomaterials.2004.07.023.

Pompella A, Emdin M, Passino C, Paolicchi A (2004) The significance of serum gamma-glutamyltransferase in cardiovascular diseases. Clin. Chem. Lab. Med. CCLM FESCC **42**: 1085–1091. doi:10.1515/CCLM.2004.224.

Pourmoghaddas A, Sanei H, Garakyaraghi M, Esteki-Ghashghaei F, Gharaati M (2014) The relation between body iron store and ferritin, and coronary artery disease. ARYA Atheroscler. **10**: 32–36.

Rapoport R, Hanukoglu I, Sklan D (1994) A Fluorometric Assay for Hydrogen Peroxide, Suitable for NAD(P)H-Dependent Superoxide Generating Redox Systems. Anal. Biochem. **218**: 309–313. doi:10.1006/abio.1994.1183.

Réty F, Clément O, Siauve N, Cuénod CA, Carnot F, Sich M, Buisine A, Frija G (2000) MR lymphography using iron oxide nanoparticles in rats: pharmacokinetics in the lymphatic system after intravenous injection. J. Magn. Reson. Imaging JMRI **12**: 734–739.

Rugal AA, Gun'ko VM, Barvinchenko VN, Turov VV, Semeshkina TV, Zarko VI (2007) Interaction of fibrinogen with nanosilica. Cent. Eur. J. Chem. **5**: 32–54. doi:10.2478/s11532-006-0067-4.

Ruiz A, Hernández Y, Cabal C, González E, Veintemillas-Verdaguer S, Martínez E, Morales MP (2013) Biodistribution and pharmacokinetics of uniform magnetite nanoparticles chemically modified with polyethylene glycol. Nanoscale **5**: 11400–11408. doi:10.1039/c3nr01412f.

Ryter SW, Alam J, Choi AMK (2006) Heme oxygenase-1/carbon monoxide: from basic science to therapeutic applications. Physiol. Rev. **86**: 583–650. doi:10.1152/physrev.00011.2005.

Sadauskas E, Wallin H, Stoltenberg M, Vogel U, Doering P, Larsen A, Danscher G (2007) Kupffer cells are central in the removal of nanoparticles from the organism. Part. Fibre Toxicol. **4**: 10. doi:10.1186/1743-8977-4-10.

Samuel Reich E (2011) Nano rules fall foul of data gap. Nature **480**: 160–161. doi:10.1038/480160a.

Santosh S, Podaralla P, Miller B (2010) Anaphylaxis with elevated serum tryptase after administration of intravenous ferumoxytol. NDT Plus **3**: 341–342. doi:10.1093/ndtplus/sfq084.

Saraswathy A, Nazeer SS, Nimi N, Arumugam S, Shenoy SJ, Jayasree RS (2014) Synthesis and characterization of dextran stabilized superparamagnetic iron oxide nanoparticles for in vivo MR imaging of liver fibrosis. Carbohydr. Polym. **101**: 760–768. doi:10.1016/j.carbpol.2013.10.015.

Sarin H (2010) Physiologic upper limits of pore size of different blood capillary types and another perspective on the dual pore theory of microvascular permeability. J. Angiogenesis Res. **2**: 14. doi:10.1186/2040-2384-2-14.

Schellekens H, Hennink WE, Brinks V (2013) The immunogenicity of polyethylene glycol: facts and fiction. Pharm. Res. **30**: 1729–1734. doi:10.1007/s11095-013-1067-7.

Scherz-Shouval R, Elazar Z (2011) Regulation of autophagy by ROS: physiology and pathology. Trends Biochem. Sci. **36**: 30–38. doi:10.1016/j.tibs.2010.07.007.

Schlachter EK, Widmer HR, Bregy A, Lönnfors-Weitzel T, Vajtai I, Corazza N, Bernau VJ, Weitzel T, Mordasini P, Slotboom J, others (2011) Metabolic pathway and distribution of superparamagnetic iron oxide nanoparticles: in vivo study. Int. J. Nanomedicine **6**: 1793.

Schrand AM, Braydich-Stolle LK, Schlager JJ, Dai L, Hussain SM (2008) Can silver nanoparticles be useful as potential biological labels? Nanotechnology **19**: 235104.

Shah NB, Dong J, Bischof JC (2011) Cellular uptake and nanoscale localization of gold nanoparticles in cancer using label-free confocal Raman microscopy. Mol. Pharm. **8**: 176–184. doi:10.1021/mp1002587.

Sharifi S, Behzadi S, Laurent S, Forrest ML, Stroeve P, Mahmoudi M (2012) Toxicity of nanomaterials. Chem. Soc. Rev. **41**: 2323–2343.

Sharma G, Kodali V, Gaffrey M, Wang W, Minard KR, Karin NJ, Teeguarden JG, Thrall BD (2013) Iron oxide nanoparticle agglomeration influences dose rates and modulates oxidative stress-mediated dose–response profiles in vitro. Nanotoxicology **8**: 663–675. doi:10.3109/17435390.2013.822115.

Sharma HS, Sharma A (2007) Nanoparticles aggravate heat stress induced cognitive deficits, blood–brain barrier disruption, edema formation and brain pathology. Prog. Brain Res. **162**: 245–273.

Sharp FR, Massa SM, Swanson RA (1999) Heat-shock protein protection. Trends Neurosci. **22**: 97–99.

Shaw SY, Westly EC, Pittet MJ, Subramanian A, Schreiber SL, Weissleder R (2008) Perturbational profiling of nanomaterial biologic activity. Proc. Natl. Acad. Sci. **105**: 7387–7392.

Simberg D, Zhang W-M, Merkulov S, McCrae K, Park J-H, Sailor MJ, Ruoslahti E (2009) Contact activation of kallikrein–kinin system by superparamagnetic iron oxide nanoparticles in vitro and in vivo. J. Controlled Release **140**. Proceedings of the Fourtheenth International Symposium on Recent Advances in Drug Delivery Systems: 301–305. doi:10.1016/j.jconrel.2009.05.035.

Singh N, Jenkins GJS, Asadi R, Doak SH (2010) Potential toxicity of superparamagnetic iron oxide nanoparticles (SPION). Nano Rev. **1**. doi:10.3402/nano.v1i0.5358. http://www.ncbi.nlm.nih.gov/pmc/articles/PMC3215220/.

Singh N, Jenkins GJS, Nelson BC, Marquis BJ, Maffeis TGG, Brown AP, Williams PM, Wright CJ, Doak SH (2012) The role of iron redox state in the genotoxicity of ultrafine superparamagnetic iron oxide nanoparticles. Biomaterials **33**: 163–170. doi:10.1016/j.biomaterials.2011.09.087.

Singh N, Manshian B, Jenkins GJS, Griffiths SM, Williams PM, Maffeis TGG, Wright CJ, Doak SH (2009) NanoGenotoxicology: the DNA damaging potential of engineered nanomaterials. Biomaterials **30**: 3891–3914. doi:10.1016/j.biomaterials.2009.04.009.

Sismanopoulos N, Delivanis D-A, Alysandratos K-D, Angelidou A, Therianou A, Kalogeromitros D, C Theoharides T (2012) Mast cells in allergic and inflammatory diseases. Curr. Pharm. Des. **18**: 2261–2277.

Soenen SJ, Baert J, De Cuyper M (2007) Optimal conditions for labelling of 3T3 fibroblasts with magnetoliposomes without affecting cellular viability. Chembiochem **8**: 2067–2077.

Soenen SJH, Himmelreich U, Nuytten N, De Cuyper M (2011) Cytotoxic effects of iron oxide nanoparticles and implications for safety in cell labelling. Biomaterials **32**: 195–205. doi:10.1016/j.biomaterials.2010.08.075.

Soenen SJH, Himmelreich U, Nuytten N, Pisanic TR, Ferrari A, De Cuyper M (2010a) Intracellular nanoparticle coating stability determines nanoparticle diagnostics efficacy and cell functionality. Small Weinh. Bergstr. Ger. **6**: 2136–2145. doi:10.1002/smll.201000763.

Soenen SJH, Nuytten N, De Meyer SF, De Smedt SC, De Cuyper M (2010b) High intracellular iron oxide nanoparticle concentrations affect cellular cytoskeleton and focal adhesion kinase-mediated signaling. Small Weinh. Bergstr. Ger. **6**: 832–842. doi:10.1002/smll.200902084.

Srinivas A, Rao PJ, Selvam G, Goparaju A, Murthy PB, Reddy PN (2012) Oxidative stress and inflammatory responses of rat following acute inhalation exposure to iron oxide nanoparticles. Hum. Exp. Toxicol. **31**: 1113–1131. doi:10.1177/0960327112446515.

Stamler JS, Lamas S, Fang FC (2001) Nitrosylation. the prototypic redox-based signaling mechanism. Cell **106**: 675–683.

Sucharová J, Suchara I (2006) Determination of 36 elements in plant reference materials with different Si contents by inductively coupled plasma mass spectrometry: Comparison of microwave digestions assisted by three types of digestion mixtures. Anal. Chim. Acta **576**: 163–176. doi:10.1016/j.aca.2006.06.004.

Sun J, Zhou S, Hou P, Yang Y, Weng J, Li X, Li M (2007) Synthesis and characterization of biocompatible Fe3O4 nanoparticles. J. Biomed. Mater. Res. A **80**: 333–341.

Suzuki Y, Yoshimaru T, Inoue T, Niide O, Ra C (2005) Role of oxidants in mast cell activation. Chem. Immunol. Allergy **87**: 32–42. doi:10.1159/000087569.

Suzuki Y, Yoshimaru T, Inoue T, Ra C (2009) Discrete generations of intracellular hydrogen peroxide and superoxide in antigen-stimulated mast cells: reciprocal regulation of store-operated Ca2+ channel activity. Mol. Immunol. **46**: 2200–2209. doi:10.1016/j.molimm.2009.04.013.

Suzuki Y, Yoshimaru T, Matsui T, Inoue T, Niide O, Nunomura S, Ra C (2003) FcεRI signaling of mast cells activates intracellular production of hydrogen peroxide: role in the regulation of calcium signals. J. Immunol. **171**: 6119–6127.

Tapiero H, Townsend DM, Tew KD (2003) Trace elements in human physiology and pathology. Copper. Biomed. Pharmacother. Bioméd. Pharmacothérapie **57**: 386–398.

Tarnuzzer RW, Colon J, Patil S, Seal S (2005) Vacancy Engineered Ceria Nanostructures for Protection from Radiation-Induced Cellular Damage. Nano Lett. **5**: 2573–2577. doi:10.1021/nl052024f.

Thankam FG, Muthu J (2014) Biosynthetic hydrogels--studies on chemical and physical characteristics on long-term cellular response for tissue engineering. J. Biomed. Mater. Res. A **102**: 2238–2247. doi:10.1002/jbm.a.34895.

Townsend DM, Tew KD, Tapiero H (2003) The importance of glutathione in human disease. Biomed. Pharmacother. Bioméd. Pharmacothérapie **57**: 145–155.

Tseng MT, Lu X, Duan X, Hardas SS, Sultana R, Wu P, Unrine JM, Graham U, Butterfield DA, Grulke EA, Yokel RA (2012) Alteration of hepatic structure and oxidative stress induced by intravenous nanoceria. Toxicol. Appl. Pharmacol. **260**: 173–182. doi:10.1016/j.taap.2012.02.008.

Tuomainen T-P, Punnonen K, Nyyssönen K, Salonen JT (1998) Association Between Body Iron Stores and the Risk of Acute Myocardial Infarction in Men. Circulation **97**: 1461–1466. doi:10.1161/01.CIR.97.15.1461.

Ulus T, Yildirir A, Demirtas S, Demir O, Sade LE, Bozbas H, Gürsoy Y, Bilgi M, Küçük MA, Müderrisoğlu H (2007) Serum gamma-glutamyl transferase activity: a new marker for stent restenosis? Atherosclerosis **195**: 348–353.

Varma HK MP (2014) Toxicity Evaluation of Dextran Coated Ferrite Nanomaterials After Acute Oral Exposure to Wistar Rats. J. Allergy Ther. **05**. doi:10.4172/2155-6121.1000166. http://omicsonline.org/open-access/toxicity-evaluation-of-dextran-coated-ferrite-nanomaterials-2155-6121.1000166.pdf.

Vogel U, Savolainen K, Wu Q, Tongeren M van, Brouwer D, Berges M (2013) Handbook of Nanosafety: Measurement, Exposure and Toxicology. Elsevier, December 17.

Walker BL, Tiong JWC, Jefferies WA (2001) Iron metabolism in mammalian cells. In , ed. BT - International Review of Cytology, **211**241–278. Academic Press.

Wallander ML, Leibold EA, Eisenstein RS (2006) Molecular control of vertebrate iron homeostasis by iron regulatory proteins. Biochim. Biophys. Acta BBA - Mol. Cell Res. **1763**. Cell Biology of Metals: 668–689. doi:10.1016/j.bbamcr.2006.05.004.

Walter PB, Knutson MD, Paler-Martinez A, Lee S, Xu Y, Viteri FE, Ames BN (2002) Iron deficiency and iron excess damage mitochondria and mitochondrial DNA in rats. Proc. Natl. Acad. Sci. U. S. A. **99**: 2264–2269. doi:10.1073/pnas.261708798.

Wang Q, Shen M, Zhao T, Xu Y, Lin J, Duan Y, Gu H (2015) Low toxicity and long circulation time of Polyampholyte-coated magnetic nanoparticles for blood pool contrast agents. Sci. Rep. **5**. doi:10.1038/srep07774. http://www.nature.com/srep/2015/150114/srep07774/full/srep07774.html.

Wang YX, Hussain SM, Krestin GP (2001) Superparamagnetic iron oxide contrast agents: physicochemical characteristics and applications in MR imaging. Eur. Radiol. **11**: 2319–2331. doi:10.1007/s003300100908.

Weissleder R, Bogdanov A, Neuwelt EA, Papisov M (1995) Long-circulating iron oxides for MR imaging. Adv. Drug Deliv. Rev. **16**. Long-circulating Drug Delivery Systems: 321–334. doi:10.1016/0169-409X(95)00033-4.

Weissleder R, Stark DD, Engelstad BL, Bacon BR, Compton CC, White DL, Jacobs P, Lewis J (1989) Superparamagnetic iron oxide: pharmacokinetics and toxicity. AJR Am. J. Roentgenol. **152**: 167–173. doi:10.2214/ajr.152.1.167.

Whitfield JB (2001) Gamma glutamyl transferase. Crit. Rev. Clin. Lab. Sci. **38**: 263–355.

Widziewicz K, Kalka J, Skonieczna M, Madej P (2012) The comet assay for the evaluation of genotoxic potential of landfill leachate. ScientificWorldJournal **2012**: 435239. doi:10.1100/2012/435239.

Wilhelm C, Billotey C, Roger J, Pons JN, Bacri J-C, Gazeau F (2003) Intracellular uptake of anionic superparamagnetic nanoparticles as a function of their surface coating. Biomaterials **24**: 1001–1011.

Wilhelm C, Gazeau F (2008) Universal cell labelling with anionic magnetic nanoparticles. Biomaterials **29**: 3161–3174.

Xu J, Shi H, Ruth M, Yu H, Lazar L, Zou B, Yang C, Wu A, Zhao J (2013) Acute Toxicity of Intravenously Administered Titanium Dioxide Nanoparticles in Mice. PLoS ONE **8**. doi:10.1371/journal.pone.0070618. http://www.ncbi.nlm.nih.gov/pmc/articles/PMC3738549/.

Yang H, Liu C, Yang D, Zhang H, Xi Z (2009) Comparative study of cytotoxicity, oxidative stress and genotoxicity induced by four typical nanomaterials: the role of particle size, shape and composition. J. Appl. Toxicol. JAT **29**: 69–78. doi:10.1002/jat.1385.

Yang S-T, Wang X, Jia G, Gu Y, Wang T, Nie H, Ge C, Wang H, Liu Y (2008) Long-term accumulation and low toxicity of single-walled carbon nanotubes in intravenously exposed mice. Toxicol. Lett. **181**: 182–189. doi:10.1016/j.toxlet.2008.07.020.

You C-C, De M, Rotello VM (2005) Monolayer-protected nanoparticle-protein interactions. Curr. Opin. Chem. Biol. **9**: 639–646. doi:10.1016/j.cbpa.2005.09.012.

Zaouali MA, Bejaoui M, Calvo M, Folch-Puy E, Pantazi E, Pasut G, Rimola A, Ben Abdennebi H, Adam R, Roselló-Catafau J (2014) Polyethylene glycol rinse solution: an effective way to prevent ischemia-reperfusion injury. World J. Gastroenterol. WJG **20**: 16203–16214. doi:10.3748/wjg.v20.i43.16203.

Zhang Y, Kohler N, Zhang M (2002) Surface modification of superparamagnetic magnetite nanoparticles and their intracellular uptake. Biomaterials **23**: 1553–1561.

Zhao W, Gan X, Su G, Wanling G, Li S, Hei Z, Yang C, Wang H (2014) The interaction between oxidative stress and mast cell activation plays a role in acute lung injuries induced by intestinal ischemia-reperfusion. J. Surg. Res. **187**: 542–552. doi:10.1016/j.jss.2013.10.033.

Zimmerman HJ (1999) Hepatotoxicity: The Adverse Effects of Drugs and Other Chemicals on the Liver 2nd Revised edition edition. Philadelphia: Lippincott Williams and Wilkins, September 1.

List of Publications

1. Mast cell infiltration and oxidative stress induction of dextran and polyethylene glycol coated superparamagnetic iron oxide nanoparticles: An acute *in vivo* study. (Under review).

2. Confocal Raman microscopic studies of superparamagnetic iron oxide nanoparticles uptake in-vitro.(manuscript under preparation)

3. Oxidative stress analysis and Comet assay of dextran and polyethylene glycol coated superparamagnetic iron oxide nanoparticles: An in-vitro study.(manuscript under preparation)

4. Divalent metal cation disturbance due to dextran and polyethylene glycol coated superparamagnetic iron oxide nanoparticles: An acute *in vivo* study.(manuscript under preparation)

Curriculum vitae

Name	: A.SABAREESWARAN
Position	: Scientist-D &Scientist-In-Charge
Address	: Histopathology Laboratory, Division of Implant biology, Biomedical Technology Wing. Sree Chitra Tirunal Institute for Medical Sciences and Technology. Thiruvananthapuram-695012.Kerala.
e-mail	: asw@sctimst.ac.in
Phone	: +91 471 25 20 251(O)

Education:

Graduate (BVSc) in veterinary science and animal husbandry (2002) from Veterinary college and Research Institute, Namakkal. Tamilnadu Veterinary and Animal Sciences University, Madhavaram, Chennai.

Post Graduate (MVSc) in Veterinary Pathology (2005) from Madras Veterinary college, Tamilnadu Veterinary and Animal Sciences University, Madhavaram, Chennai.

Research and development:

Working as a scientist in the area of medical device development and testing at Sree chitra tirunal institute for medical sciences and technology for the past 9 years.

Carried out biocompatibility evaluation of various metals, ceramics, polymers and composites intended for soft and hard tissue application as per international standards in an accredited laboratory.

Carried out preclinical evaluation of the following medical devices namely, modified chitra mechanical heart valve, biological heart valve, bare and drug eluting coronary vascular stents, small and large diameter vascular grafts, left ventricular assist device, haemoconcentrator, blood oxygenator, dental composites, tissue engineered bone substitutes, cartilage, cornea, wound dressings and nano drug delivery system as study pathologist.

Publications

Research articles: 15 Nos **Book**: One

Appendix

Phase II reagents

Dulbecco Modified Eagle's Medium (DMEM) preparation

Dissolved one vial containing powder DMEM in 50 ml FCS, added 50 ml water until complete dissolution using a magnet stirrer and sterilized by filtration through sterile Millipore filter (0.22 mm)

Flouresceindiacetate (FDA) /Propidiumiodide (PI) staining working solution

Component	Volume
Culture medium without FCS	5 ml
FDA (5 mg of FDA in 1 ml acetone)	8 µl
PI (2 mg of PI in 1 ml PBS)	50 µl

1X Phosphate buffer saline (pH-7.4)

Dissolved the following in 800 ml distilled water

NaCl – 8 g

KCl – 0.2 g

Na_2HPO_4 – 1.44 g

KH_2PO_4 – 0.24 g

Adjusted the pH to 7.4 using HCl.

Made up the volume to 1000 ml with additional distilled water

Sterilized by autoclaving.

Phase III reagents

Neutral buffered formalin

Disodium hydrogen phosphate anhydrous (6.5 g) (Merck, India), Sodium dihydrogen phosphate monohydrate (4 g) (Merck, India), 100 ml of formaldehyde 37-41% (Merck, India) and 900 ml distilled water. The salts were dissolved by stirring, pH of the solution was adjusted to 7 and made up to one litre.

Harris's Haematoxylin

Haematoxylin (Merck) was dissolved in absolute alcohol by stirring in a magnetic stirrer. Potasium alum (Merck) was dissolved in water by gentle heating with the help of an electric heater (Bajaj electricals, Pune). Haematoxylin solution was poured into the alum solution while it was hot and allowed to boil rapidly. This was stirred using a glass rod. Mercuric oxide and sodium iodate were slowly added to it. The reaction vessel was then plunged into a basin of cold water. Glacial acetic acid was added to the reagent and filtered.

Eosin stain

Eosin (water soluble) (Merck, India) was mixed with isopropyl alcohol in a ratio of 10:1000 (gm/ml) using a magnetic stirrer.

Acid alcohol

Seven hundred millilitres of isopropyl alcohol was made up to 1000 ml with distilled water. From this 10 ml was discarded and 10 ml of con. HCl (Merck, India) was added to it.

Scott's tap water

Potassium bicarbonate - 2 grams

Magnesium sulphate - 20 grams

Distilled water - 1 litre

Potassium bicarbonate was dissolved in a little of water. Magnesium sulphate was dissolved in water in a separate beaker. Dissolved bicarbonate was poured into the magnesium sulphate solution and mixed well. The solution was then made up to one litre with water.

Sorensen's phosphate buffer

Stock A - 0.2 M Na_2HPO_4

Stock B - 0.2 M NaH_2PO_4

Sorensen's phosphate buffer (0.1 M) was prepared by mixing 40.5 ml of stock A and 9.5 ml of stock B.

3% buffered gluteraldehyde

The stock 8% gluteraldehyde (Polyscience, USA) was diluted to 3% using Sorensen's phosphate buffer.

Perl's Prussian blue stain.

5% Potassium Ferrocyanide:

Potassium ferrocyanide(Merck) -25.0 gm

Distilled water -500.0 ml

5% Hydrochloric Acid:

Hydrochloric acid, conc. -25.0 ml

Distilled water - 475.0 ml

Working Solution:

5% potassium ferrocyanide -25.0 ml

5% hydrochloric acid -25.0 ml

Neutral fast red stain

Neutral fast red (sigma) - 1.0 g

Distilled water - 100.0 ml

Glacial acetic acid - 1.0 ml

Cresyl violet stain

0.5% Cresyl Echt Violet:

Cresyl Echt Violet Acetate (Sigma)- 0.5 gm

Distilled water - 100.0 ml

Toluidine blue stain

Toluidine blue stock solution:

Toluidine blue O (Sigma) – 0.5g dissolved in 50 ml 70% Alcohol

1% NaCl solution:

NaCl (Merck) – 0.5g in 50 ml distilled water

Working solution

Toluidine blue stock 5 ml and 1% NaCl solution 45 ml (Make fresh)